Evolutionary divergence in proteins: Experimental and theoretical studies on the stability and electrochemical properties of cytochrome b_5

By

Sudharsan Parthasarathy

Submitted to the graduate degree program in Molecular BioSciences and the Graduate Faculty of the University of Kansas in partial fulfillment of the requirements for the degree of Doctor of Philosophy.

_____

Chairperson: Professor. Krzysztof Kuczera

_____

Professor. David R. Benson

_____

Professor. Mark Richter

_____

Associate Professor. Audrey Lamb

_____

Associate Professor. Hao Zhu

Date Defended: 16th December 2011

The Dissertation Committee for Sudharsan Parthasarathy

certifies that this is the approved version of the following dissertation:

Evolutionary divergence in proteins: Experimental and theoretical studies on the stability and electrochemical properties of cytochrome b_5

_____

Chairperson : Professor. Krzyszof Kuczera

Date approved: December 16th 2011

Abstract

Cytochrome b5 (CYB5) is a small ubiquitous heme binding protein whose biochemical function is electron transfer. Two isoforms of CYB5 are found in mammals, which are named based on their specific subcellular localization. One isoform is localized to the outer membrane of mitochondria (OMb5) and the other isoform is localized to the endoplasmic reticulum (Mcb5). Available evidence indicates that Mc and OM b5 isoforms arose from a gene duplication event that led to functional divergence. High sequence identity is observed when comparing individual isoforms across mammalian organisms. A highly conserved protein fold is also a feature when comparing the two isoforms. However the two isoforms differ remarkably with respect to their biophysical and biochemical properties. This dissertation focusses on analyzing the specific differences in Mc and OM b5 amino acid sequences that translate into subtle differences in structure, and to correlate them with differences in the biophysical properties of the two isoforms. A combination of experimental and theoretical methods has been used in order to study the differences between Mcb5 and Omb5. In chapter 3, I describe the X-ray crystal structures of the rat Omb5 (rOMb5) and human Omb5 (hOMb5), which reveal a striking difference in structure due to a difference in buried residue 21. The presence of Leu at position 21 in hOMb5 causes a displacement of the first two residues in beta 5, and consequent loss of two of the three hydrogen bonds between beta 5 and beta 4. Hydrogen bonding between the residues is instead mediated by two well ordered, fully buried water molecules. MD simulations of the hOMb5 protein, with and without the water molecules, provided mechanistic insight into the similarity in biophysical properties between hOMb5 and rOMb5. This study also provided information on the versatility of the CYB5 fold to resist internal mutations. Chapter 4 is a mutation based study that attempts to combine the most stabilizing features of OMb5 and Mcb5. The model proteins used here are rOMb5 and the bovine Mcb5 (bMcb5). We performed a systematic incorporation of amino acids from rOMb5 into the corresponding positions in bMcb5 which culminated in generating a hybrid protein (hybb5) that combined the most stabilizing features of the two proteins. We were successful in generating a series of mutants of increasing stability that altered both heme binding strength and apo protein stability. Further investigation revealed that rOMb5 displayed greater stability on account of the amino acid at position 71 (Leu). The presence of Leu in OMb5 isoforms results in generation of a more compact empty heme binding pocket that plays a major part in stabilizing OMb5 in contrast to Mcb5 isoforms which contain a more polar residue (Ser) at position 71. Chapter 5 utilizes the mutants generated as part of the study in chapter 4 to understand the factors responsible for modulating the redox potential difference in Omb5 and Mcb5. The initial part of the chapter focusses on measurement of redox potentials of the wild type proteins and the mutants. A constant redox potential difference of 60 mV was observed when comparing Omb5 and Mcb5 proteins in different mammals. Crystal structures of

a point mutant of bMcb5 (McS71L) and hybb5 were also generated and studied using molecular dynamics. Analysis of the crystal structures of bMcb5, McS71L, hybb5, rOMb5 and hOM5b revealed an in-plane rotation of the heme of approximately 13°. This in-plane rotation was consistently observed in all the proteins which contained Leu at position 71. The results obtained from experiments in chapter 5 lead us to propose that evolutionary divergence of the two isoforms (Mcb5 and Omb5) was favored by mutations at position 71. The nature of residue at position 71 influences two main factors responsible for modulating the redox potential; (a) the rotational isomer preference with respect to heme binding and (b) the in-plane rotation of the heme within the heme binding pocket. Thus, following the mutation at position 71 in mammals, it is possible that the two isoforms of CYB5 localized to different organelles and interacted with a new set of binding partners, as determined by their redox potentials, in order to accomplish a wider range of biochemical functions.

Acknowledgements

I would like to thank Prof. Krzysztof Kuczera and Prof. David Benson for accepting me into their labs and provide me with the skillset and knowledge for the advancement of my career. I am truly indebted to them given the circumstances with which I began my graduate career in their laboratories. Also my research would not have progressed without the suggestions of my committee members Prof. Mark Richter, Dr. Audrey Lamb and Dr. Hao Zhu for which I am eternally grateful. Special mention also goes out to my previous committee members Dr. Jennifer Laurence and Dr. David Davido for their assistance during my graduate work.

I would like to also thank Prof. Mario Rivera, Dr. Emily Scott, Prof. Russ Middaugh in their help with equipment that enabled me to perform key experiments required for my research. I am indebted to Dr. Scott and her lab members, Dr. Natasha DeVore and Patrick Porubsky with respect to assistance in protein purification and X-ray crystallography discussions throughout my graduate time in KU. I would also like to thank Dr. Justin Douglas and Sarah Neuenswander with regard to assistance in performing NMR experiments. Dr. Chris Olsen of Prof. Middaugh's lab was extremely valuable in providing assistance with DSC experiments, and I am indebted to his help with respect to this.

Finally to my wife Raghavi, my dear kutti Aditi, my appa and amma and my family members Sundar chitappa , Shantha aunty and my dear 'urundai' Urmilla, thank you, thank you, thank you. Without your help, I don't know how I could have accomplished these achievements. Without your words of encouragement and support, I could not have done this. Amma and appa (naan pass aiten), this thesis is dedicated to you. Thank you once again.

Table of Contents

Chapter 4: Step by step incorporation of rOMb5 residues into bMcb5 aimed to increase stability of bMcb5

Chapter 5: Divergence of biochemical properties of CYB5; insight into the redox potential difference between isoforms

List of Figures

List of Tables

Chapter 1: Introduction

Mammalian cytochrome b_5 (CYB5) proteins were first discovered by Strittmater and Ball in 1952 in microsomal factions of rat liver cells and characterised as an iron -protoporphyrin IX (heme b) binding protein [134, 132]. CYB5 first isolated from liver microsomes was dubbed microsomal CYB5 (Mcb5, more recently defined as CYB5A) [122, 140, 60]. Further characterisation of the protein by Spatz and Strittmater revealed that the full length protein is composed of two distinct regions: a water soluble cytosolic domain that contains the heme binding region and a C-terminal hydrophobic membrane anchoring segment [130]. A second isoform of CYB5 was isolated and purified from the outer membrane of rat liver mitochondria (after trypsin digestion), and was labelled outer mitochondrial CYB5 (OMb5, more recently designated CYB5B) [49, 58]. Available evidence indicates that CYB5A and CYB5B isoforms are a result of a gene duplication event that gave rise to independent proteins with different subcellular localizations [53], the localization determined by the sequence of the C-terminus [89, 32]. A soluble form of CYB5 from erythrocytes [34] is considered a splice variant of CYB5A lacking the membrane anchoring segment [53]. Biophysical and biochemical studies have been performed extensively on the souble heme binding domain of CYB5A and CYB5B, in part supported by the result that proteolyzed (specifically tryptic digest) CYB5A does not differ from full length CYB5A with respect to spectral properties [133]. Both CYB5A and CYB5B display virtually identical UV-visible and EPR spectra [112]. The spectra are also virtually identical when examining CYB5 proteins across various species [97]. As an example, the UV-visible spectrum of oxidised and reduced bovine Mcb5 is shown in figure 1.1

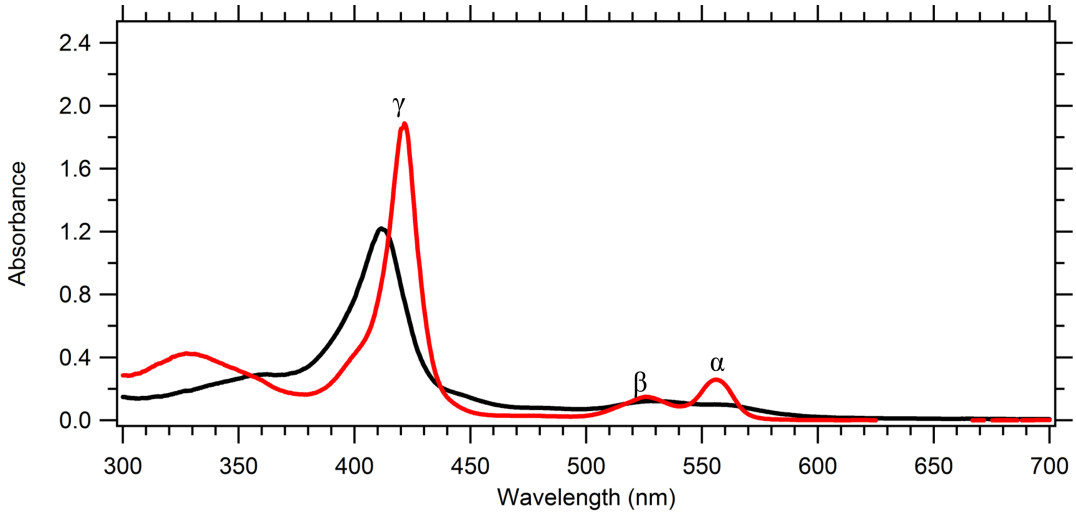

Figure 1.1: UV-Visible spectrum of oxidised (black) and reduced (red) Mcb5 bound to heme b. The visible bands appear prominently in the reduced spectrum with the α band occuring at 556 nm and the β band occuring at 523 nm. The Soret band (γ peak) shifts from 412 nm in the oxidised state to 423 nm in the reduced state.

Many proteins exist as fusion enzymes that harbour CYB5 as an independent domain along with additional functional domains. CYB5 domains are inserted anywhere along the length of the protein. For example $\Delta 5$ and $\Delta 6$ fatty acid desaturases contain the CYB5 domain at the N-terminus, $\triangle 9$ fatty acid desat-

urases contain the CYB5 domain at the C-terminus and nitrate reductases have the CYB5 domain inserted in the middle of the protein [122]. These fusion proteins are speculated to have risen due to wide range of gene manipulation events early in evolution including gene duplication and gene insertion following which they have evolved independently [68]. It has been proposed that incorporation of the CYB5 fold in fusion proteins also reduces the conformational search space sampled by protein partners to accomplish effective electron transfer between the protein partners [33].

1.1 Functions of CYB5

Extensive functional characterisation has been carried out on CYB5A proteins including *in vitro* redox interaction with protein partners and *in vivo* modulation of expression.

1.1.1 *In vitro* studies of CYB5: Interaction with known redox partners

Fatty acid desaturation A well-studied biochemical system involving CYB5A is the fatty acid desaturase reaction. The desaturation of fatty acids from saturated lipids is an important component of metabolism yielding many products that are responsible for vital cellular functions. Unsaturated fatty acids are key membrane components that regulate membrane fluidity and serve as precursors to signalling molecules such as prostaglandins and leukotrienes [140, 94, 73]. Fatty acid desaturases along with CYB5A introduce double bonds into the acyl chains, generating the unsaturated fatty acid. CYB5A, in addition to $\Delta 5$ and $\Delta 6$ fatty acid desaturases, participates in cholesterol biosynthesis by acting as an electron donor for the action of $\triangle 7$- Sterol $\delta 5$ desaturase [107, 48]. These are a few examples of the involvement of CYB5 in the synthesis of a wide variety of important lipids. The products of CYB5A mediated lipid reactions are critical molecules involved in a range of biological functions including signaling, gene expression and maintenance of homeostasis [52, 94].

Cytochrome P450 reduction Over three decades of research have produced extensive reviews [140, 122] and a textbook [100] detailing the biochemistry of cytochrome P450 (CYP450); in particular the role of CYB5A in mediating the reaction catalyzed by CYP450. CYP450 isoforms are mixed function oxidases that enable the oxidation of a wide variety of substances including endogenous molecules (vitamins, steroids, fatty acids) and exogenous molecules (therapeutic molecules, carcinogens) [140]. The mechanism involving CYB5A in CYP450 mediated oxidation reaction still remains unclear with CYB5A displaying different effects on the action of CYP450. There are three main roles of CYB5A in CYP450 mediated reactions: (i) In some cases CYB5A is absolutely necessary for CYP450 activity, For example, CYB5A is an obligate component for CYP450- 2B4 in the oxidation of methoxyfluorane. (ii) CYB5A can function as a stimulant for the action of CYP450, as shown by the fact that CYB5A increased metabolism of N,N-dimethylaniline by CYP450- 2B1 by a factor of 5. (iii) CYB5A can inhibit the action of CYP450, as in the case of benzphetamine metabolism by CYP450- 2B4 [140, 122]. Researchers have generally agreed that the influence of CYB5A on the action of CYP450 is dependent on experimental conditions, type of substrate used and also the isoform of CYP450 [122]. It is also believed that complexation of CYB5A and CYP450 affects the

redox potential of the components that lead to the oxidation of substrates. This is hypothesised to be a result of structural changes in CYP450 and/or CYB5A on complex formation [106, 122].

Methemoglobin reduction Circulating hemoglobin, to be functional, must maintain the heme iron in the Fe(II) state. Sometimes the iron is oxidized and the resulting hemoglobin (methemoglobin) is incapable of binding oxygen. Erythrocyte CYB5A has been identified as the protein partner that helps maintaining hemoglobin in its reduced state [86, 34]. CYB5A acts as an electron transfer protein that transfers electrons to methemoglobin from nicotinamide adenine dinucleotide (NADH) bound in NADH-CYB5 reductase (CYB5R3) [140]. A medical case also exists where a person with congenital methemoglobinaemia (a disease characterised by increased concentration of methemoglobin) was linked to a deficiency of CYB5A [54].

1.1.2 *In vivo* characterization of CYB5 function

Recently the generation of tissue specific (liver) CYB5A [45] and global CYB5A knockout mice [88, 46] has opened exciting avenues for research into the functional role of CYB5A in areas including liver disease and drug metabolism. Hepatic CYB5A knockout mice displayed diminished capacity to metabolize a series of probe drugs [45] along with an increased expression of CYP450. Global CYB5A knockout mice [88] displayed significant differences in drug metabolism in extra hepatic tissues (lung, intestine, kidney) and male CYB5A knockout mice showed reduced testosterone production. A similar study showed that global CYB5A mice showed differences in lipid composition in skin compared to wild type mice and displayed typical symptoms of methemoglobinemia (Concentration of methemoglobin in blood was greater than 3%)[46]. Conclusions from the knockout mouse experiments confirmed the roles of CYB5A in CYP450 mediated drug metabolism, fatty acid metabolism, testosterone production and methemoglobin reduction *in viv*o [46].

Very little work on CYB5B expression and function has been performed. The earliest study [59]showed an inhibition of NADH-semidehydroascorbic acid reductase activity in liver cells by anti-CYB5B antibodies. Both CYB5A and CYB5B were shown to be involved in modulating the activity of CYP450-17A1 with respect to the production of androgens in the testes [129]. Further experiments [16] also indicate that CYB5B and CYB5A act in different mechanisms thus affecting the action of CYP450-17A1 on different substrates. The authors showed that both CYB5A and CYB5B stimulated the C17,20 lyase activity of CYBP450-17A1 leading to production of a key hormone dehydroepiandrosterone. In the same study, they revealed that overexpression of CYB5A exclusively stimulated CYP450-17A1 catalyzed formation of another hormone, androsterone. Notably, a recent microarray study followed by peptide sequencing identified the over expression of CYB5B in Hodgkin lymphoma when compared to normal bone marrow cells [92].

1.2 Sequence comparison of mammalian CYB5 isoforms

Sequence alignment of the cytosolic region of known examples of mammalian CYB5A and CYB5B, using Clustal W [25] is shown in figure 1.4. Comparison of the sequences of mammalian CYB5A revealed a high percentage of sequence identity (84- 97%) and sequence similarity (93-98%) [4]. This trend is maintained within the CYB5B family. However, when comparing the cytosolic regions of bovine CYB5A and rat

```
         1        11        21        31        41        51        61        71        81
bCYB5A SKAVKYYTLEEIQKHNNSKSTWLILHYKVYDLTKFLEEHPGGEEVLREQAGGDATENFEDVGHSTDARELSKTFIIGELHPDDRSKITKP
rCYB5B DPAVTYYRLEEVAKRNTAEETWMVIHGRVYDITRFLSEHPGGEEVLLEQAGADATESFEDVGHSPDAREMLKQYYIGDVHPNDLKPKDGD
       . **.** ***: *:*.:::.**:::* :***:*:**.********* ****.****.*******.****: * : **::**:* .
```

Figure 1.2: Sequence alignment of the heme binding domains of bovine CYB5A (bCYB5A) and rat CYB5B (rCYB5B). The first crystal structures of mammalian CYB5A and CYB5B were that of bCYB5A and rCYB5B. They form the basis sequences for experiments described in this dissertation. Sequence alignment was performed with Clustal W [25]. Conserved amino acid residues are marked by '*' (identical), ':' (highly conserved) or '.' (weakly conserved). Iron coordinating His residues are underlined and indicated in bold. The numbering system used here is based on the lipase fragment of bMCb5 introduced by Mathews [83].

CYB5B (the basis proteins used here figure1.2), the sequence identity between CYB5A and CYB5B is reduced to 57%.

Based on phylogenetic analysis of the sequences of CYB5A and CYB5B, it was proposed that CYB5A and CYB5B genes arose from a common ancestor, which during the course of evolution duplicated to form independently evolving CYB5A and CYB5B proteins with specific subcellular localizations [53]. The difference in sequence is not reflected in the structures of CYB5A and CYB5B (detailed in the following section) but is the reason for the variation in biophysical and biochemical properties of CYB5A and CYB5B proteins (the basis of this dissertation).

1.3 Structures of CYB5A and CYB5B

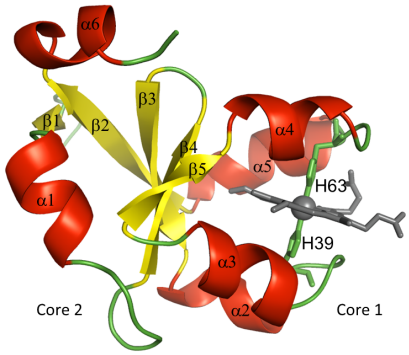

Figure 1.3: Structure of bCYB5A (1CYO) depicted as cartoons. Secondary structure elements α helices are colored red, β strands are colored yellow and loops are colored green. Stick figures of heme are colored gray with the Fe atom modelled as a sphere. His 63 and His 39 (green sticks) are shown co-ordinated to the Fe atom. Based on Matthews' scheme [83], the order of numbering the secondary structural elements is in the order of their appearence in the structure.

Bovine liver microsomal cytochrome b5 (bCYB5A) [140] was the first CYB5 to have its structure elucidated. The original structure, solved by X-ray crystallography, had a resolution of 2.8 Å [84] and was subsequently determined to a higher resolution of 1.5 Å (PDB id 1CYO) [35]. The second CYB5 to have its structure determined by X-ray crystallography was the rat outer mitochondrial CYB5 (rCYB5B) and this was solved to a resolution of 2.7Å (PDB id 1B5M) [118]. A structure with a resolution of 2.0 Å (PDB code 3MUS)

was more recently obtained. A crystal structure of human CYB5B is also available at a resolution of 1.45 Å (PDB code 3NER) [104]. At present no other crystal structures of wild-type mammalian CYB5A or CYB5B proteins exist. However, three dimensional structures determined by nuclear magnetic resonance (NMR) spectroscopy are available for the bovine, rat, rabbit and human isoforms of CYB5A [10, 14, 98, 152]. Throughout this document, bCYB5A and rCYB5B are used as representatives of the CYB5A and CYB5B isoforms respectively.

CYB5 belongs to the $\alpha + \beta$ class of proteins. As shown for Mcb5 (See figure 1.3) the structure consists of two hydrophobic cores separated by a five-stranded β sheet. There are five α helices and a short C-terminal 3_{10} helix (α6). The hydrophobic core 1 includes helices α2- α5, with the heme sandwiched between two helix- turn- helix motifs. Heme iron is ligated by two His residues, the first (His39) is in a loop with the sequence HPGG between helices α2 and α3, and the second (His63) in a loop with the sequence VGHS between helices α4 and α5 [83, 84]. The sequence HPGG is a conserved motif that is seen in all proteins of the mammalian CYB5 superfamily and the sequence VGHS is maintained in all examples of CYB5A and CYB5B. Helices α1 and α6 belong to core 2 of the CYB5A fold. The five stranded β sheet separates the two hydrophobic cores although we consider β5 (residues 51-54) to be part of core 1 because it is located between core 1 helices α3 and α4 [104].

The binding of heme in CYB5 is an example of bis-histidine (bis-His) hexacoordination wherein two histidines coordinate to the iron via the N^{ϵ} atom. After coordination, binding of heme with the protein is predominantly through hydrophobic interactions. Characteristic properties of the heme binding site include the presence of highly aliphatic amino acid side chains (Ala, Leu, Met, Ile, Val) lining the heme binding pocket [108]. Aromatic amino acids such as Tyr, Trp, Phe also commonly interact with the porphyrin ring [68]via T stacking and π stacking interactions with the porphyrin ring [74, 128].

Mammalian CYB5A and CYB5B contain a large number of conserved acidic amino acid residues. These acidic residues (Asp or Glu) are mainly located in the four helix bundle of core 1 (see figure 1.5a). Three conserved residues E44, E48 and D60 whose side chains protrude into the solvent along with one of the heme propionates are proposed to interact with the redox partners of CYB5 [122]. The location of all these acidic side chain groups including the heme propionate is along one side of the protein, thereby creating a negatively charged zone in the protein. These acidic residues play a key role in binding between CYB5 proteins and their redox partners via electrostatic interactions [116, 117]. Molecules like CYP450, methemoglobin, fatty acid desaturases are physiologically relevant partners of CYB5 and model redox acceptors such as cytochrome c are shown to interact *in vitro* with these acidic amino acids [122].

```
CYB5A                1         11        21        31        41        51        61        71        81
Human                DEAVKYYTLE EIQKHNHSKS TWLILHHKVY DLTKFLEEHP GGEEVLREQA GGDATENFED VGHSTDAREM SKTFIIGELH PDDRPKLNKP
Chimpanzee           DEAVKYYTLE EILKHNHSKS TWLILHHKVY DLTKFLEEHP GGEEVLREQA GGDATENFED VGHSTDAREM SKTFIIGELH PDDRPKLNKP
Rhesus Monkey        DEAVKYYTLE EIQKHNHSKS TWLILHHKVY DLTKFLEEHP GGEEVLREQA GGDATENFED VGHSTDAREM SKTYIIGELH PDDRPKLSKP
Marmoset             DEAVKYYTLE EIQKHNHSKS TWLILHHKVY DLTKFLEEHP GGEEVLREQA GGDATENFED VGHSTDAREL SKTYIIGELH PDDRPKLNKP
Rat                  DKDVKYYTLE EIQKHKDSKS TWVILHHKVY DLTKFLEEHP GGEEVLREQA GGDATENFED VGHSTDAREL SKTYIIGELH PDDRSKIAKP
Mouse                DKDVKYYTLE EIQKHKDSKS TWVILHHKVY DLTKFLEEHP GGEEVLREQA GGDATENFED VGHSTDAREL SKTYIIGELH PDDRSKIAKP
Rabbit               DKDVKYYTLE EIKKHNHSKS TWLILHHKVY DLTKFLEEHP GGEEVLREQA GGDATENFED VGHSTDAREL SKTFIIGELH PDDRSKLSKP
Bovine               SKAVKYYTLE EIQKHNNSKS TWLILHYKVY DLTKFLEEHP GGEEVLREQA GGDATENFED VGHSTDAREL SKTFIIGELH PDDRSKITKP
Sheep                SKPVKYYTLE EIQKHNHSKS TWLILHYKVY DLTKFLEEHP GGEEVLREQA GGDATENFED VGHSTDAREL SKTFIIGELH PDDRSKITKP
Pig                  DKAVKYYTLE EIQKHNNSKS TWLILHHKVY DLTKFLEEHP GGEEVLREQA GGDATENFED VGHSTDAREL SKTFIIGELH PDDRSKIAKP
Horse                DKAVKYYTLE EIKKHNHSKS TWLILHHKVY DLTKFLDEHP GGEEVLREQA GGDATENFED IGHSTDAREL SKTFIIGELH PDDRSKIAKP
Dog                  DQTVKYYTLE EIQKHNHSKS TWLILHHKVY DLTKFLEEHP GGEEVLREQA GGDATENFED VGHSTDAREL SKTFIIGELH PDDRAKINKP
Opossum              GEKVKYYTLE EIQKHNHSKS TWLILHHQVY DLTKFLEEHP GGEEVLREQA GGDATENFED VGHSTDAREL SKTYIIGELH PDDRDKIKKP
                     .: ******** ** **:.*** **:***::** ******:*** ********** ********** :********** ***:******* **** *: **

CYB5B                1         11        21        31        41        51        61        71        81
Human                ETSVTYYRLE EVAKRNSLKE LWLVIHGRVY DVTRFLNEHP GGEEVLLEQA GVDASESFED VGHSSDAREM LKQYYIGDIH PSDLKPESGS
Chimpanzee           ETSVTYYRLE EVAKRNSLKE LWLVIHGRVY DVTRFLNEHP GGEEVLLEQA GVDASESFED VGHSSDAREM LKQYYIGDIH PSDLKPESGS
Rhesus Monkey        ETSVTYYRLE EVAKRNSLKE LWLVIHGRVY DVTRFLNEHP GGEEVLLEQA GVDASESFED VGHSSDAREM LKQYYIGDIH PSDLKPENGS
Marmoset             DTSATYYRLE EVAKRNSLKE LWLVIHGRVY DVTRFLNEHP GGEEVLLEQA GVDASESFED VGHSSDAREM LKQYYIGDIH PNDLKPENGS
Orangutan            ETSVTYYRME EVAKRNSLKE LWLVIHGRVY DVTRFLNEHP GGEEVLLEQA GVDASESFED VGHSSDAREM LKQYYIGDIH PSDLKPENGS
Rat                  DPAVTYYRLE EVAKRNTAEE TWMVIHGRVY DITRFLSEHP GGEEVLLEQA GADATESFED VGHSPDAREM LKQYYIGDVH PNDLKPKDGD
Mouse                EPSVTYYRLE EVAKRNSAEE TWMVIHGRVY DITRFLSEHP GGEEVLLEQA GADATESFED VGHSPDAREM LKQYYIGDVH PSDLKPKGDD
Rabbit               ETSVTYYRLE EVAKRNSPKD LWLVIHGRVY DITRFLNEHP GGEEVLLEQA GVDASESFED VGHSSDAREM LKQYYIGDVH PSDLKPGSGR
Bovine               ETSVTYYRLE EVAKRNSPKD IWLVIHGRVY DVSRFLDEHP GGEEVLMEQA GGDATESFED VGHSSDAREM LKQYYIGDVH PNDLKPGGGS
Pig                  ETSVTYYRLE EVAKRNSPKE LWLVIHGRVY DVTRFMNEHP GGEEVLMEQA GRDATESFED VGHSSDAREM LKQYYIGDVH PNDLKSESGK
Horse                ETSVTYYRLE EVAKRNSSKE IWLVIHGRVY DVTRFLNEHP GGEEVLLEQA GADASESFED VGHSSDAREM LKQYYIGDVH PNDLKPEGGG
Dog                  EAAVTYYRLE EVAKRNSLKE IWLVIHGRVY DVTDFLKEHP GGEEVLLEQA GADASESFED VGHSSDAREM LKQYYIGDVH PDDLKPESGS
Opossum              EASVTYYRLE EVAKRNSEKE TWLVIHGRVY DITRFLDEHP GGGEVLMEQA GRDATESFDD VGHSSDAKEM LKQYYVGEVH PSDRKAEGSE
                     :.:******:* ******: :: *:******** *::  *:.*** ** ***:*** * **:***:* ****.**:** *****:*::* *.* *. ..
```

Figure 1.4: Complete sequence alignment of the tryptic fragments of mammalian CYB5A (above) and CYB5B (below) using ClustalW [25]. Conserved amino acid residues are marked by '*' (identical), ':' (highly conserved) or '.' (weakly conserved).

```
          1        11        21        31        41 ↓    ↓  51        ↓61         71         81
bCYB5A SKAVKYYTLEEIQKHNNSKSTWLILHYKVYDLTKFLEEHPGGEEVLREQAGGDATENFEDVGHSTDARELSKTFIIGELHPDDRSKITKP
rCYB5B DPAVTYYRLEEVAKRNTAEETWMVIHGRVYDITRFLSEHPGGEEVLLEQAGADATESFEDVGHSPDAREMLKQYYIGDVHPNDLKPKDGD
       . **.** ***: *:*.::.**:::* :***:*:**.********* ****.****.*******.****: * : **::**:* .
```

(a)

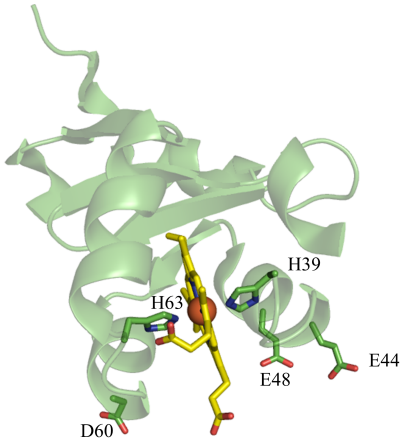

(b)

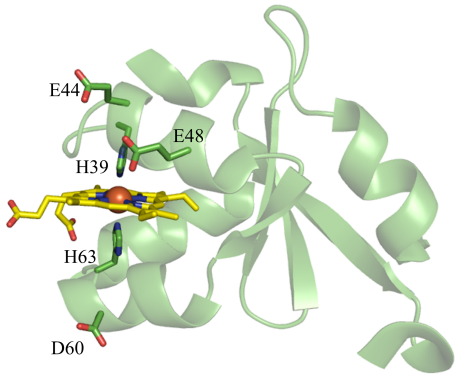

(c)

Figure 1.5: Sequence and structural representation of conserved electrostatic features in CYB5 proteins. (a) Sequence comparison of bCYB5B and rCYB5A, note the particularly high number of acidic residues occuring in the heme binding pocket. Residues lining the heme binding pocket are coloured red, arrow marks indicate the amino acids mentioned in the text. Conserved amino acid residues are marked by '*' (identical), ':' (highly conserved) or '.' (weakly conserved). (b) and (c) Alternate views of the acidic residues along with the heme propionate. The polypeptide is coloured green and the heme is shown in yellow. The iron atom of heme is depicted as a sphere, coordinating His residues (His39 and His63), Glu44, Glu48 and Asp60 are shown as sticks. The protein used here is bCYB5A (PDB code 1CYO).

Given the difference in sequence, atomic structures of CYB5A and CYB5B display remarkable similarity. When structurally aligned (see figure 1.6), the backbone atoms of both proteins display a root mean square deviation (R.M.S.D) of only 0.6 Å. When comparing side chain torsion angles, the difference between the corresponding amino acids in the two isoforms is less than 60°. It can be said that the structural similarity between CYB5A and CYB5B is not limited only to the backbone atoms [71].

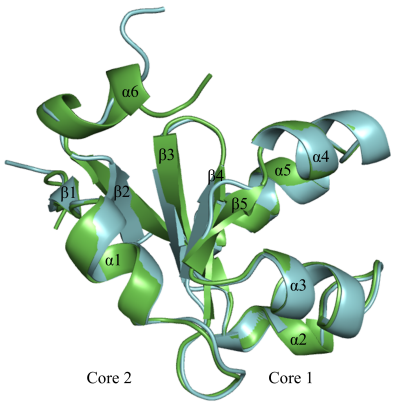

Figure 1.6: Structural alignment of bCYB5A (1CYO) and rCYB5B (3MUS). Alignment of the backbone atoms was performed with Pymol (www.pymol.org) and polypeptides are depicted as cartoons. The structure of bCYB5A is colored green and rCYB5B is colored blue.

1.4 CYB5 without heme: The apoprotein

The CYB5 holoprotein is similar to classic globin proteins in that the final structure (CYB5 fold) is dependent on the binding of the ligand (heme b). One of the earliest studies on apoCYB5 [56] revealed that the apoprotein adopts a structure markedly different from that of the holoprotein. Circular dichroism and ultracentrifugation experiments revealed that apoCYB5 is significantly less compact than the holoprotein, unfolded by lower ethanol concentrations, and showed increased succeptibility to trypsin digestion. Of particular interest in this study was the unaffected signal of Trp (Trp22) when comparing CD spectra of the holoprotein and the apoprotein which suggested the presence of a regular hydrophobic environment around the Trp residue.

Structural characterization of apoCYB5 (see figure 1.7 b) was performed using NMR spectroscopy. The data revealed a stabilized compact hydrophobic core and a highly unstructured component [90]. Further structural refinement of apoCYB5 [40] revealed that the majority of core 1 (heme binding region) was unfolded. The secondary structural elements (all part of core 2), that were found well-formed in the absence of heme were helices $\alpha 1$ and $\alpha 2$, and β strands $\beta 1$- $\beta 4$, all of which define the fold of core 2. Interestingly $\beta 5$, which occurs at the interface of core 1 and core 2, showed a only a very weak interaction with $\beta 4$, indicating that minor and short transitions to the holoprotein fold were occurring at the interface[41]. It is generally accepted now that the core 2 of the apoprotein adopts a similar structure to that of the holoprotein.

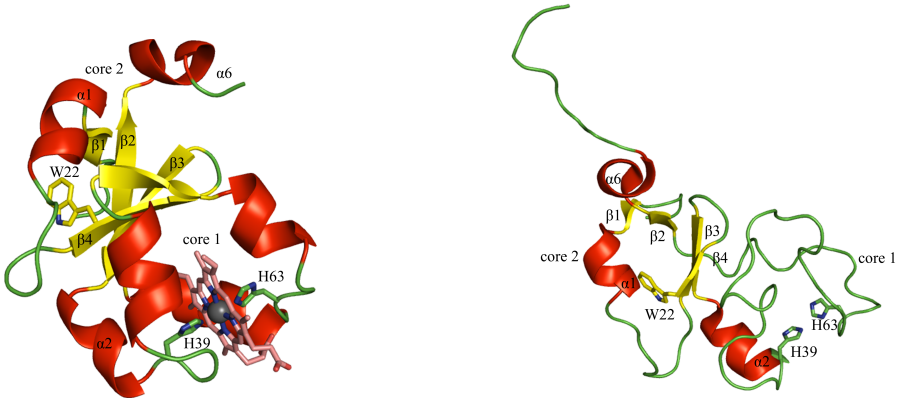

Figure 1.7: Comparison of the environment of Trp22 in the holoprotein and the apoprotein. (a) Structure of bCYB5A (PDB code CYO) depicted in cartoon. (b) Structure of rat apoCYB5A (PDB code 1I8C). Both figures show the overall distribution of secondary structural elements. α helices are colored red, β strands are coloured yellow and loops are coloured green. Iron ligating His residues and Trp 22 are shown as sticks. The heme in figure (b) is colored salmon with the iron atom shown as grey spheres.

1.5 Comparison of biophysical and biochemical properties of CYB5A and CYB5B

CYB5A and CYB5B function as redox proteins. The protein is capable of accepting or donating one electron at a time when participating in a redox coupled reaction. Electrochemical studies[113] have revealed that rCYB5B has a redox potential (-102 mV vs Standard hydrogen Electrode (SHE)) significantly more negative than that of bCYB5A (+ 0.8 mV vs SHE) [141]. Amino acid sequence comparison (vide supra) also shows that the distribution of charged amino acids around the heme binding pocket is similar in CYB5A and CYB5B which suggests that electrostatic contribution to the redox potential should also be similar in the two isoforms. The difference in the redox potential in spite of similar structure is an area investigated in this thesis.

The thermodynamic stability of the holoprotein can be considered to be a combination of two factors: (a) free energy of folding of the apo-protein and (b) free energy of binding of the heme by the apoprotein. Direct comparison of heme binding (by Isothermal titration calorimetry) is very difficult given that heme is insoluble, forms aggregates in aqueous solution and forms non specific interactions by binding to exposed hydrophobic regions of the apo-protein. Heme binding strengths are instead estimated by kinetic studies such as heme transfer experiments with a heme acceptor like apo-myoglobin [27]. Another method of evaluating relative heme binding strengths is by 1-D NMR spectroscopy, the details of which are in chapter 3.

Thermal and chemical chemical dentaturation studies comparing rCYB5B and bCYB5A revealed that rCYB5B was considerably more stable [125]. The heme binding strength of the isoforms was also different, with rCYB5B having a lower rate of heme dissociation that bCYB5A. However when comparing the apoproteins, it was seen that both rCYB5B and bCYB5A had similar stability at physiologically relevant temperatures ($\triangle G_{\text{native} \rightarrow \text{unfolded}} \approx 2$ kcal/mol at 25 °C) [29]. This is evidence that heme binding differ-

entially stabilizes the isoforms and the overall stability of the protein is a function of heme binding and apoprotein stability.

Initial studies [27], on understanding the stability difference, focused on the systematic incorporation of bCYB5A residues into rCYB5B following a careful comparison of sequence and structure. A hydrophobic patch (described in detail in Chapter 3) was identified as the stabilizing component in rCYB5B and when replaced with residues of bCYB5A, the rCYB5B mutants showed less thermal stability and a faster rate of heme dissociation. The key residue in this hydrophobic patch was the residue at position 71 (Ser in all known examples of CYB5A and Leu in all known examples of CYB5B). The hydrophobic patch and the associated network of interactions was disrupted in rCYB5B when Leu71 replaced by Ser and this accelerated heme dissociation and decreased thermal stability of both the holoprotein and the apoprotein.

Molecular dynamics (MD) simulations, at the nano second time scale, have also been performed to understand microscopic motions involved in modulating the biophysical and biochemical behaviour of CYB5 proteins [131, 71, 24]. The first study [131] was performed on bCYB5A and was 2.9 ns in length. The study showed the formation of a cleft that resulted in increased solvent exposure of the hydrophobic patch and the residues lining the heme binding core. The authors proposed that the biological implication of the cleft opening was the increased hydrophobic interactions between CYB5 and its protein partners that would facilitate electron transfer. MD simulations performed on bCYB5A and rCYB5B in our group [71] also reproduced the cleft opening event first described by Storch and Daggett [131]. The cleft opening event in bCYB5A was subsequently implicated to crystal contact effects and an extended simulation (8.5 ns) of bCYB5A and rCYB5B [24] showed the absence of the cleft formation in both proteins at the nano second time scale. In fact, the MD simulations of bCYB5A and rCYB5A showed little difference in dynamic behavior [24]. The authors concluded that the CYB5 protein fold was extremely resistant to mutations but differed in subtle dynamic behaviour that could explain the biophysical and biochemical differences in the two isoforms. However hydrogen-deuterium exhange experiments (H-D X) monitored by NMR spectroscopy [127] revealed distinct differences in the polypeptide dynamics when comparing bCYB5A and rCYB5B.

The research described in this dissertation represents an attempt to understand the evolutionary divergence in CYB5 proteins with respect to their biophysical and biochemical properties using both experimental and theoretical methods. In chapter 3, the ability of the CYB5 fold to accommodate mutations is investigated by comparing X-ray crystal structures and MD simulations of hCYB5B, rCYB5B and bCYB5A. In chapter 4, mutations are systematically introduced into bCYB5A (using bCYB5A as the model) in an attempt to replicate the heme environment of rCYB5B (a model of CYB5B proteins). This chapter also looks at individual contributions of heme binding and apoprotein stability that are responsible for overall stability of the protein. Finally, chapter 5 compares the difference in redox potential between CYB5A and CYB5B isoforms using redox potentiometric measurements and MD simulations. Understanding of the redox potential difference is clarified through investigations with the core 1 motif swap mutants described in Chapter 4.

Chapter 2: Materials and methods

2.1 Protein expression and purification

Details of all proteins and their nomenclature are provided in the appropriate chapters. Gene expression and protein purification systems for rat CYB5B (rCYB5B) [6], bovine CYB5A (bCYB5B) [6], human CYB5A (hCYB5A) [33], human CYB5B (hCYB5B) [7], the S71L mutant of bCYB5A (McS71L) [135] and the L32I/S71L double mutant of bCYB5A (Mc2m) [135] have been previously reported. The genes encoding McS71L and Mc2m were generated by Dr. Na Sun in our laboratory, as were those for two unreported mutants of bCYB5A that are used in the present work: the L23M/L25I/L32I/S70L quadruple mutant (Mc4m) and the S18A/L23M/L25I/L32I/R47L/S70L sextuple mutant (Mc6m). Starting from the previously reported pET11a plasmid harboring the gene for Mc2m, the QuikChange® site-directed mutagenesis kit (Agilent technologies, Santa Clara, CA) was used to construct Mc4m in one step. The QuikChange® site-directed mutagenesis kit was also used to generate the Mc6m mutant in two steps. The recombinant constructs were transformed into *E. coli* XL1 blue competent cells for amplification.

The gene coding for hybb5, a dodecamer amino acid mutant of bCYB5A (see Chapter 3 for a full list of mutations), was purchased from Genscript Inc (Piscataway, NJ, USA), and was initially set in a pUC57 plasmid. Sub cloning into the plasmid, pET11a with restriction sites created by NdeI and BamHI, was performed using the polymerase chain reaction (PCR) and suitably designed primers. Prior to transformation in expression hosts, the plasmids were checked for correct coding sequence at the DNA sequencing center, University of Kansas Medical Center. The recombinant plasmids carrying the genes were transformed into *E.coli* BL21 (DE3) cells for protein expression. An overnight seed culture (1% volume, incubated at 37º C, with 200 rpm agitation) was used to inoculate 1 liter of Luria Bertani broth containing ampicillin (100 mg/L). The growth of bacteria was carried out at 37° C, with 200 rpm agitation till $OD_{600} \approx 0.8$. The bacterial cultures were induced with isopropyl β-D-1- thiogalactopyranoside (0.5 - 1.0 mM) and further incubated for 7 hours at 25° C, with 150 rpm agitation. All subsequent steps were performed at 4° C unless specifically mentioned. The bacterial suspension was centrifuged at 6000 rpm for 20 minutes using an Avanti J-E® centrifuge and the cell pellet was frozen and stored at -80° C overnight.

The frozen pellet was thawed and resuspended in 20 mM Tris buffer, pH 7.0 (3 mL/g of cell pellet). Phenylmethylsulfonyl fluoride (PMSF) dissolved in ethanol was added to a final concentration of 50 μM. The cells were lysed by sonication and the cell lysate was centrifuged at 20,000 rpm for 60 minutes. The supernatant contained holoprotein as indicated by the red color, but also contained significant levels of apoprotein. It was therefore subjected to heme reconstitution at room temperature. The amount of heme needed was determined as follows. A sample of the cell lysate and a hemin stock solution in DMSO (5 mg/mL) were diluted 10 fold. The diluted hemin solution was titrated slowly (in 10 μL volumes) to the diluted cell lysate under constant stirring and wavelength scans were recorded from 350 - 700 nm using a Cary Bio 100 UV- visible spectrophotometer (Varian Inc, Lexington, MA, USA). Wavelength scans were continued until A_{412} (Soret band λ_{max}) reached a maximum. Using these data we determined the appropriate volume of the heme stock solution needed to be added to the undiluted cell lysate. This was added in small aliquots with vigorous stirring. The reconstituted cell lysate was then centrifuged at 20,000 rpm for

2.5 hours. The supernatant was filtered to remove heme particulates using a 0.22μm filter (Millipore Inc, Billerica, MA, USA) before FPLC purification.

All purification procedures were performed using an ÄKTApurifier ™, and all chromatography resins and columns were purchased from GE Healthcare (Piscataway, NJ, USA). The reconstituted cell lysate was loaded onto a Q-sepharose anion exchange column and eluted using a gradient of 0- 1.0 M NaCl in 20 mM Tris buffer, pH 7.0. Red fractions containing the holoprotein were pooled and subjected to a second round of purification, to remove apoprotein, using a Phenyl Sepharose™ hydrophobic interaction column with a reverse gradient of 1.0- 0.0 M NaCl in the above mentioned buffer. The fractions containing protein were concentrated, using an Amicon ® Ultra Centrifugal filter unit (Millipore Inc) to a final voume of 1.0 ml and subjected to size exclusion chromatograhy using a Superdex™ 200 column. Purity was confirmed by the presence of a single protein band in native gel electrophoresis. The protein was also analyzed by electro-spray ionization mass spectrometry (ESI-MS; KU mass spectrometry laboratory) to confirm the expected molecular weight of the proteins. Concentrations of the holoprotein were estimated using the absorbance at the Soret band (λ_{max} = 412 nm, ε_{max} = 130000 M^{-1} cm^{-1}). Protein yields were typically 20 - 25 mg/L of bacterial culture.

2.2 X-ray crystal structures of the proteins

Concentrated solutions of protein (typically 25- 30 mg/ml in 20 mM Tris-HCl, pH7.0) were crystallized by the hanging drop vapour diffusion method. Detailed methods of crystallization including conditions and solution methods for each specific protein are described below. Data collection and refinement statistics are provided in Table 2.1 and Table 2.2 respectively. The structures of hCYB5B, rCYB5B and hybb5 were determined by Dr. Simon Terzyan at the Oklahoma Medical Research Foundation. The McS71L structure and a new structure of rCYB5B was solved by Dr. Scott Lovell at the KU Protein Structure Facility. The structure solution of rCYB5B (herein called rCYB5Bnew) was repeated in order to correct data processing errors in the published structure of rCYB5B (PDB code 3MUS) [104].

2.2.1 Crystallization and structure solution of hCYB5B

Hanging drop solutions of hCYB5B were made by mixing equal volumes of protein and a reservoir solution composed of 30% PEG8K, 0.1M HEPES buffer (pH 6.8) and 0.2 M magnesium acetate. Equilibration at 5°C was done against the reservoir solution. The crystals were first equilibrated in a reservoir solution of similar composition but containing 36% PEG8K before crycooling at 100 K using a gas stream of nitrogen. Data collection was performed at the Cornell High Energy Synchrotron Source (CHESS) F1 station (Cornell University, Ithaca, NY). The X- ray source was tuned to 0.976 Å, and data were collected at 1.45 Å using an ADSC Quantum 4 CCD detector. A crystal-detector distance of 125 mm and an exposure time of 60 s were used to collect high resolution data sets. For low resolution data sets, a crystal-detector distance of 200 mm and an exposure time of 20 s were used. The program suite HKL2000 [101] was used to process all the data. The crystal was found to belong to the space group $P2_1$ and contained two molecules of hCYB5B per asymmetric unit.

	hCYB5B	rCYB5B	rCYB5Bnew	hybb5	McS71L
Space group	$P2_1$	$P2_12_12_1$	$P2_12_12_1$	C2	$P2_1$
Unit cell parameters	a = 37.32 Å b = 40.03 Å c = 58.74 Å β = 98.61°	a = 46.26 Å b = 71.13 Å c = 72.80 Å	a = 38.61 Å b = 67.85 Å c = 70.34 Å	a =110.67 Å b = 30.65 Å c = 23.55 Å β = 95.65°	a = 43.53 Å b = 92.71 Å c = 48.99 Å β = 113.11°
Resolution (Å)	30-1.45(1.5-1.45)†	10.3-1.98	70.34-1.25 (1.32-1.25)†	27.5-1.7	92.71-2.4
R_{merge}(%)	5.7(45.3)†	6.3	6.6 (75.7)†	5(15.2)†	12.8(78.5)†
# Reflections	29891(2709)†	14715(741)†	49,228 (2,643)†	8707(848)†	51974(15234)†
Completeness (%)	97.6(89.3)†	87(60.8)†	100 (100)†	98.4(95.3)†	99.2(99.5)†
Redundancy	3.1(2.4)†	–	6.4 (6.2)†	4	3.4(3.5)†

Table 2.1: Data collection statistics for the crystal structures. †Numbers in parenthesis are for the highest resolution shell. ‡The structure of rCYB5B was repeated to correct previous errors (see text)

	hCYB5B	rCYB5B	rCYB5Bnew	hybb5	McS71L
Reflections (working)	14452	13089	49,228	7435	14452
Reflections (free)	1131	1507	2,643	898	761
$R_{working}$ (%)	17.7	17.89	13.7	17.6	20.1
R_{free} (%)	21.5	22.3	15.2	22.9	24.4
# Non hydrogen atoms					
Protein	1448	1380	1352	666	2593
Heme	86	86	172	43	172
Solvent	296	133	233	142	39
R.M.S deviation					
Bond length (Å)	0.019	0.017	0.011	0.018	0.010
Bond angle (°)	1.7	1.22	1.328	1.77	1.10
Average B factor					
Protein	18.83	28.7	14.7	15.43	42.3
Solvent	34.3	45.4	26.7	30.2	38.5

Table 2.2: Refinement statistics of the crystal structures

Molecular replacement, with AMoRe [95], was used to determine the orientation and position of the molecules in the unit cell using the heme free model of the quintuple mutant of rCYB5B (PDB ID 1LJ0)[27]. The CNS program suite [20] was used to perform several cycles of initial refinement. One cycle of simulated

annealing using the slowcool protocol from 5000 K was performed along with several cycles of positional and isotropic individual temperature factor refinement. The final model was generated using the graphics program TURBO-FRODO (http://www.afmb.univ-mrs.fr/-TURBO-) using $2|F_o|$ - $|F_c|$ difference Fourier maps. Water molecules were added to the structure using the water-pick program of CNS. The refined structure from CNS was subjected to further refinement using REFMAC [93] with the complete data set and individual temperature factors. The final coordinates for hCYB5B (1.45 Å) have been deposited in the Protein Data Bank (PDB) with PDB code 3NER [104].

2.2.2 Crystallization and structure solution of rCYB5B (PDB code 3MUS)

Crystallization of rCYB5B utilized conditions identical to those described above for hCYB5B. Room temperature data collection was performed on a four-circle Siemens diffractometer equipped with a multi wire area detector. The crystallography programs SAIDE and SAINT (http://www.xray.utmb.edu/saint.html) were used to index, integrate and scale the crystallographic reflections. The crystal structure was redetermined by molecular replacement and initially refined using the program TNT [138]. Final refinement was performed using the CNS suite. The programs COOT [37]and TURBO-FRODO were used for model building. The final cooordinates for rCYB5B (1.98 Å) have been deposited in the PDB code 3MUS [104]. Unfortunately, only 60% of data were used for the highest resolution shell in solving the structure while typical protein crystal structures of similar resolution use 90% of the data in the highest resolution shell. Given this problem, a new crystallization setup of rCYB5B was performed at the Protein Structure laboratory, University of Kansas (PSL- KU) and the structure was solved by Dr.Scott Lovell.

2.2.3 Crystallization and structure solution of hybb5

Thin plate crystals of hybb5 were formed in hanging drops of equal volumes of protein and reservoir buffer (27%PEG8K, 0.2M Mg Acetate, PIPES pH 7.0) that was equilibrated at 5°C. Data were collected on a Mar345 image plate mounted on Rigaku RU-H3R generator equipped with Osmic blue optics. The refinement and models of the final structure were generated using methods identical to those described above for hCYB5B. Coordinates of the final structure (1.7 Å) have been deposited with PDB code 3OZZ.

2.2.4 Crystallization and structure solution of McS71L

The S71L mutant of bCYB5A (McS71L) was screened for crystallization by the sitting drop vapour diffusion technique using Compact jr crystal screen plates (Emerald Biosystems, Bainbridge Island, WA, USA). Needle-like crystals were obtained within 24 hours from 20% (w/v) PEG 8K, 100 mM Tris pH 8.5, 200 mM $MgCl_2$ but did not display any diffraction when subjected to an in-house X-ray source. The initial conditions were further refined using the Additive HT screen (Hampton Research, Aliso Viejo, CA). Plate shaped crystals were obtained from 20% (w/v) PEG 8K, 100 mM Tris-HCl pH 8.5, 200 mM $MgCl_2$ 10 mM $CuCl_2$.

The crystals of McS71L were subjected to diffraction at the Advance Photon Source (APS, Argonne National Laboratory, Argonne, IL) IMCA-CAT beamline 17ID using a Decris pilatus 6M pixel array detector.

The intensities of the reflections were integrated and scaled using XDS [62] and Scala [39]. The program Pointless [39] was used to check the Laue class which indicated that the space group was $P2_1$. A previously determined structure of bCYB5A (PDB code 1EHB) was used to solve the structure using the molecular replacement method. The molecules were located by MOLREP [139] and initially refined with the program REFMAC [93]. Further refinement of the structure was done with the program BUSTER [17] and the model was built manually by COOT. The final structure (2.4 Å) was validated using the program MOLPROBITY [77].

2.2.5 Crystallization and structure solution of rCYB5Bnew

Purified rCYB5B was concentrated to 25 mg/mL in 20 mM Tris-HCl pH 7.0, and screened for crystallization (Compact Jr. (Emerald Biosystems)) sitting drop vapor diffusion plates at 20 ºC using 0.5μL of protein and 0.5μL of crystallization solution equilibrated against 100μL of the latter. Small prismatic crystals (Figure 1) were obtained in approximately 3 days from the Crystal Screen HT (Hampton Research) condition C4 (30% (w/v) PEG 8000, 100 sodium cacodylate pH 6.5, 200 mM sodium acetate). Crystals were transferred to a fresh drop of composed of 80% crystallization solution and 20% PEG400 before flash freezing in liquid nitrogen for data collection. Data were collected at the Advanced Photon Source beamline 17-ID using a Dectris Pilatus 6M pixel array detector.

Intensities were integrated and scaled using XDS [62] and Scala [39] respectively. Structure solution was conducted by molecular replacement with MOLREP [139] using an isomorphous structure, PDB code 3MUS, as the search model. Following initial refinement with Phenix [2], difference electron density (Fo-Fc) greater than 3σ was observed near the heme molecule methyl groups which indicated that the heme molecule adopts two orientations. Therefore, the heme molecules were modeled in two orientations. Refinement with anisotropic atomic displacement parameters was conducted with Phenix and manual model building with COOT [37]. Structure validation was conducted with MOLPROBITY [77].

The structure of rCYB5B (PDB code 3MUS) and rCYB5Bnew have very low RMSD (RMSD = 0.4 Å) when structurally aligned with one another (see figures 2.1a and 2.1b) . In addition when only atoms of the backbone (C_α , C, N and O) are considered, the RMSD is reduced to 0.3 Å. This gives us confidence in the usage of the rCYB5B structure for the interpretation of data in chapter 3 and chapter 4. In addition the availability of the new rCYB5B structure (rCYB5Bnew) provides credence to the data presented in chapter 5.

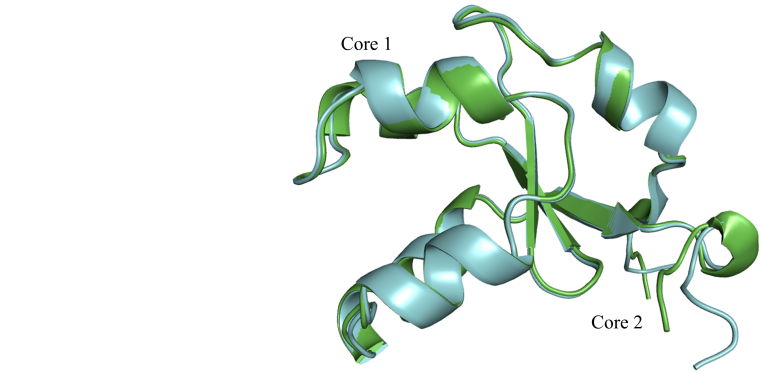

(a)

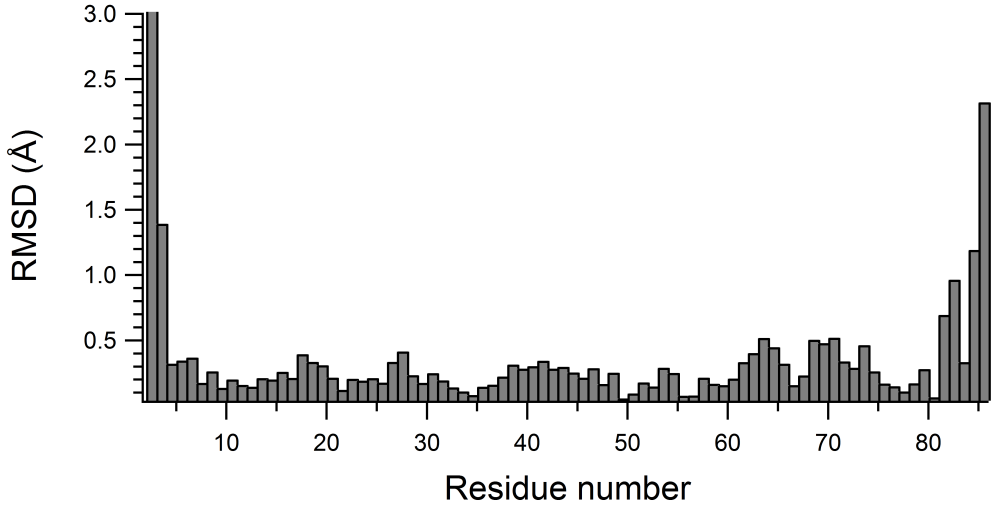

(b)

Figure 2.1: Structural alignment of rCYB5B structures. (a) The backbone atoms (residues 4-84) corresponding to the structures of rCYB5B (PDB code 3MUS) and rCYB5Bnew are aligned. The proteins are represented in cartoon form, with rCYB5B (3MUS) colored blue and rCYB5Bnew colored green. (b) C_α RMSD plot comparing rCYB5B (3MUS) and rCYB5Bnew

2.3 Holoprotein thermal denaturation

Heat denaturation experiments of holoproteins were performed using a Cary Bio 100 UV- visible spectrophotometer (Varian Inc, Lexington, MA, USA) outfitted with a Peltier-thermostated multiple cell holder and a dedicated temperature monitor probe ($\pm$ 0.1° C). Proteins, at a concentration of 3- 5 µM, were buffered using 50 mM sodium phosphate at pH 7.0. The temperature was increased in increments of 1 °C, and absorbance values were recorded once equilibration had been achieved. For ferric holoprotein thermal denaturation experiments, a standard 1 ml quartz cuvette with a 1 cm path length was used. The cuvette was equipped with a tight fitting polytetrafluoroethylene (PTFE) cap to prevent evaporation of the solvent.

Ferrous holoprotein thermal denaturation experiments were conducted using a modified 3 ml quartz cuvette, 1 cm path length, with an opening sealed by a rubber septum. Prior to each experiment, a stream of N_2 gas was bubbled through the buffer solution for 30 minutes to displace oxygen dissolved in the buffer.

Sodium dithionite was added separately to degassed buffer in a 5 mL conical flask to give a final concentration of 0.1 mM. The flask was fitted with a septum, and the solution was further degassed, using the N_2 stream, to displace any adventitious nitrogen. Ferric proteins were reduced to the ferrous state by adding an aliquot of degassed aqueous sodium dithionite solution (0.1 mM) in buffer. All experiments with the ferrous protein were performed under a positive pressure atmosphere of N_2 gas. Protein denaturation was monitored using the absorbance at 412 nm for the ferric proteins and 422 nm for the ferrous proteins.

The data were fit, using the program Igor Pro (ver 4.03, WaveMetrics Inc, OR), to an equation describing a two state denaturation process (equations were provided to us by Prof. Juliette Lecomte, Johns Hopkins University, MD) [26] which corrects for baselines having non-zero slopes, to obtain the thermal denaturation midpoint (Tm) values. Holoprotein thermal denaturation reactions were only partially reversible, and therefore no attempt was made to extract any thermodynamic information from the data.

2.4 Molecular Dynamics simulations

Ten nanosecond molecular dynamics (MD) simulations were performed on the proteins using the CHARMM program (ver. 33a1, [19]). All atom topology and parameter sets (ver. 22) along with dihedral cross term corrections (CMAP) were used in all calculations [81]. X-ray crystal structures of the proteins were used as the starting structures for the MD simulations. Missing hydrogen atoms were added to complete all atom models using the HBUILD module of CHARMM [21]. The proteins were then subjected to a gradual energy minimization in vacuum to prevent any atomic clashes. Energy minimized proteins were neutralized by the addition of Na^+ and Cl^- counter ions to an ionic strength of 0.15 M. Counter ions were added using the Solvator module in CHARMM-GUI [61]. The entire system (protein +counter ions) was immersed in a truncated octahedral water cell, built by cutting off corners from a cube of edge length 70 Å. Water molecules overlapping the protein and counter ions were removed yielding the final simulation systems (see Table 2.3for proteins used in simulations and setup details). Water molecules combined with the counter ions were subjected to an initial equilibration of 0.1 ns in the presence of a fixed solute. A final equilibration of 0.1 ns was performed on the whole system before the trajectory production stage.

	PDB code	Protein atoms	Solvent atoms	Counter ions (Na^+ + Cl^-)
bCYB5A	1CYO	1377	15448	20 + 11
rCYB5B	3MUS	1436	15354	22 + 10
hCYB5B	3NER	1422	15572	21 + 11
McS71L	–	1385	15406	20 + 11
hybb5	3OZZ	1373	15502	20 + 11

Table 2.3: Final MD system before equilibration

Equilibration and MD simulations were performed at a constant temperature (300 K) and pressure (1 atm). The Hoover thermostat method [3] was used to maintain constant temperature and the Langevin piston method [43] was used to maintain constant temperature. The IMAGE facility in CHARMM was used

to generate periodic boundary conditions and to solvate the system. The particle- mesh Ewald method [38] was used to expand long-range forces in the calculation of electrostatic interactions. The Ewald parameter, κ, was set to 0.34 $Å^{-1}$, the grid spacing parameter L was set to 64 and the cutoff distance was set to 12 Å. Bonds involving hydrogen atoms in the system were kept fixed using the SHAKE algorithm [119]. A 2-fs time step was used in association with the Leapfrog integrator [3]. At every 250 steps (0.5 ps), coordinates were saved yielding a total of 20,000 coordinate frames for subsequent analysis.

Before analysis of the trajectories, the solute was centered in the solvent box and a rigid body rotation was applied to the protein backbone atoms. This enabled the investigation of internal protein structure fluctuations by removing overall rotational and translational motions. Solvent accessible surface area of the CYB5Bs was calculated using Lee and Richards's algorithm [70]with a probe radius of 1.6 Å. Trajectories were visualized using the molecular graphics packages VMD [55] and PyMOL (The PyMOL Molecular Graphics System, Version 1.3, Schrödinger, LLC).

2.5 ^{1}H Nuclear Magnetic Resonance (NMR) spectroscopy

^{1}H NMR spectra were recorded for the proteins at 25 °C using a Bruker- Avance (Bruker Biospin Corp, Billerica MA) spectrometer functioning at 500.13 MHz ^{1}H NMR frequency. The purified protein solution (in 20 mM Tris buffer pH 7.2) was exchanged into deuterated potassium phosphate buffer (μ = 0.1 M and pD =7.0, not corrected for isotope effects) using an Amicon ® Ultra Centrifugal filter unit (Millipore Inc) that had a molecular weight cutoff of 3000 daltons. It was concentrated to a final concentration of 1.5- 2.0 mM and a volume of 600 μL. Spectra were acquired with water presaturation , 16 K data points, 0.3 sec relaxation delay and 1024 scans over a 60 ppm spectral width. Resonances of some heme substituents were assigned on the basis of previously published data [7, 112, 115].

2.6 Redox potentiometry experiments

Redox potentiometry experiments were conducted on the proteins using a modification of a previously described protocol [36]. The redox cell consisted of a 5 mL beaker with a stir bar and a calomel/platinum electrode (241 mV versus the Standard Hydrogen Electrode (SHE), Radiometer Analytical, France) connected to a pH meter operating in voltage mode. Absorption spectra were recorded using a USB 2000 fiber optic spectrophotometer outfitted with a dip probe (Ocean Optics, Dunedin, FL). The entire setup was housed under a nitrogen-hydrogen atmosphere in a glove box (Coy Laboratories, Grass Lake, MI). All experiments were conducted in 50 mM sodium phosphate buffer, pH 7.0 [μ = 0.019 M] with the protein concentration at 10 μM and the redox mediator concentrations at 1 μM each. For reductive and oxidative titrations, appropriate volumes of a sodium dithionite stock solution (4 mM) or a potassium ferricyanide stock solution (1 mM), respectively, were added using a Hamilton microsyringe. Changes in oxidation state of the heme were monitored using the α band at 557 nm (for heme holoproteins) or 547 nm (for mesoheme holoproteins), and the voltage was recorded after equilibrium had been achieved (typically 15 minutes). Data were corrected for deviation by subtracting the absorbance at the isosbestic wavelength and were fit to a one-electron Nernst equation using Igor Pro (ver 4.03, WaveMetrics Inc, OR). The redox mediators

used, with their standard potentials against SHE, were: methyl viologen (-430 mV), benzyl viologen (-311 mV), anthraquinone-2-sulfonic acid (-225 mV), anthraquinone-2,6-disulfonic acid Sodium salt (-184 mV), 2-hydroxy-1,4-naphthoquinone (-152 mV), 2,5 dihydroxy-1,4-benzoquinone (-60 mV), 5,8-dihydroxy-1,4-naphthoquinone (-50 mV), pyocyanin (-34 mV), duroquinone (+5 mV), 5- hydroxyl-1,4-naphthoquinone (+33 mV), 1,4-naphthoquinone (+50 mV), phenazine methosulfate (+80 mV), 2,6-dimethylbenzoquinone (+115 mV), 1,2-naphthoquinone (+157 mV), 2-methyl-1,4-benzoquinone (+175 mV), 1,2-naphthoquinone-4- sulfonic acid (+210 mV). The electrode was calibrated with a suspension of Quinhydrone in potassium phosphate buffer pH 7.0.

2.7 Apoprotein experiments

2.7.1 Apoprotein preparation

The heme bound to the holoproteins was removed by a modification of the Teale acid-ketone extraction method [12] with all operations performed at 4 °C. The holoprotein solution (10 μM in 20 mM Tris pH 7.0), in a 50 mL centrifuge tube submerged in an ice/water slurry, was reduced in pH to 2.0 using 0.1 N HCl. Cold ethyl methyl ketone (2-butanone) was added to the tube immediately, the tube was vigourously agitated and then left to stand for 10-15 mins. After an adequate period of separation, the organic layer (top layer with heme) was removed and the butanone wash was repeated twice. After the final butanone extraction step, the aqueous phase (contains dissolved apoprotein) was transferred to a Slide-A-Lyzer® (Thermo Fisher Scientific Inc, Rockford IL) 3.5 KDa Molecular weight cutoff dialysis cassette. Four dialysis steps, each for a duration of 4 hours, were performed in 4 L of 20 mM potassium phosphate buffer, pH 7.0, stored overnight in the cold room (4 °C). The apoprotein solution was then concentrated and buffer exchanged into 50 mM Sodium- Potassium phosphate buffer (Potassium phosphate solution buffered to pH 7.0 with sodium hydroxide) using an AmiconUltra centifugal filter unit (15 mL volume with a molecular weight cutoff of 3 kDa). The apoproteins were used within 48 hours of preparation in all experiments.

2.7.2 Circular Dichroism spectroscopy

Circular dichroism (CD) spectra were recorded using on a Jasco J-810 (Jasco Inc, Easton, MD) spec- tropolarimeter equipped with a Peltier thermoelectric type temperature control system. Spectra were acquired at 1.0 nm intervals with a scan rate of 1 nm/sec, a response time of 4 seconds, and represent the average of five scans. Apoprotein concentrations were 15- 20 μM in 50 mM sodium-potassium phosphate buffer pH 7.0. A cuvette of 1 mm path length was used for far-UV experiments (190-260 nm). Background correction was accomplished by subtraction of a spectrum recorded at the same temperature and containing only buffer.

2.7.3 Apoprotein thermal denaturation

Apoprotein thermal denaturation was monitored using CD spectroscopy. To test for isodichroic behavior during apoprotein unfolding, far-UV CD spectra were recorded at 5° C intervals between 25 °C and 75 °C. Increments of 3 °C were used in the thermal denaturation experiments, for which the mean residue ellipticity at 222 nm (θ_{222}) over a 5 minute period was recorded and averaged. An identical set of measurements

was performed using a blank sample, and subtracted to correct for background changes. Samples were equilibrated for 5 minutes at each temperature prior to recording data. Normalized data were fit to a two-state equation described by Constans et al [26] using Igor Pro (ver 4.03, WaveMetrics Inc, OR).

2.7.4 Differential Scanning Calorimetry (DSC)

DSC experiments were performed on the apoproteins using a VP-DSC microcalorimeter (Microcal Inc, Piscataway, NJ) using a sample containing 1- 2 mg/ml of apo-protein in 50 mM sodium-potassium phosphate buffer pH 7.0. Before each experiment, the protein sample and the buffers were degassed at 25 mm Hg vacuum for 15 minutes. Initial baselines were made using repeated scans in which the sample chamber also contained buffer. Protein- buffer and buffer-buffer 'upscans' (low temperature to high temperature) were all performed at a scan rate of 1° C/min. A statistical mechanics based deconvolution module as implemented in the Origin® v7.0 suite of programs (OriginLab Corp, Northampton, MA) was used to calculate thermodynamic parameters.

Chapter 3: Divergence within a given isoform of CYB5: structural and molecular dynamics studies of human CYB5B and rat CYB5B

3.1 Introduction

Mammalian cytochrome b_5 (CYB5) is an important heme binding protein that is membrane anchored to specific organelles in the cell. The divergence of two genes gave rise to separate isoforms of CYB5 which are named based on their subcellular localization. One isoform, present in the endoplasmic reticulum membrane, is known as microsomal cytochrome b_5 and is now named as type A cytochrome b_5 (CYB5A). The other isoform is localized at the outer mitochondrial membrane, is known as the outer mitochondrial cytochrome b_5 and is named as type B cytochrome b_5 (CYB5B) [69, 66]. CYB5As participate in a number of electron transfer reactions with protein partners such as cytochrome P450 and fatty acid desaturases. The biological role of CYB5B has been shown, especially in modulating CYP450 activity [16, 129, 122] and a recent study has discovered overexpression of CYB5B in malignant lymphoma cells [92].

CYB5s are composed of two domains, a cytoplasmic N-terminal domain also called the heme binding domain and a hydrophobic C-terminal domain also called the membrane anchoring domain. The hydrophilic heme binding domain folds independently and has spectroscopic properties that are identical to that of the full length protein [133]. Structural studies have focused mainly on N-terminal fragments owing to their greater solubility. Commonly reported N-terminal fragments arise from enzymatic treatment of the full length protein by trypsin or lipase[130]. The lipase fragment was generated due to a nonspecific cleavage following lipase treatment when attempting to free full length CYB5A from the microsomal membrane. Reported X-ray structures of wild type mammalian proteins, to date, exist only for the bovine CYB5A (bCYB5A) (both tryptic and lipase fragment) [35, 147] and rat CYB5B (rCYB5B) [118]. The crystal structure of rCYB5B is of lower resolution (2.7 Å) when compared to the resolution of the crystal structures of bCYB5A (lipase fragment = 1.5 Å, tryptic fragment = 1.9 Å). The amino acid numbering scheme adopted for this work has been based on the system developed for the bCYB5A lipase fragment [84] and is illustrated in Figure 3.1.

The CYB5 fold can be considered to contain two distinct hydrophobic cores that are separated by a five stranded β sheet [140] (see Figure 3.1). Core 1 contains the heme molecule with the Fe atom co-ordinated to two histidine residues contained in helix-loop-helix motifs. The first helix-loop-helix motif is composed of helices $\alpha 2$ and $\alpha 3$ separated by a conserved loop bearing the sequence HPGG. The second helix-loop-helix motif is composed of secondary structural elements $\alpha 4$, $\alpha 5$ and a loop with the sequence VGHS. Helices $\alpha 1$ and $\alpha 6$ (a C-terminal 3_{10}-helix) make up core 2. Residues 51-54, which reside between helices $\alpha 3$ and $\alpha 4$, make up $\beta 5$, which we consider to be within the core 1 region of the protein.

Our lab has focused on understanding the biophysical and biochemical differences between the two CYB5 isoforms. The first CYB5B gene to be identified was that of rCYB5B [112]. Biophysical analysis, in collaboration with Dr.Benson's group, of rCYB5B revealed that rCYB5B was significantly more stable than bCYB5A [6]. rCYB5B was also seen to have a redox potential more negative than that of bCYB5A [114]. The second CYB5B gene to be synthesised was the human protein (hCYB5B) [7]. Biophysical analysis indicated that hCYB5B had the stability properties similar to rCYB5B and likewise had a redox potential

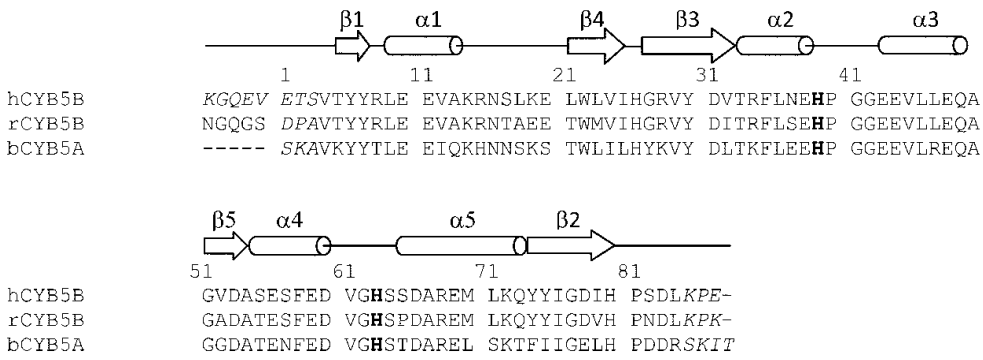

Figure 3.1: Amino acid residues of hCYB5B and rCYB5B aligned with bCYB5A. The numbering system used here uses the scheme first introduced by Mathews [84]. α- helices are depicted as cylinders and β strands are shown as arrows. Histidines that co-ordinate to the heme are shown in bold, italicized residues appear disordered in the final X-ray structure.

more negative than that of bCYb5A. However, the redox potential of hCYB5B was found to be more positive than that of rCYB5B [7]. The crystal structures of rCYB5B and hCYB5B were solved to high resolution (see chapter 2 for details) prior to my work in Dr. Benson's group, but were not published.

The amino acid sequence alignment of CYB5As and CYB5Bs have revealed that the amino acid sequence in CYB5B has diverged significantly more than that of CYB5As (See figure 1.4). Within CYB5As the amino acid sequence from different mammalian organisms are highly homologous. Comparison of the variation in the two isoforms has revealed the presence of key mutations in CYB5Bs. The amino acids at the respective positions in CYB5As are identical (see table 3.1). These mutations, in CYB5B, are typically in positions that likely affect surface properties and internal organization of the CYB5 fold, and are identified to be part of a hydrophobic patch that differentiates CYB5A and CYB5B with respect to their biophysical and biochemical properties [114].

rCYB5B and hCYB5B (hCYB5B) are two proteins that represent the divergence within type B cytochrome b_5s. Our refined structure of rCYB5B (2.0 Å) also enables a meaningful comparison of the two orthologous proteins. Two well ordered water molecules were seen in hCYB5B (absent in rCYB5B) that prompted us to investigate the role of those water molecules. MD simulations were performed on rCYB5B and hCYB5B as part of this investigation. The work described in this chapter has been published [104].

3.2 Results

3.2.1 Crystal structure comparison of bCYB5A, rCYB5B and hCYB5B

The earliest crystal structure of rCYB5B [118] was solved to a resolution of 2.7 Å (PDB code 1B5M) and contained one molecule in the aymmetric unit. The present structure of rCYB5B (PDB code 3MUS, 2.0 Å resolution) has two molecules in its asymmetric unit. The crystal structure of hCYB5B, solved to 1.45 Å resolution, also shows two molecules in the asymmetric unit. Molecules A of the aymmetric unit of both hCYB5B and rCYB5B are compared with the crystal structure of bCYB5A (PDB code 1CYO).

Organism	Amino acid position number										
	18	47	36	32	23	25	58	71	30	21	50
Human	Ser	Arg	Leu	Leu	Leu	Leu	Phe	Ser	Tyr	Thr	Ala
Rat	Ser	Arg	Leu	Leu	Val	Leu	Phe	Ser	Tyr	Thr	Ala
Rabbit	Ser	Arg	Leu	Leu	Leu	Leu	Phe	Ser	Tyr	Thr	Ala
Bovine	Ser	Arg	Leu	Leu	Leu	Leu	Phe	Ser	Tyr	Thr	Ala
Sheep	Ser	Arg	Leu	Leu	Leu	Leu	Phe	Ser	Tyr	Thr	Ala
Pig	Ser	Arg	Leu	Leu	Leu	Leu	Phe	Ser	Tyr	Thr	Ala
Horse	Ser	Arg	Leu	Leu	Leu	Leu	Phe	Ser	Tyr	Thr	Ala
Dog	Ser	Arg	Leu	Leu	Leu	Leu	Phe	Ser	Tyr	Thr	Ala
Opposum	Ser	Arg	Leu	Leu	Leu	Leu	Phe	Ser	Tyr	Thr	Ala

(a) Hydrophobic network in mammalian CYB5A orthologs

Organism	Amino acid position number										
	18	47	36	32	23	25	58	71	30	21	50
Human	Leu	Leu	Leu	Val	Leu	Ile	Phe	Leu	Tyr	Leu	Ala
Rat	Ala	Leu	Leu	Ile	Met	Ile	Phe	Leu	Tyr	Thr	Ala
Rabbit	Pro	Leu	Leu	Leu	Leu	Ile	Phe	Leu	Tyr	Leu	Ala
Bovine	Pro	Met	Leu	Leu	Leu	Ile	Phe	Leu	Tyr	Ile	Ala
Pig	Pro	Met	Met	Leu	Leu	Ile	Phe	Leu	Tyr	Leu	Ala
Horse	Ser	Leu	Leu	Leu	Leu	Ile	Phe	Leu	Tyr	Ile	Ala
Dog	Leu	Leu	Leu	Leu	Leu	Ile	Phe	Leu	Tyr	Ile	Ala
Opposum	Glu	Met	Leu	Leu	Leu	Ile	Phe	Leu	Tyr	Thr	Ala

(b) Hydrophobic network in all known CYB5B orthologs

Table 3.1: Comparison of hydrophobic network in mammalian CYB5A and CYB5B

Average main chain crystallographic temperature factors (B factors) for the hCYB5B peptide fragment (see figure 3.2) indicates less dynamic behavior for the β sheet strands (average B factor 12.5) when compared to the solvent exposed α helical regions (Average B factor 17.2). This is consistent with NMR experiments of both CYB5A and CYB5B proteins [10, 126].

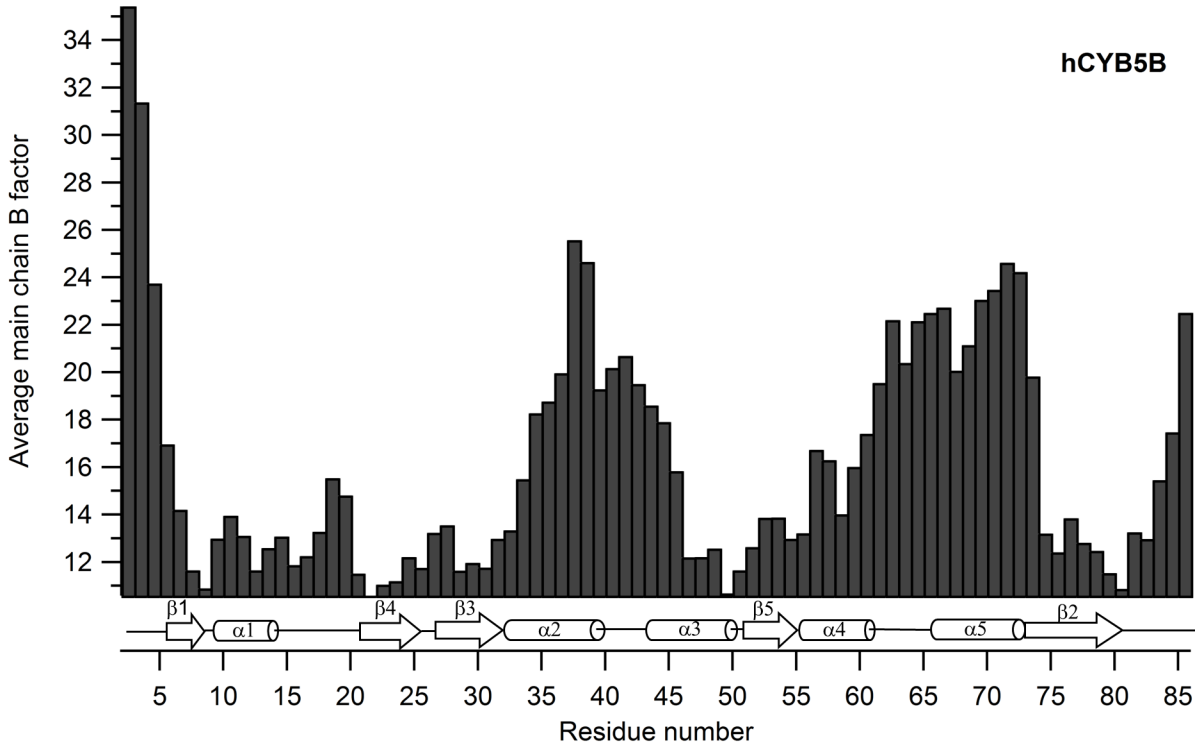

Figure 3.2: B factor plot of hCYB5B across the polypeptide. Secondary structure elements are indicated along the X-axis.

Small differences are seen in the root mean square deviation (RMSD) of the Cα (see figure 3.3) atoms for the protein in the two molecules of the asymmetric unit in both rCYB5B (average RMSD 0.23 Å) and hCYB5B (average RMSD 0.29 Å). Comparison of bCYB5A and rCYB5B indicate virtually identical folds with an average RMSD of 0.56 Å (See figure 3.4). However, significant differences appear when comparing rCYB5B and hCYB5B, especially spanning amino acid residues 50- 54 that are part of secondary structure element β5 (See figure 3.5).

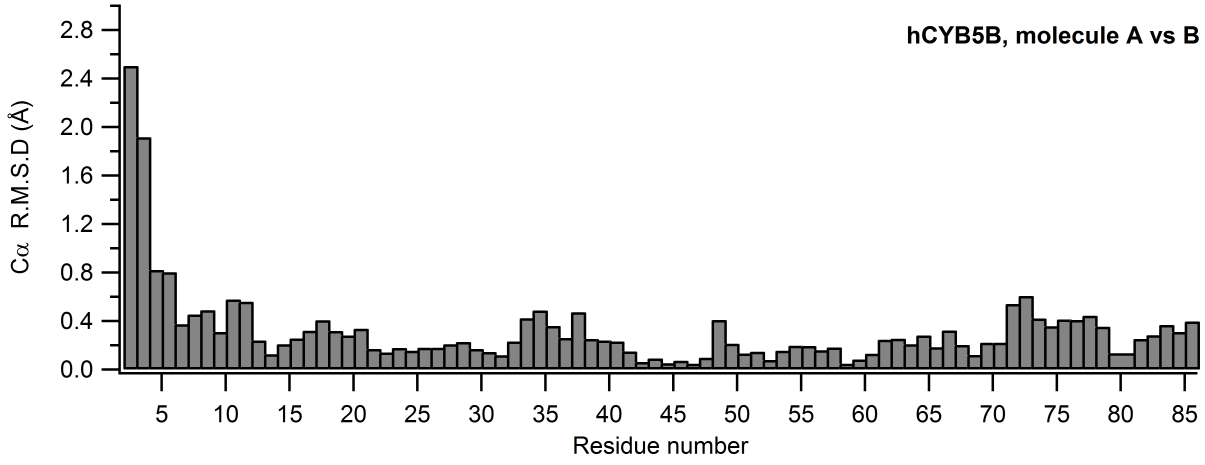

(a)

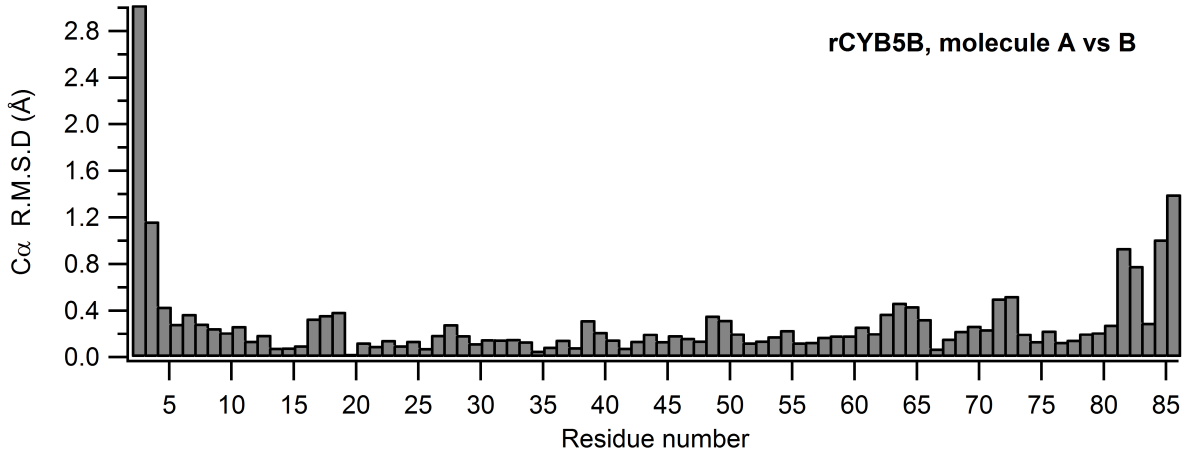

(b)

Figure 3.3: Comparison of the two molecules in the asymmetric units.

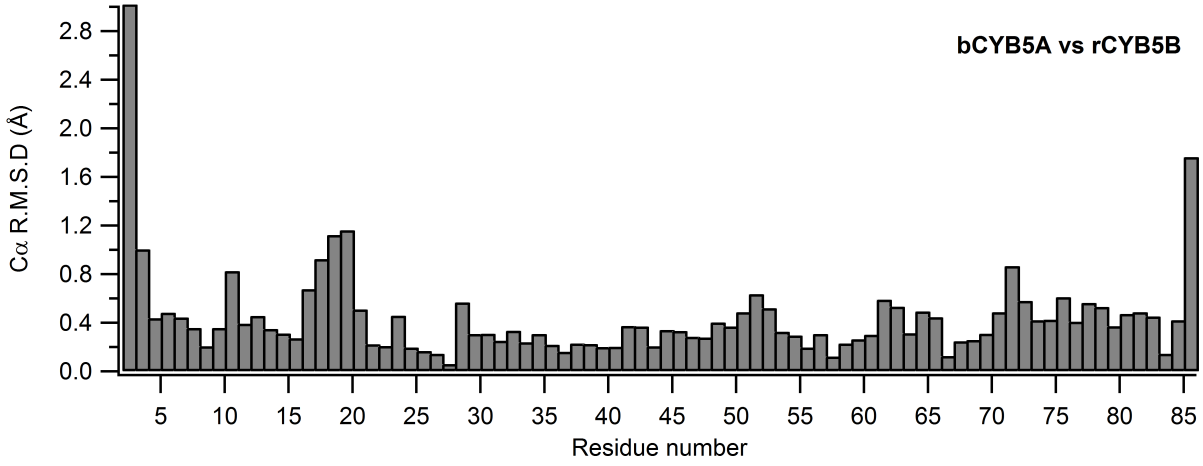

Figure 3.4: Comparison of bCYB5A and rCYB5B

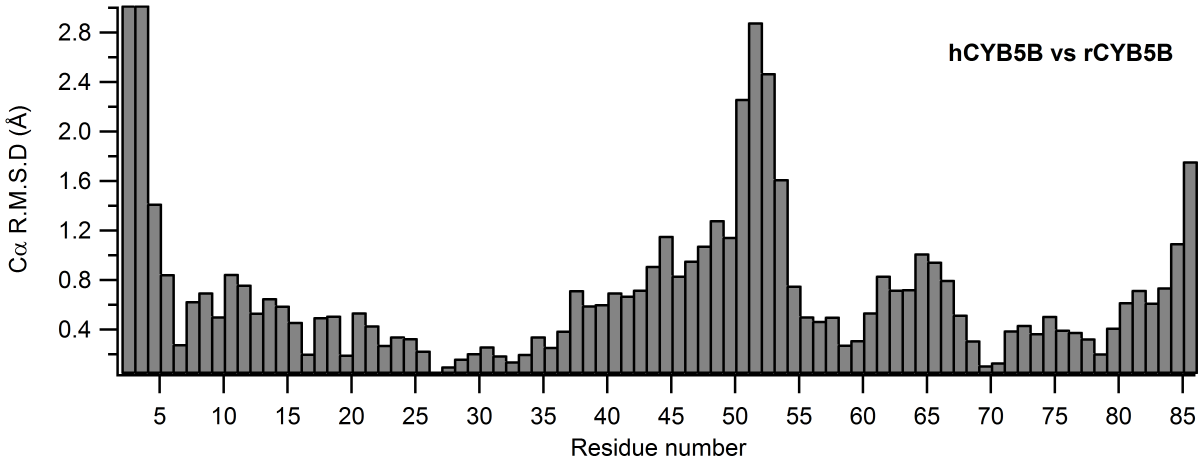

Figure 3.5: Comparison of hCYB5B and rCYB5B

3.2.2 Comparison of the Hydrophobic patch in rCYB5B and hCYB5B

An extensive patch of hydrophobic interactions exists for rCYB5B proteins; interactions that involve heme and the amino acid side chains at the core1/ core 2 interface. These interactions, as demonstrated by mutagenesis studies [6, 27, 30, 135], contribute largely to the increased stability of rCYB5B versus bCYB5A. In rCYB5B, the hydrophobic interactions start with van der Waals contact between the solvent exposed side chain of Ala18 and Leu47. The hydrophobic network continues with sequential interactions between the side chains of Leu47, Leu36, Ile32, Met23, and Ile25 and finishes with van der Waals interactions between Leu71, Ile25 and Phe58. Hydrophobic interactions with heme occur with the side chains of Met23, Ile25, Ile32, Leu71 and Phe58 (See figure 3.6a). In mammalian CYB5A orthologs, the corresponding region is less hydrophobic largely owing to the presence of more polar amino acids at positions 18 (Ser), 47 (Arg) and 71 (Ser).

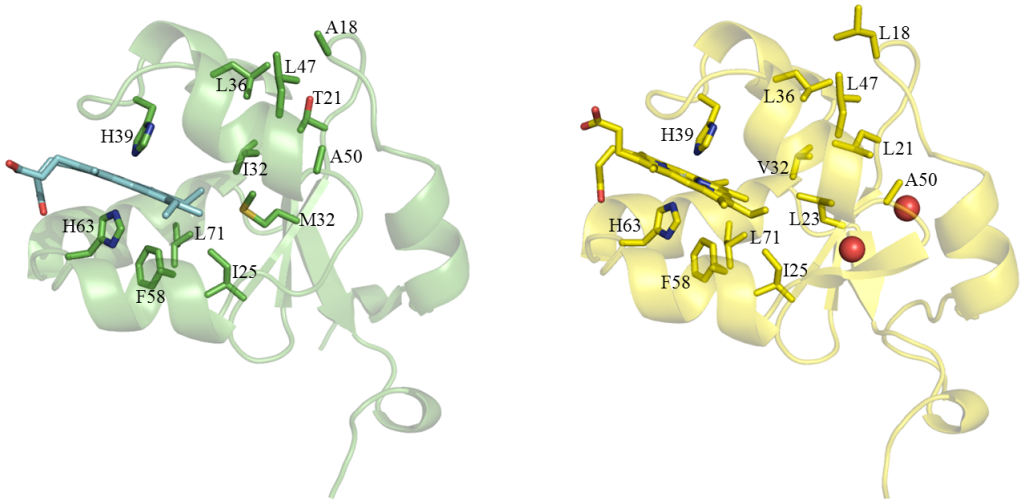

(a) rCYB5B (b) hCYB5B

Figure 3.6: Comparison of the hydrophobic pocket in rCYB5B (green) and hCYB5B (yellow). The polypeptide is shown as cartoon with the amino acid residues lining the hydrophobic pocket and heme depicted as sticks. Water molecules in hCYB5B are shown as red spheres.

With respect to the hydrophobic pocket, hCYB5B displays differences at three positions which are relatively conservative when compared to rCYB5B: 18 (Leu vs Ala), 23 (Leu vs Met) and 32 (Val vs Ile). The mutations at positions 23 and 32 of hCYB5B preserve the hydrophobic interactions as seen in rCYB5B hydrophobic cluster. The solvent-exposed side chain of Leu18 in hCYB5B engages in a more extensive van der Waals interaction with both Leu47 and Leu36 than does Ala18 in rCYB5B (See figure 3.6b).

Residue 21 in rCYB5B is Thr that participates in a hydrophobic interaction to Leu47 (C-C distance 4.4 Å) and to Ala50 (C-C distance 3.4 Å). These interactions are through the γ-CH_3 group of Thr 21 with the γ-CH_3 group of Leu47 and the γ-CH_3 group of Thr21 with the β-CH_3 group of Ala50. The hydrophobic pocket in rCYB5A is thus extended in rCYB5B via Ala50 and Thr21. Residues 15-20 comprise a loop that connects secondary structure elements $\alpha 1$ and $\beta 4$ and is hereby referred to as the $\alpha 1/\beta 4$ loop. More specifically, a type 1 β turn is formed by residues 17-20. In addition the backbone CO of Thr17 forms a strong hydrogen bond (O-O distance 2.9 Å) with the side chain hydroxyl of Thr21. The amino acid at position 21, in known CYB5A proteins, is Thr. Thr21 in the bCYB5A structure displays identical interactions as seen for the Thr21 residue in the rCYB5B structure.

3.2.3 A closer look at $\beta 4$ and $\beta 5$

Amino acid position 21 in hCYB5B differs from rCYB5B by replacing a polar residue (Thr in rCYB5B) with a bulkier and more hydrophobic residue (Leu in hCYB5B). The presence of Leu, in hCYB5B, however changes the nature of interactions within the hydrophobic cluster when compared to rCYB5B (See figures 3.6a and 3.6bfor an overview). The bulkier Leu side chain in hCYB5B prevents the formation of side chain hydrogen bonds within the $\alpha 1/\beta 4$ loop when compared to rCYB5B (See figure 3.7). The hydrophobic network in hCYB5B also is extended due to van der Waals interactions between the side chain of Leu21

with the side chains of Leu47, Ala50 , Leu23 and Leu36. The enhanced van der Waals interaction in hCYB5B and the necessity to accomodate a bulkier, hydrophobic Leu21 side chain causes the movement of the Ala50 side chain. Specifically, the β methyl group of Ala50 is displaced approximately 2.5 Å compared to its position in rCYB5B (see figure 3.5).

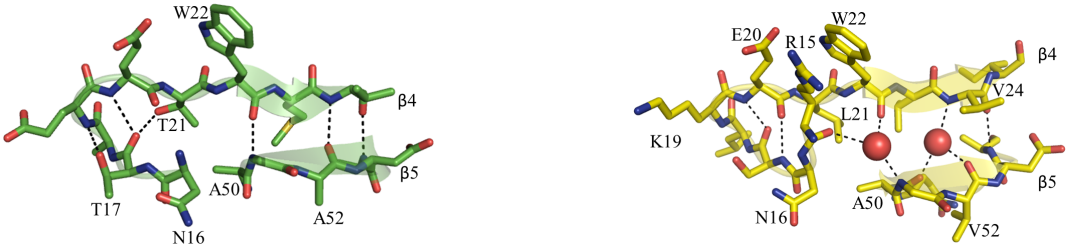

(a) rCYB5B (b) hCYB5B

Figure 3.7: Comparion of $\alpha 1/\beta 4$ loop, $\beta 4$ and $\beta 5$ in rCYB5B (green) and hCYB5B (yellow). Residues lining the secondary structural elements are shown as sticks. The water molecules are shown as red spheres and hydrogen bonds are depicted as black dashes.

The effect of the movement of Ala50 and its neighbouring residues (51-53) is seen in the loss of hydrogen bonds between β4 and β5. Specifically, the hydrogen bond between α-CO of Trp22 in β4 and the α-NH of Gly51 in β5 and the hydrogen bond between α-NH of Val24 in β4 and the α-CO of Val52 in β5 are disrupted. Two water molecules instead are involved in hydrogen bonding between those residues in β4 and β5 (WAT11 and WAT194 respectively). These 2 water molecules are completely buried (solvent accessible suface area of both water molecules = 0.0 Å^2) and are well resolved. Figure 3.9 shows the hydrogen bonding network in the β sheet of hCYB5B along with hydrogen bond distances.

WAT11 forms very strong hydrogen bonds with α-CO of Trp22 in β4 (O-O distance = 2.66 Å) and the α-NH of Gly51 in β5 (O-N distance = 2.79 Å). WAT11 also shows hydrogen bond interactions with the α-CO of Arg15 (O-O distance = 3.1 Å) and the α-CO of Val12 (O-O distance = 3.0 Å). WAT194 forms hydrogen bonds with the α-NH of Val24 in β4 (O-N distance = 2.86 Å) and the α-CO of Val52 in β5 (O-O distance = 2.65 Å). It also forms a hydrogen bond with the α-CO of Gln49 (O-O distance = 2.7 Å, see figure 3.7b).

No other hydrogen bonding interactions are seen for either of these 2 water molecules. Though the two water molecules are sandwiched between the β strands, they are too far apart for a water-water hydrogen bond (O-O distance = 4.9 Å). WAT11 and WAT194 display lower B-factors in the crystal structure (13.3 and 16.5 respectively) when compared to the average B-factor of the crystal water molecules (34.4). The amino acid backbone atoms in β4 and β5 have B-factors that are similar to the B-factors of the sandwiched water molecules and also form very short hydrogen bonds with them. (See figure 3.10) When the backbone atoms of molecule B and molecule A in the asymmetric unit in hCYB5B were aligned, the difference in distance between the water molecules sandwiched between the β sheets was less than 0.5 Å. All these observations are indicative of structurally well preserved water molecules with strong hydrogen bonding interactions to the β sheet.

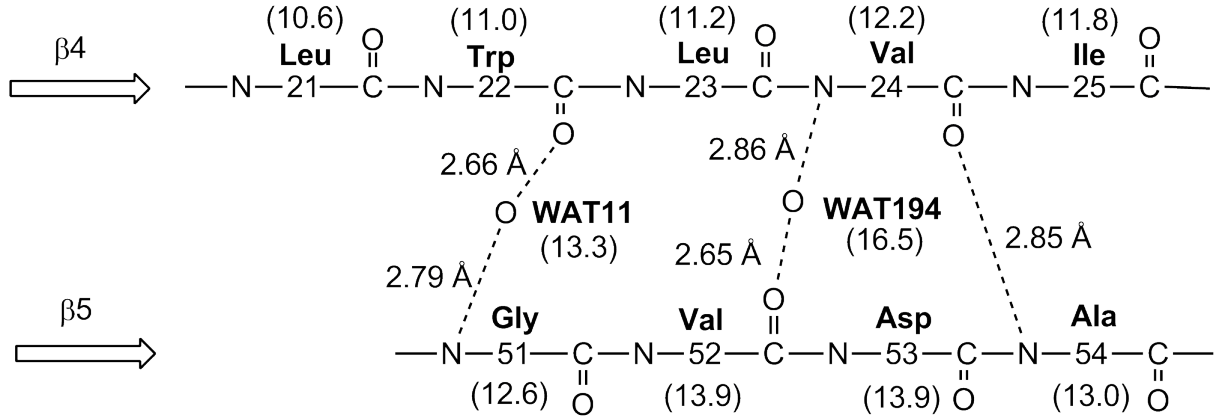

Figure 3.10: Diagram of interactions within β4 and β5. Hydrogen bonds between residues are indicated by dashed lines and the numbers correspong to the lengths. Numbers in parentheses correspond to B-factors of both the main chain atoms and the buried water molecules.

As an approach to compare solution properties of rCYB5B and hCYB5B and to look at details of atomic and structural changes in the two proteins, we performed 10 ns MD simulations. The crystal structure of

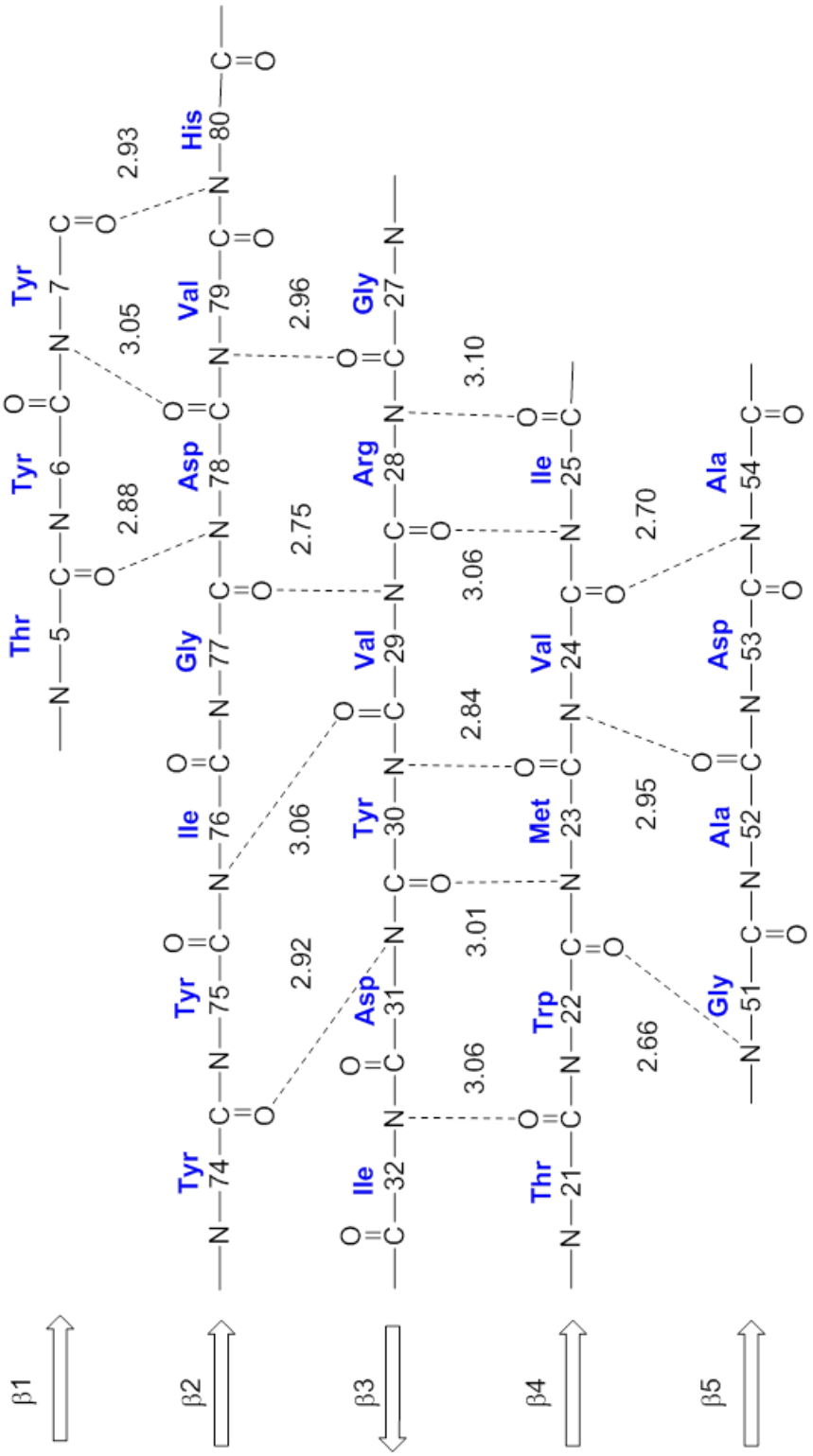

Figure 3.8: Hydrogen bonding network in rCYB5B β sheet. The hydrogen bonds are shown as dashed lines and the numbers represent the lengths of hydrogen bonds in Å

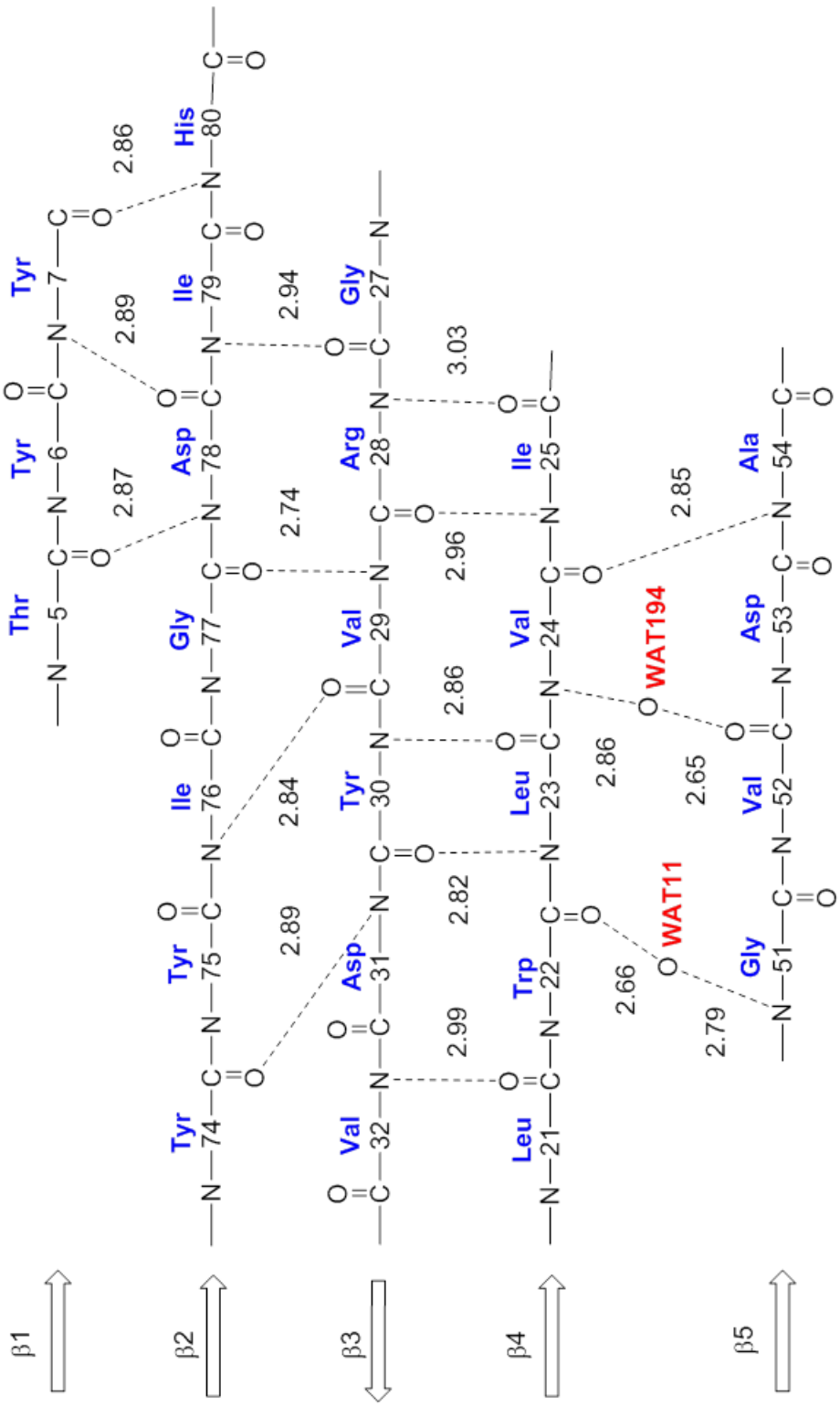

Figure 3.9: Hydrogen bonding network in hCYB5B β sheet. The hydrogen bonds are shown as dashed lines and the numbers represent the lengths of hydrogen bonds in Å.

	Backbone RMSF	Heme RMSF	Backbone RMSD	Heme RMSD
hCYB5Bnw	0.7	0.9	0.9	1.1
hCYB5Bw	0.6	0.9	0.5	0.9
rCYB5B	0.7	0.8	0.6	1.0

Table 3.2: Backbone RMSD and RMSF of the three CYB5B simulations (Å). *Backbone atoms are defined by Cα, C and N atoms of amino acid residues 4-84*

hCYB5B was treated in two ways; one in which the two water molecules sandwiched between $\beta 4$ and $\beta 5$ were retained (hCYB5Bw, henceforth) and one in which the water molecules were removed from the starting structure (hCYB5Bnw). Results from the MD simulations of 3 proteins (hCYB5Bnw, hCYB5Bw and rCYB5B, vide infra) helped us elucidate the role that the water molecules played in maintaining structural integrity of hCYB5Bw when compared to hCYB5Bnw and rCYB5B. The starting structures of the three proteins are shown in Figure 3.11.

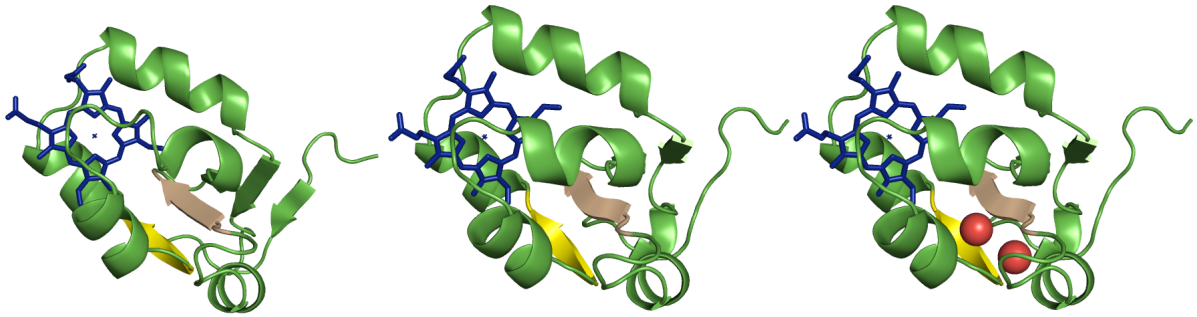

(a) (b) (c)

Figure 3.11: Experimental structures of CYB5Bs. The polypeptide is depicted in green with secondary structural elements $\beta 4$ and $\beta 5$ colored wheat and yellow respectively. Water molecules in hCYB5w are shown as red spheres. (a) rCYB5B, (b) hCYB5Bnw and (c) hCYB5Bw

3.3 General Structural Analysis of MD simulations

Analysis of MD simulations of the three proteins indicated that the average polypeptide backbone structure was very similar to that of the starting experimental structure. The root mean square deviation (RMSD) and fluctuation (RMSF) of both the polypeptide backbone and the heme prosthetic group are given in Table 3.2.

The three CYB5B protein simulations do not reveal a significant deviation from their respective starting experimental coordinates, with average protein backbone RMSD values being less than 1.0 Å in all cases. Individual amino acid residue RMSDs and RMSFs in all three cases are shown in Figure 3.12. The RMSD plot of hCYB5Bnw MD simulation shows the maximum deviation ($\approx$ 2.0 Å) at amino acid residues 51-54 which in large part corresponds to β sheet strand $\beta 5$. The RMSD increase in the hCYB5Bnw simulation can be attributed to the absence of WAT11 and WAT194, which results in formation of hydrogen bonds between $\beta 4$ and $\beta 5$. The hydrogen bonds, which form during the pre-production equilibration step, are virtually identical to those observed between $\beta 4$ and $\beta 5$ in the rCYB5B crystal structure and MD simulation. They

stay intact through the 10 ns hCYB5B simulation, as shown by the low RMSF value in the corresponding residues (See Figure 3.12b).

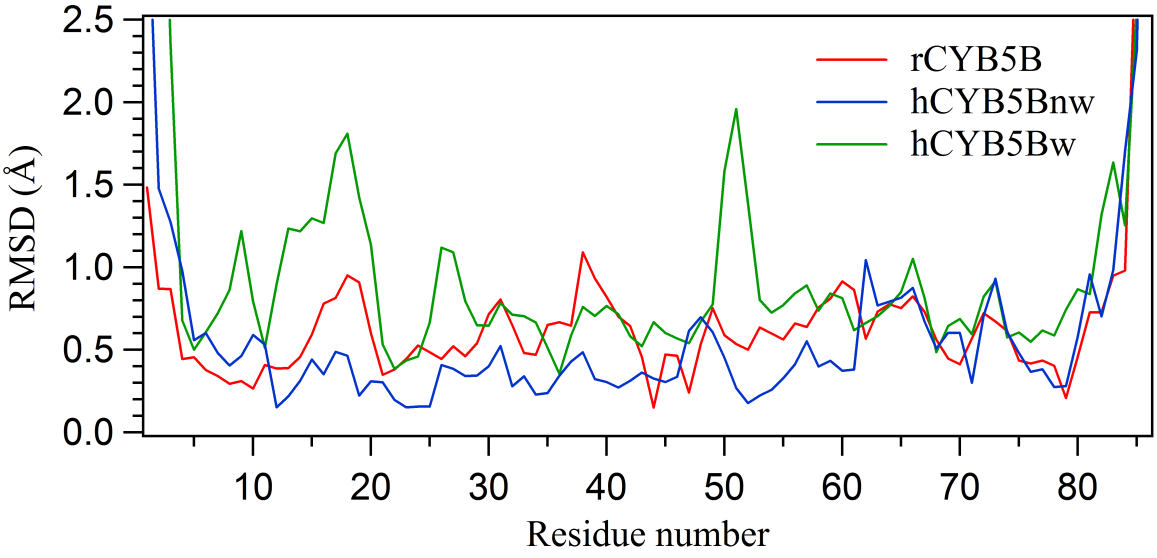

(a)

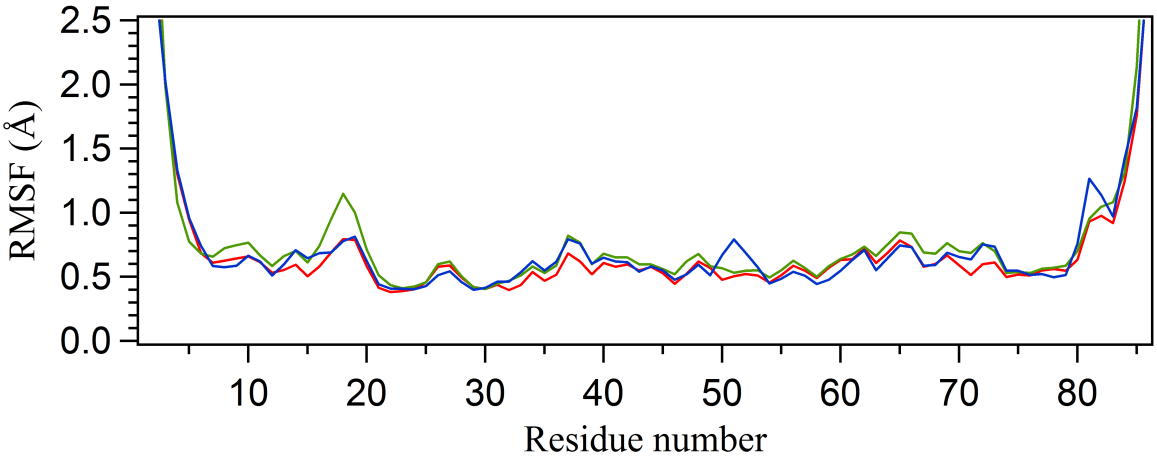

(b)

Figure 3.12: MD simulations- Backbone analysis (a) Backbone RMSD plots of the average trajectory structure and the starting X- ray coordinates in the 10ns simulations. (b) Backbone RMSF plots in the three CYB5B simulations. The colour scheme shown in (a) is the same for (b)

hCYB5B also shows a significant deviation at amino acid residues 15- 20 (1.5 - 2.0 Å). This deviation can be attributed to the reorganization of the Leu 21 side chain due to the formation of new hydrogen bonds between $\beta 4$ and $\beta 5$ and to avoid steric interference. In the case of hCYB5Bw, RMSD and RMSF values for residues in $\beta 4$ and $\beta 5$ are less than 1 Å, indicating maintenance of the structural elements throughout the simulation. Analysis of WAT11 and WAT194 in the hCYB5Bw simulation is discussed in a separate section.

3.3.1 Solvent Accessibility

Comparison of the solvent accessible surface area (SASA) in the three simulations is shown in Figure 3.13. SASA comparison of the three proteins helps to compare heme binding pocket changes, and support RMSD and RMSF comparisons of MD simulations. Given the presence of WAT11 and WAT194 in hCYB5Bw, a significant change in SASA can give us clues about possible solvent movement events within the protein.

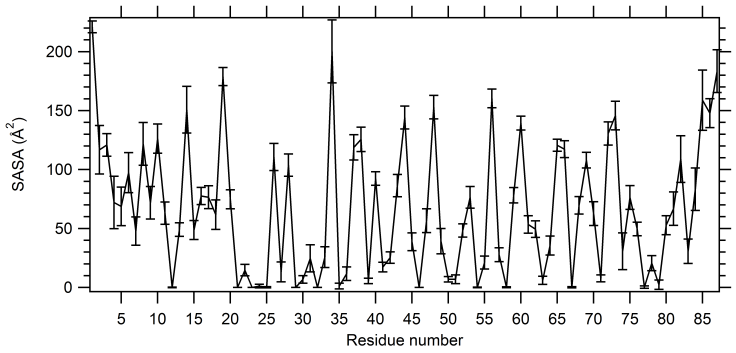

(a)

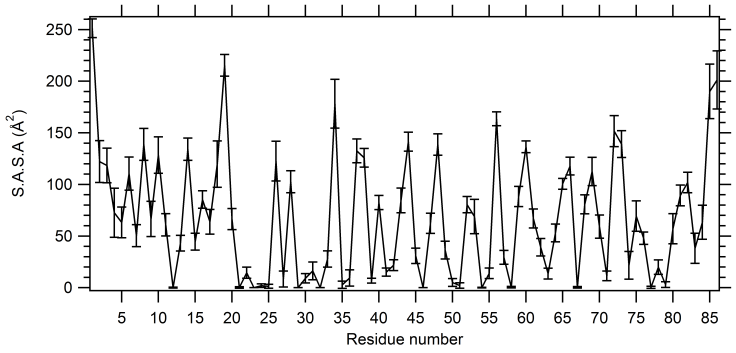

(b)

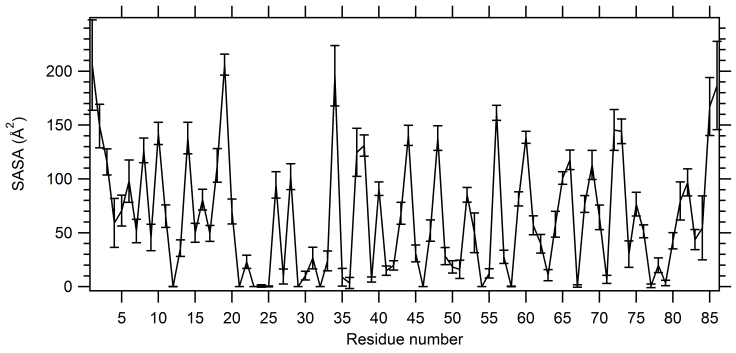

(c)

Figure 3.13: Average SASA of the three MD simulations. Error bars indicate the standard deviation. (a) rCYB5B, (b) hCYB5Bnw and (c) hCYB5Bw

As seen in Figure 3.13, differences in polypeptide residue surface area of the three MD simulations are not statistically significant. Minor differences are seen in residues that are exposed to the solvent and are

	SASA (Å^2)
rCYB5B	242 ± 18 (222)
hCYB5Bnw	243 ±17 (218)
hCYB5Bw	243 ± 18 (218)

Table 3.3: Average SASA of heme, SASA calculated from X-ray crystal structures is enclosed in parentheses

mainly due to fluctuations in side chain dynamics. The data, however, support the RMSF plots indicating the lack of change in structural elements of hCYB5Bw when compared to the starting crystal structure. A similar trend is seen with the hCYB5Bnw and rCYB5B SASA plots.

The average heme SASA values throughout the three 10 ns simulations are shown in Table 3.3. The values indicate that the presence or absence of water in hCYB5B simulations has not changed the dynamics of the heme binding pocket. SASA of heme has been implicated as a factor that controls redox potential of heme binding proteins [108]. The similarity of the heme SASA values in the MD simulations is consistent with the similarity of their redox potentials as determined in the research described in chapter 5.

3.3.2 Behavior of WAT11 and WAT194 in the hCYB5Bw simulation

The RMSD and RMSF plots (see Figure 3.12) show that the presence of water molecules in the hCYB5Bw starting structure does not cause variation of overall polypeptide secondary structure through the 10 ns MD simulation. In the crystal structure of hCYB5Bw, WAT 194 mediates the hydrogen bond between Val24 and Val52 and WAT11 mediates the hydrogen bond between Trp22 in β4 and Gly51 in β5. Analyses of β4 and β5 in both the hCYB5B and hCYB5Bw MD simulation are shown in Table 3.4. This is a closer look at the amino acid residues involved in direct hydrogen bond formation with respect to the hCYB5B MD simulation and water mediated hydrogen bonds in hCYB5Bw MD simulations.

	Trp22- Gly 51	Val24- Val52	Trp22- WAT11	Gly51- WAT11
hCYB5Bnw	2.9 ± 0.2	3.5 ± 0.3	–	–
hCYB5Bw	5.1 ± 0.4	4.7 ± 0.3	30.4 ± 14.8	29.3 ± 14.3

Table 3.4: Distance between water molecules and amino acid residues involved in β4 and β5 hydrogen bonding (Å) during the MD simulations. Note the high standard deviation in distances between Trp22 and WAT11 and Gly51 and WAT11

There is very little fluctuation as seen from the low standard deviation when comparing β4 and β5 residues and indicates maintenance of hydrogen bonds in both hCYB5B and hCYB5Bw MD simulations. However, visual inspection of the hCYB5Bw MD trajectories showed rapid exchange of the WAT11 that is involved in mediating the hydrogen bond between Trp22 in β4 and Gly51 in β5 with the bulk solvent (also see Table 3.4 for definitive evidence). The second water molecule, WAT194, retains its relative position during the MD simulation when compared to the starting crystal structure of hCYB5Bw. WAT194 mediated hydrogen bonds involving Val24 and Val52 in β4 and β5 respectively are also preserved.

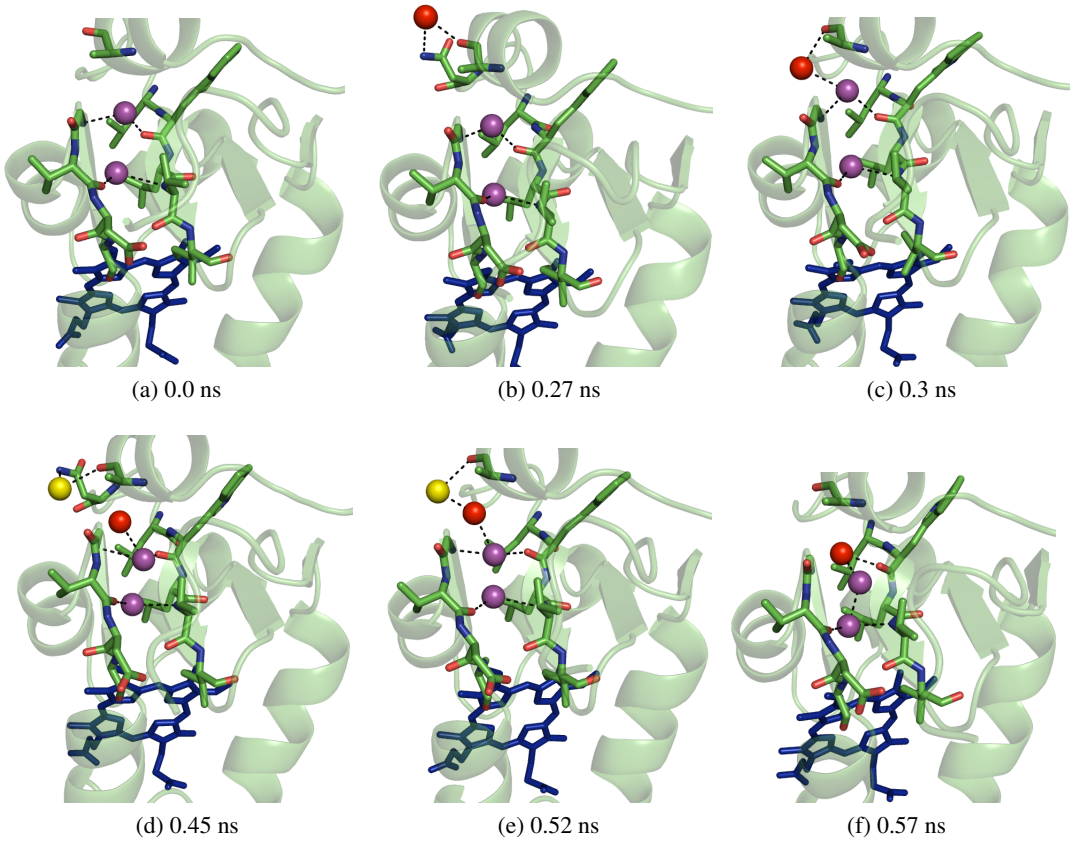

(a) 0.0 ns (b) 0.27 ns (c) 0.3 ns

(d) 0.45 ns (e) 0.52 ns (f) 0.57 ns

Figure 3.14: Initial stage of entry of water molecules. Waters are shown as spheres, waters of crystallization (WAT11 and WAT194) are depicted as purple spheres, the polypeptide is shown in green cartoon with residues in $\beta 4$ and $\beta 5$, Ala 13 and Asn 16 are depicted in sticks. Heme is shown as sticks and colored blue. Hydrogen bonds are shown as black dashes. (a) Starting structure immediately after equilibration (b) The incoming water molecule, wat1877 colored red, forms hydrogen bonds with Asn 16 and Ala 13. (c) wat1877 forms a hydrogen bond with WAT11. (d) Bulk solvent molecule, wat4142 colored yellow, initially hydrogen bonds with Asn 16 and Ala13 and then helps in formation of the water chain as shown in (e). (f) Entry of bulk solvent wat1877 into the β sheet by hydrogen bonding with backbone O of Trp 22.

The movement of water molecules is illustrated in three parts. The waters of crystallization, colored purple, are denoted in uppercase and those from the bulk solvent box are designated lower case letters. There exists 2 distinct regions from which bulk water molecules can enter and exit. The first site involves the solvent accessible area between the last turn of helix $\alpha 1$ and the beginning of $\beta 4$. During entry, the incoming bulk solvent molecule (coloured red, wat1877) makes initial contact with the polypeptide at the sidechain N of Asn16 and the backbone O of Ala13. The backbone O of Ala13 along with another bulk solvent molecule (coloured yellow, wat4142) are involved in guiding the incoming water molecule. A water chain is formed, with hydrogen bonds between the bulk water molecules (wat4142, wat1877) and the water of crystallization (WAT11). The positions of the bulk solvent molecule (both wat1877 and wat4142), in the initial steps, are identical to a water molecule in the crystal structure (water molecule 121 in the PDB file, which is not included in the starting structure in MD simulation) which also forms hydrogen bonds with Arg 16 and Ala 13 (See figure 3.14).

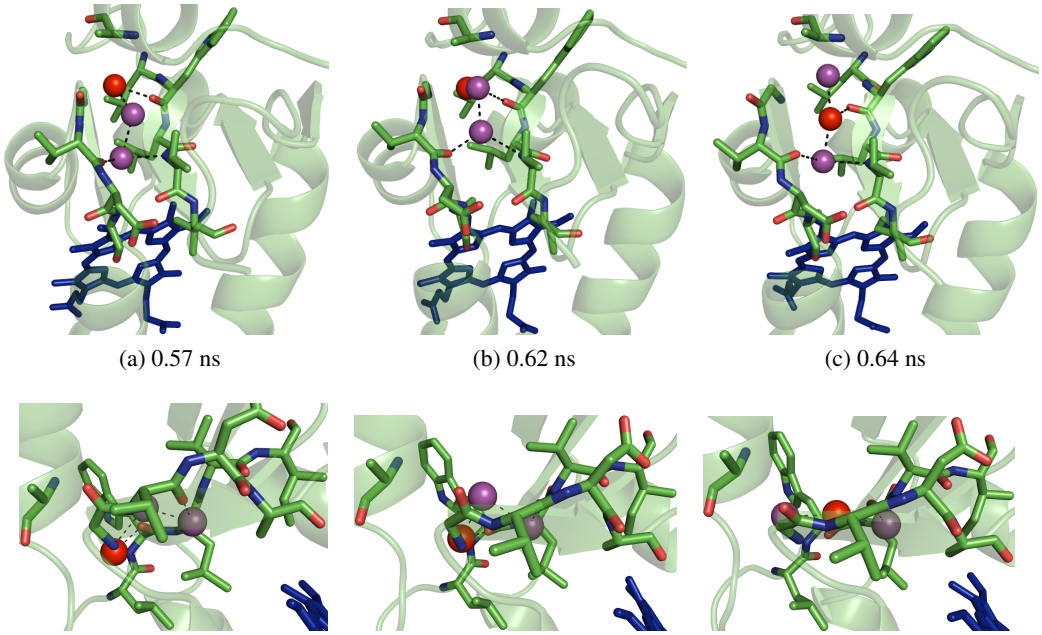

(a) 0.57 ns (b) 0.62 ns (c) 0.64 ns

(d) (e) (f)

Figure 3.15: Movement of water molecules within the β sheet. Panels (d), (e) and (f) are rotated frames of (a), (b) and (c) repectively such that the viewer is looking at the plane formed by the β strands. The protein is depicted as a green cartoon with the residues of the β sheet shown as sticks. Heme is shown as blue sticks. Water molecules are shown as spheres with the waters of crystallization coloured purple and bulk solvent (wat1877) coloured red respectively. Hydrogen bonds are shown as black dashes. There is disruption of the hydrogen bond network which leads to the exchange of bulk solvent with the waters of cyrstallization. Fig (f) clearly shows the string of three water molecules between the β strands.

After the initial step, the incoming water molecule sandwiches between $\beta 4$ and $\beta 5$, by either mediating the hydrogen bond between Trp22 and Gly51 or becoming involved in hydrogen bonding with the two resident water molecules. At any given point two or three water molecules can exist between $\beta 4$ and $\beta 5$. The water molecule (WAT194) involved in hydrogen bonding to Val24 and Val52 remains relatively unchanged terms of hydrogen bonds formed to the protein. (see Figure 3.15). The incoming water molecule (wat1877, coloured red) exchanges with one of the crystal waters present (WAT11, coloured purple). It does so by disrupting the hydrogen bonding between WAT11 and the backbone N atom of Gly 51 in $\beta 4$. It also forms a hydrogen bond to the backbone O atom in $\beta 5$. This results in sandwiching of the incoming water molecule between the β strands and formation of intermolecular hydrogen bonds between the three water molecules.

During the course of the MD simulation, WAT11 and WAT194 come closer. This pushes the sandwiched water molecule (wat1877) out of the plane defined by $\beta 4$ and $\beta 5$. The exit of the sandwiched water molecule (wat1877) is further facilitated by the formation of a hydrogen bond with the backbone O of Gly51. Subsequent steps involve solvent- solvent hydrogen bonding that helps in complete removal of the exiting water molecule. There are three distinct occurances of three water molecules between $\beta 4$ and $\beta 5$; in two instances the bulk solvent molecule is successful in completely displacing the water molecule mediating the

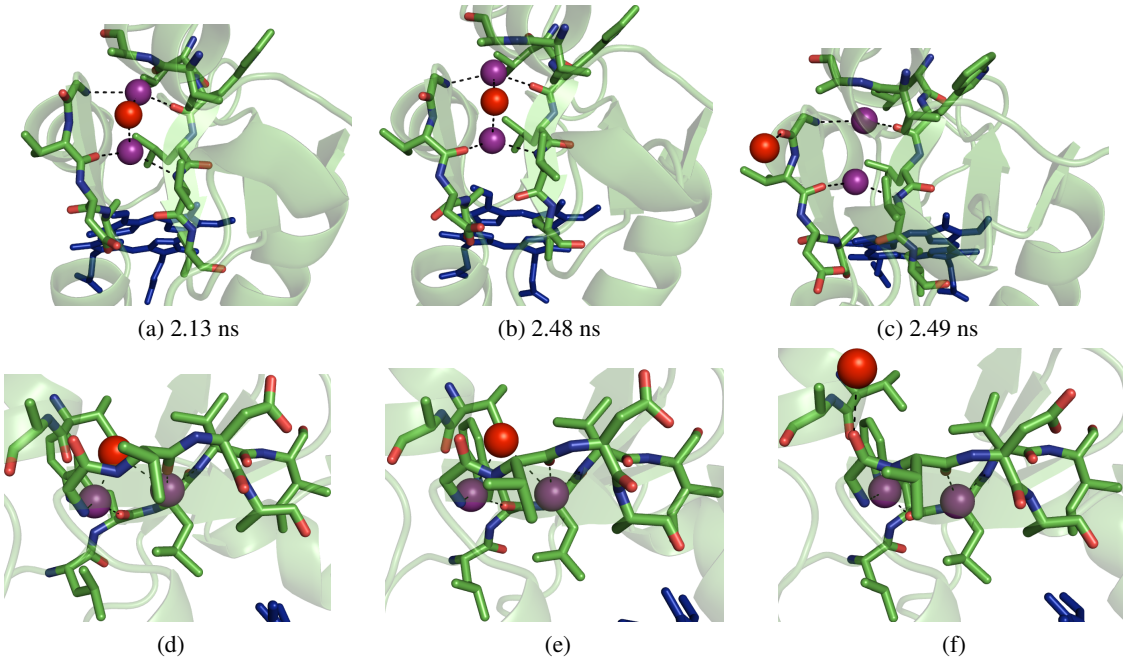

(a) 2.13 ns (b) 2.48 ns (c) 2.49 ns

(d) (e) (f)

Figure 3.16: Exit of the water molecule from the β strands. Panels (d), (e) and (f) are rotated frames of (a), (b) and (c) repectively such that the viewer is looking at the plane formed by the β strands. The protein is depicted as a green cartoon with the residues of the β sheet shown as sticks. Heme is shown as blue sticks. Water molecules are shown as spheres with the waters of crystallization coloured purple and bulk solvent (wat1877) coloured red respectively. Hydrogen bonds are shown as black dashes. The two crystallization waters come closer leading to the steric push of the sandwiched water molecule out of the plane defined by the β strands as seen in (a) and (b). The formation of a hydrogen bond with the exiting water molecule and the backbone O of Gly 51, as seen in (f), is the final step in removal of the sandwiched water molecule.

hydrogen bond between Trp22 and Gly51. WAT194 plays a major role however in the exit of the resident water molecule (see figure 3.16) by providing a steric force in pushing out one of the two water molecules. The retention of WAT194 prevents hydrogen bond formation between Trp22 in β4 and Gly51 in β4 when WAT11 exits, resulting in a void that can be quickly occupied by a water molecule from the bulk solvent. Subsequent steps involve solvent- solvent hydrogen bonding that helps in complete removal of the exiting water molecule. Within the MD simulation of hCYB5Bw, it was observed that the entry and exit sites within the polypeptide are interchangeable, with both sites being equally involved in the water exchange event. However, none of the water entry or exit events were accompanied by any protein conformational changes (See figure 3.17).

3.3.3 Rare Leu rotamer seen in the hCYB5B simulation

The MD simulation of hCYB5Bnw (starting crystal structure from which WAT11 and WAT194 were removed) revealed small but important changes. Amino acid residues 50-52 showed a significant deviation from the X-ray structure co-ordinates as seen in figure 3.12a. This change is due to formation of normal β sheet hydrogen bonds between Val24 and Val52 and between Trp22 and Gly51. Hydrogen bonds form during the pre-production equilibration stage and are identical to those observed in the rCYB5B MD simu-

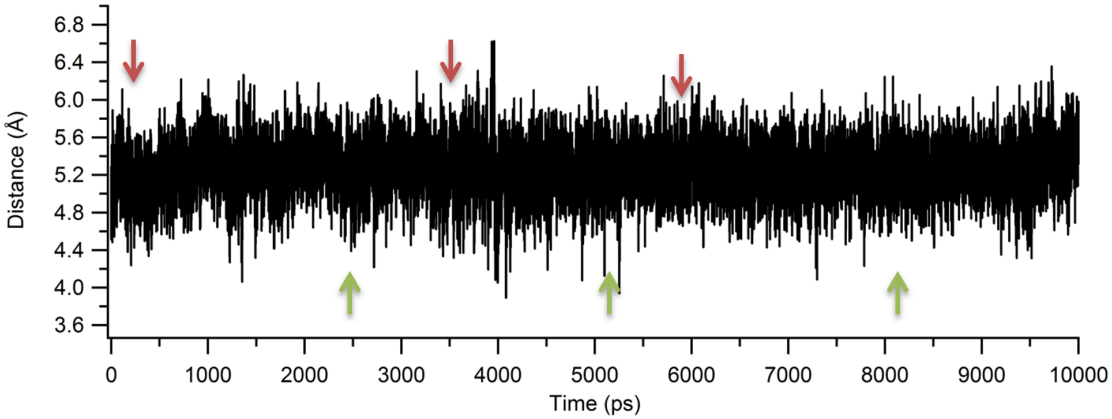

Figure 3.17: Distance between Gly51 (backbone N) and Trp22 (backbone O) in Å. Red arrows indicate the water entry event and the green arrows indicate the water exit event

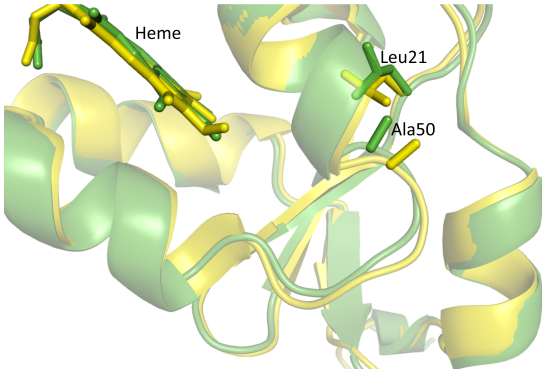

Figure 3.18: Structural alignment of hCYB5B crystal structure (yellow) and structure post equilibration (green). The polypeptide is depicted as cartoons and the heme, Ala50 and Leu21 are shown as sticks. Note the change in Leu side chain conformation after equilibration and the burial of the Ala50 side chain.

lation. Visual inspection of the trajectories as well as low RMSF values seen for the corresponsing residues (See figure 3.12b) suggest the maintanence of the hydrogen bonds throughout the 10 ns simulation. Amino acid residues 15-19, spanning the $\alpha 1/\beta 4$ loop, also show significant backbone deviation with Leu18 showing the maximum deviation. This is due to movement of the Ala50 side chain. The methyl side chain of Ala50 moves deeper into the interior of the protein as the hydrogen bonds between $\beta 4$ and $\beta 5$ form. Correspondingly the side chain of Leu21 also is reorganised to prevent steric clashes (See figure 3.18).

Leu21 in the hCYB5B crystal structure has a side chain conformation that is found in 34% of Leu residues in β sheets. The side chain angles χ_1 and χ_2 have the values 178° and 65° in Leu21 and are referred to as 'tp' based on the convention of Lovell et al [78]. After equilibration, Leu21 adopts a rotamer conformation that is observed in only 3% of Leu residues in β sheets the side chain angles χ_1 and χ_2 have the values -160° and 169° respectively (referred to as 'tt'). A possiblity from this rotamer conformation is the introduction of strain in the Leu side chain arising due to the formation of the hydrogen bonds between $\beta 4$ and $\beta 5$.

3.4 Discussion

The structure and MD simulations of hCYB5B have revealed the ability of CYB5 proteins to maintain an intact fold by accomodating various insertions, deletions and mutations. It has previously been referred to as an 'adaptible module' due to its ability to do the same [68]. The ability to accomodate a non-conservative internal mutation is demonstrated in hCYB5B, which incorporates two or three buried water molecules within the protein interior to preserve the CYB5 fold. Common examples of buried water molecules are associated with proteins possessing large internal cavities [145]. More recently, statistical analysis and MD simulations of 842 non redundant protein structures revealed that amino acid residues not found in secondary structural elements such as α helices and β sheets are commonly involved in hydrogen bonding with buried water molecules [18, 103]. Buried water moleules are also predominantly involved in mediating protein-ligand interactions [79]. In that context, the presence of water molecules sandwiched between β strands is quite rare as seen in the hCYB5B crystal structure. A well documented example of such a phenomenon in other proteins is a conserved water molecule between β strands seen in lectins [76].

The crystallographic data and MD simulations comparing rCYB5B and hCYB5B have revealed a greater ease for the entry of water between β4 and β5 in hCYB5B than in rCYB5B. This difference, however, is not reflected in either of the biochemical and biophysical properties of rCYB5B and hCYB5B. hCYB5B and rCYB5B have identical themal denaturation midpoints ($T_m \approx 85^\circ$ C) [5] and display similar redox potentials (See chapter 5). It is possible that the increased hydrophobic packing in hCYB5B, due to the Leu21 side chain, compensates for the energetic penalty imposed by the loss of two of the three hydrogen bonds between β4 and β5. It has already been shown, through mutagenic studies, that the more hydrophobic pocket at the core1/ core 2 interface in CYB5Bs contributes to greater stability when compared to CYB5As.

The entry and presence of three water molecules between β4 and β5 may suggest an intermediate in the β sheet formation of hCYB5B fold. A previous study using trypsin also revealed conserved buried water molecules that bridge hydrogen bonds between amino acid residues at the termini of β - strands; these water molecules are considered to represent intermediates of β sheet formation when the protein folds [44]. In this context, the hydrogen bond between Ala54 in β5 and Val24 in β4 may be the strongest and most important to maintain the hCYB5B fold. This may be the case in all CYB5s as well, supported by the conservation of Ala at position 54 in both CYB5A and CYB5B sequences (see figure 1.4).

CYB5 unfolding can be divided into two major steps; heme release from the polypeptide and subsequent unfolding of the heme free (apo) CYB5. In the apo form of CYB5, core 1 (composed of secondary structural elements α2- α5 and β5) completely unfold with dissociation of β5 from β4. Core 2 on the other hand retains holo CYB5 like structural characteristics [31, 42, 40, 27, 30]. The key step in the release of heme from the polypeptide is the breakage of the His-Fe bonds. More recent studies strongly suggest that the His39-Fe coordination bond is the first to break in the heme release process [127, 57]. The His- Fe bonds act as structural anchors to maintain secondary structural elements α2- α5 since the amino acids composing these helices are of low-helix propensity.

Two independent MD simulations of bCYB5A have revealed that heme release and associated conformational changes in core 1 are likely to begin in the vicinity of β5. The studies also observed the formation of a large surface cleft and resulted in the loss of the hydrogen bond mediating Gly51 in β5 and Trp22 in β4

[6, 131]. Structurally, the dissociation of β4 from β5 would disrupt helices α3 and α4 of core 1 and disrupt the coordination bonds between His39-Fe and His 63-Fe. Given this possible mechanism, it suggests that in addition to the His-Fe coordination, the β4-β5 interaction act as structural anchor points for maintanence of the helical bundle in core 1. In the hCYB5B crystal structure and MD simulation, two (sometimes three) water molecules are found within the β4- β5 interacting strands. Only the normal hydrogen bond between Val24 in β4 and Ala54 in β5 prevents the complete separation of β4 and β5.

Ala54 is an invariant residue found in mammalian forms of both CYB5A and CYB5B. It participates in extensive interactions both within the polypeptide and the heme molecule in the holo CYB5. The methyl side chain of Ala54 participates in an extensive interaction with the hydrophobic patches of both CYB5A and CYB5B (interacts with Leu23 sidechain) and heme. An additional interaction of Ala54 is through a hydrogen bond with another invariant residue Phe58 (α CO forms a hydrogen bond with the backbone NH of Phe58) that is located in the secondary structural unit α4 and hydrophobic patches. Phe58 participates in an edge-to-face interaction with heme and the phenyl sidechain of Phe58 participates in a π- stacking interaction with His63 (an iron coordinating residue). NMR (HD exchange) experiments have shown that Ala54 and Phe58 display very slow rates of exchange pertaining to the backbone NH [10, 127]. From the present work and available literature, we can conclude that a key step to complete unfolding of the core 1 in CYB5 would be the increased solvent exposure of Ala54 and Phe 58, subsequent steps would involve increased solvent exposure of other residue backbones in core 1 and heme release. Another important conclusion from this work is the importance of the third hydrogen bond in the β sheet (between Ala54 in β5 and Val24 in β4) in preserving the intact CYB5B fold, as seen in hCYB5B, and in maintaining the biophysical properties of the CYB5B family.

Chapter 4: Step by step incorporation of rOMb5 residues into bMcb5 aimed to increase stability of bMcb5

4.1 Introduction

Mammalian organisms contain two isoforms of a small heme binding redox protein called cytochrome b_5 (CYB5). CYB5 exists as a membrane anchored protein whose C-terminus determines the organelle to which it is incorporated [60]. The protein anchored to the endoplasmic reticulum membrane is called microsomal CYB5 (CYB5A, Mcb5 for this chapter) and the isoform anchored to the outer membrane of the mitochondria is called outer mitochondrial CYB5 (CYB5B, OMb5 for this chapter). These two isoforms arose from a common primordial gene that duplicated and evolved separately to give rise to organelle specific CYB5s [53]. Physiologically, Mcb5 is known to interact with a number of proteins in redox reactions including cytochrome P450, fatty acid desaturases [106, 94] and Omb5 is involved in modulation of NADH-semidehydroascorbic acid reductase activity in liver cells [59]. More recently Omb5 is known to interact with cytochrome P450- 17A1, using different mechanisms to modulate the function of cytochrome P450-17A1 on its steroid substrates [16].

Mcb5 isolated from bovine liver micrososmes (bMcb5) was the first CYB5 protein whose atomic structure (2.8 Å) was obtained[84]. A refined structure at a final resolution of 1.5 Å [35] was reported in 1996. The first structure of OMb5 to be solved was that of the CYB5 from rat (rOMb5, PDB code 1B5M) [118]. The overall fold is highly conserved in the two isoforms, the secondary structural elements follow the order β1-α1- β4-β3-α2-α3-β5-α4-α5-β2-α6. The heme, via the iron atom, is coordinated to two histidines (See figure 1.3). The histidines are housed in two helix-loop-helix motifs that make up core 1 of the protein. Core 2 of the CYB5 fold consists of helices α1, α6 and a 5 stranded β sheet (β1 -β5). The structural components are identical in both Mcb5 and OMb5 across different species (R.M.S.D when aligning 1CYO and 1B5M $\approx$ 0.6 Å) in spite of the difference in the amino acid sequences of the respective proteins.

4.1.1 Comparison of biophysical properties between the two isoforms

The stability of CYB5 holoprotein can be considered to be the sum of two parameters, the free energy of folding of the heme free protein (apoprotein) and the free energy of heme binding by the apoprotein [91] (See equation 4.1). The overall stability of the apoprotein is lower than that of the holoprotein [105].

$$\triangle G_{folding}(holoprotein) = \triangle G_{folding}(apoprotein) + \triangle G_{hemebinding} \tag{4.1}$$

Holoprotein denaturation studies [125] revealed that bMcb5 was significantly less stable than rOMb5. The stability difference between the two isoforms was consistent in both thermal denaturation experiments (T_m rOMb5 = 85.6 °C, T_m bMcb5 = 65.5 °C) and chemical denaturation experiments using guanidium hydrochloride as chaotropic agent.

The evaluation of heme binding strength was accomplished by two methods, heme transfer to apomyoglobin and NMR spectroscopy. Silchenko *et al* [125] observed that in heme transfer experiments, the rate of heme transfer was significantly faster for bMcb5 than for rOMb5. 1D-NMR spectroscopy revealed that the

binding of heme to CYB5 differs when comparing bMcb5 and rOMb5 [112, 141]. When freshly expressed CYB5 is reconstituted with heme, it can bind to the protein in two orientations that differ by a 180° rotation about the porphyrin's α, γ meso axis (See figure 4.1).

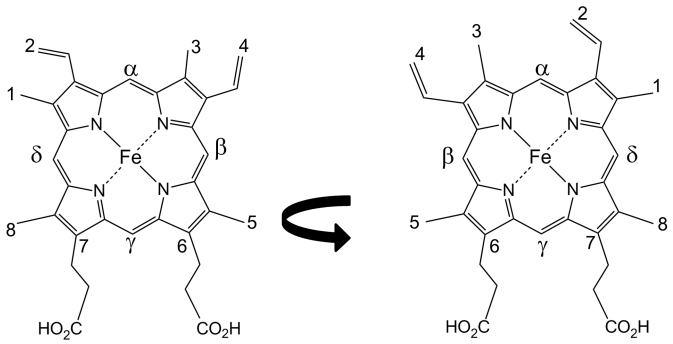

Figure 4.1: Two heme orientations that result in heme binding disorder in CYB5 proteins

Heme orientation in CYB5 proteins is heterogeneous due to binding of the heme in the two orientations. The two forms of the protein bound to different heme orientations, are steroisomers (specifically diastereomers) and therefore are hypothetically separable. Heme binding by apocytochrome b5 is a kinetically driven process, so the two possible isomeric proteins that can be obtained are formed in an approximately 1:1 ratio, but one of the two isomers is favored at equilibrium. Studies involving the selectivity in heme binding was first investigated using bMcb5 [67]. Equilibrium in bMc b5 occurs within two days at pH 7 and 25 C, with a final ratio of major (A) to minor (B) orientations of ~8:1 as demonstrated by NMR spectroscopy (The major orientation was designated as A and all subsequent studies have referred to that orientation as A) [141, 135]. In contrast, when freshly purified, the heme binding ratio in rOMb5 is 1:1 (A:B) and does not change at physiological temperatures [112, 125]. This ratio is altered slightly only when rOMb5 is heated to 68 °C for 8 hours (1:1.3, A:B ratio [125]). The ratio stays at this value even after extended incubation at 25 ºC, indicating that heme is kinetically trapped under physiologically relevant conditions. rOMb5 was the first protein in the CYB5 family shown to exhibit kinetically trapped ferric heme, and to display preference in binding to the B heme orientation [125]. As seen for rOMb5 and bMcb5, the temperature at which the heme binding ratio changes can be used to qualitatively estimate the relative heme binding strengths when comparing the two proteins and associated mutants.

Analysis of the sequences and structures (see figure 4.2) of the two isoforms revealed important details that help explain the biophysical differences between the two isoforms. Importantly a hydrophobic cluster surrounding the heme was identified which differed at residues 18, 32, 47, 25 and 71 (see figure 4.2(b) and figure 4.2 (c)). It was hypothesised that presence of more hydrophobic interactions in the heme pocket of rOMb5 was responsible for its greater stability when compared to bMcb5.

```
        1         11        21        31        41        51        61        71        81
bMcb5   SKAVKYYTLEEIQKHNNSKSTWLILHYKVYDLTKFLEEHPGGEEVLREQAGGDATENFEDVGHSTDARELSKTFIIGELHPDDRSKITKP
rOmb5   DPAVTYYRLEEVAKRNTAEETWMVIHGRVYDITRFLSEHPGGEEVLLEQAGADATESFEDVGHSPDAREMLKQYYIGDVHPNDLKPKDGD
        . **.** ***: *:*.:::.**:::* :***:*:**.********* ****.****.*******.****: * : **::**:* .
```

(a)

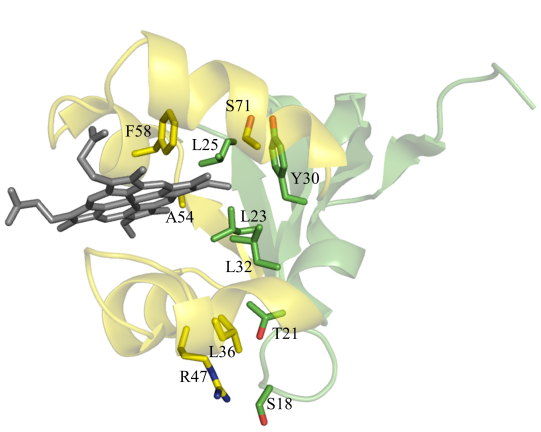

(b) bMcb5

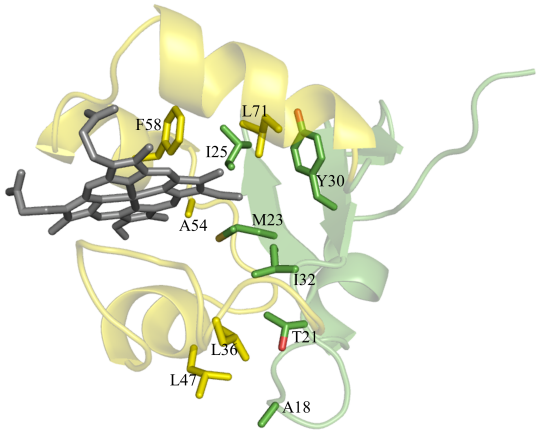

(c) rOMb5

Figure 4.2: Comparison of sequences and structures of bMcb5 and rOMb5 (a) Clustal X [25] alignment of bMcb5 and rOMb5. Residues lining the heme binding pocket are coloured red, with the histidines coordinated to the heme underlined. Specific differences pertaining to this chapter are colored green. Conserved amino acid residues are marked by '*' (identical), ':' (highly conserved) or '.' (weakly conserved). (b) Structure of bMcb5 (PDB code 1CYO [35]) in cartoon form. The backbone is colored yellow for residues in core 1 and colored green for residues in core 2. Specific amino acids and the heme (colored grey) are shown as sticks. (c) Structure of rOMb5 (PDB code 1B5M [118]) in cartoon form. The coloring scheme is identical as in figure (b).The residues contributing to the hydrophobic network in rOM b5, and the corresponding residues in bMc b5, are shown as sticks

Initial studies aimed at characterizing the biophysical differences between rOMb5 and bMcb5 involved a systematic replacement of the residues (see figure 4.2 for positions of the residues in the corresponding proteins) present in the hydrophobic cluster of rOMb5 with the corresponding bMcb5 residues [6]. The series of mutations included rOMb5 I32L, rOMb5 A18S/L47R and rOMb5 I32L/L47R/A18S that disrupted the network of hydrophobic interactions on one side of the heme. Thermal denaturation experiments of the corresponding holoproteins revealed a steady decrease in T_m values when going from the single mutant to the triple mutant (rOMb5 > rOMb5 I32L > rOMb5 A18S/L47R > rOMb5 I32L/L47R/A18S) [6]. The fastest rate of heme reorientation in this set of mutants was seen in rOMb5 I32L/L47R/A18S mutant which exibited a heme reorientation at 45 °C (6 hrs incubation), a temperature at which heme is kinetically trapped in rOM b5 [6].

The series of mutations was extended, on the opposite side of the heme, to study the influence of positions 71 (rOMb5 L71S) and 25 (rOMb5 I25L) [27]. No significant difference was seen in the T_m of rOMb5 I25L (84.7 °C) when compared to rOMb5. The rOMb5 S71L mutation, however, displayed a significantly lower T_m (75.3 °C) when compared to rOMb5. A quintuple mutant of rOMb5, which incorporated all the mutations mentioned above, had a T_m (69.7 °C) that was very close to that of bMcb5 [27]. Thus system-

atic replacement of the heme binding pocket of rOMb5 with the corresponding bMcb5 amino acid residues created a destabilized holoprotein.

Removal of heme from the CYB5 holoproteins results in complete unfolding of core 1 [90]. Core 2 of the apoCYB5 is well folded with secondary structural elements α1, α2 and β1- β4 all retaining structure similar to the holoprotein [40]. A direct comparison of the wild type apo bMcb5 and apo rOMb5 was performed in our laboratory [29]. In that study, it was found that the T_m of apo rOMb5 (51 °C) is higher than the T_m of apo bMcb5 (44 °C). This was attributed to peristence of hydrophobic interactions in core 1 of rOMb5 despite removal of heme that led to a more collapsed empty heme binding pocket than is present in apo-bMc b5. This results in a larger increase in solvent exposure of the polypeptide for apo-rOM b5 than for apo-bMc b5 upon unfolding and, thus, a greater change in solvent structure [29]. Results from the same study indicated that bMcb5 had residual non-random secondary structure even on unfolding. This was attributed to a more robust β sheet network that maintained structural homogeneity of the less stable apo bMcb5 core 2 [29].

The disruption of the hydrophobic network in rOMb5 and its effects on the apoprotein stability was also studied in our laboratory [30]. In those studies, the apo form of the mutant rOMb5 L71S displayed a far lower T_m value (33 °C) than that of even apo bMcb5. Circular dichroism spectroscopy experiments also revealed complete disorder within core 1 of apo rOMb5 L71S that also extended into core 2. This study showed the importance of Leu at position 71 (present in the disordered region of core 1 in apo rOMb5) in maintaining the structure within core 2 of apo rOMb5.

Further analysis of the structures of holo bMcb5 and holo rOMb5 revealed the presence of a motif present in core 2 of bMcb5 [143]. The amino acid at position 22 (located in core 2) in both bMcb5 and rOMb5 is Trp. The nature of amino acids in the vicinity of Trp22, however, differs in the case of the two proteins. In bMcb5, Trp22 is involved in a π stacking interaction with His15. In addition, His15 in bMcb5 is stabilized by a hydrogen bonding network involving Ser20 and Glu11 (see figure 4.3 a). In the case of rOMb5, the amino acids at corresponding positions are Arg15 and Glu20 (see figure 4.3 b). A protein engineering study at our laboratory [142] aimed at increasing the stability of rOMb5 generated a double mutant (rOMb5 R15H/E20S, OM2m herein) that had a much higher holoprotein T_m (~ 93 °C). The holoprotein effect was a result of a more stable apo OM2m (T_m = 65 °C).

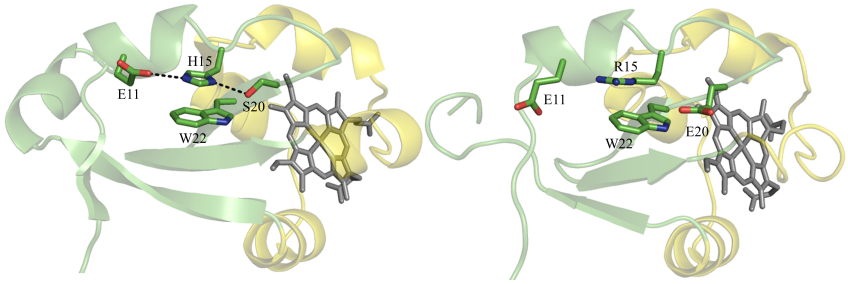

(a) bMcb5 (b) rOMb5

Figure 4.3: Difference in packing of residues present in Core 2. Holoprotein structures of bMcb5 (PDB code 1CYO) and rOMb5 (PDB code 1B5M) are shown as cartoons. Residues lining core 1 are colored yellow and residues lining core 1 are colored green. Heme is colored grey and shown as sticks. Specific residues demarking the differences in the two proteins are also shown as sticks. Hydrogen bonds are indicated as black dashes.

Recent studies in our group have aimed at incorporating residues from core 1 of rOMb5 into corresponding positions in bMcb5. The first study in this series was the creation of a point mutant that replaced Ser71 of bMcb5 with Leu (McS71L herein) [135]. McS71L holoprotein displayed unique behavior with respect to heme binding when compared to bMcb5. The equilibrium heme orientation ratio (A:B) at 25 °C was 1:8 in McS71L; a complete reversal of heme orientation preference when compared to bMcb5. In addition, based on NMR experiments and heme transfer data, it was seen that McS71L bound heme more weakly than wild type bMcb5 [135].

This chapter details experiments that involved a step-by-step replacement of the entire hydrophobic patch of rOMb5 into Mcb5 (Mc6m). Six additional mutations were added to Mc6m that introduced the core 1 of rOMb5 into bMcb5 to give a hybrid protein which we will refer to as hybb5. Details of the complete set of mutants and comparison to bMcb5 and rOMb5 are given in figure 4.4.

```
                    3       11        21        31        41        51
Mcb5        -------AVKYYTLEEIQKHNNSKSTWLILHYKVYDLTKFLEEHPGGEEVLREQAGGDAT
McS71L      -------AVKYYTLEEIQKHNNSKSTWLILHYKVYDLTKFLEEHPGGEEVLREQAGGDAT
Mc2m        -------AVKYYTLEEIQKHNNSKSTWLIIHYKVYDITKFLEEHPGGEEVLREQAGGDAT
Mc4m        -------AVKYYTLEEIQKHNNSKSTWMIIHYKVYDITKFLEEHPGGEEVLREQAGGDAT
Mc6m        -------AVKYYTLEEIQKHNNAKSTWMIIHYKVYDITKFLEEHPGGEEVLLEQAGGDAT
hybb5       -------AVKYYTLEEIQKHNNAKSTWMIIHYKVYDITRFLSEHPGGEEVLLEQAGADAT
rOMb5       -------AVTYYRLEEVAKRNTAEETWMVIHGRVYDITRFLSEHPGGEEVLLEQAGADAT

                   61        71
Mcb5        ENFEDVGHSTDARELSKTFIIGELHPDDR--- 82
McS71L      ENFEDVGHSTDARELLKTFIIGELHPDDR--- 82
Mc2m        ENFEDVGHSTDARELLKTFIIGELHPDDR--- 82
Mc4m        ENFEDVGHSTDARELLKTFIIGELHPDDR--- 82
Mc6m        ENFEDVGHSTDARELLKTFIIGELHPDDR--- 82
hybb5       ESFEDVGHSPDAREMLKTFIIGELHPDDR--- 82
rOMb5       ESFEDVGHSPDAREMLKQYYIGDVHPNDL--- 82
```

Figure 4.4: Complete set of mutants in Mcb5 along with nomenclature. The mutations are colored blue and underlined, residues lining core 1 are colored red.

4.2 Results and Discussion

4.2.1 Thermal denaturation of the mutants

UV- Vis spectroscopy was used to monitor the effect of temperature on the stability of the mutant and wild type proteins. In these experiments, heme changes from the bis-His ligated form (present in CYB5) to free or nonspecifically bound heme. Spectrophotometrically, the bis-His ligated form has a sharp Soret band with a λ_{max} of 412 nm while free/non specifically bound heme has a broader Soret band and λ_{max} of 390 nm. Changes in the absorbance in the Soret band at 412 nm is used to monitor the unfolding of holo CYB5. The data and the corresponding fits are shown in figure 4.5. T_m values obtained from the curves by fits to an equation describing two-state unfolding are reported in table 4.1.

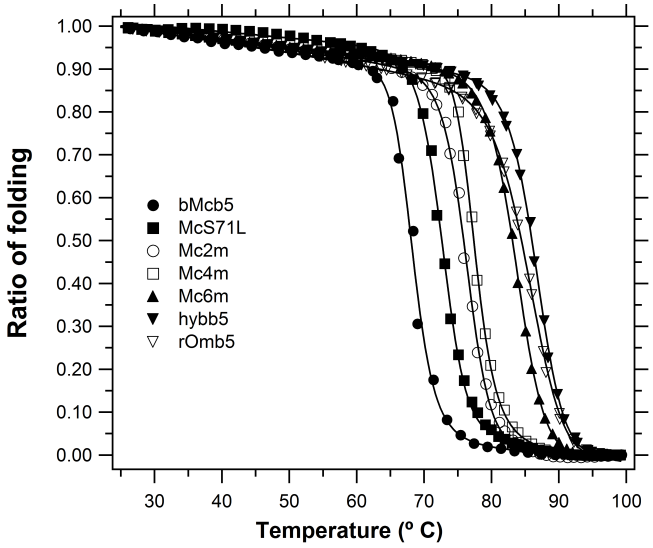

Figure 4.5: Thermal denaturation of holoproteins.

Protein	T_m value (°C)†
bMcb5	67.6 ± 0.3
McS71L	74.9 ± 0.2
Mc2m	76.4 ± 0.4
Mc4m	78.3 ± 0.1
Mc6m	83.1 ± 0.4
hybb5	86.5 ± 0.3
rOMb5	85.5 ± 0.5

Table 4.1: Average thermal denaturation midpoint values. †Obtained from three independent experiments

Replacement of Ser71 in bMcb5 with Leu led to an increase in holoprotein thermal stability; the mutation increased the T_m value by ~ 7 °C. Previously published work [135] had indicated that McS71L bound heme

more weakly than wt bMcb5. This led us to the conclusion that the enhancement of holoprotein thermal stability in McS71L was primarily a consequence of apo protein stabilization. Successive replacement of the hydrophobic pocket surrounding the heme (in Mc2m and Mc4m) only led to a modest increase in T_m value compared to McS71L.

The next significant increase in T_m value was seen in the mutant Mc6m wherein the entire hydrophobic cluster in the heme binding pocket of bMcb5 was replaced with the corresponding residues in rOMb5 (see figure 4.2). The T_m of Mc6m was only slightly lower than the T_m value of wt rOMb5. The introduction of six additional core 1 residues of rOMb5 into Mc6m (hybb5) yielded a protein that was only slightly more stable than rOMb5. In fact the T_m of hybb5 is only 1 °C higher than that of wt rOMb5. We next turned our attention to the effects of the mutations on strength of heme binding.

4.2.2 ^{1}H 1D-NMR spectroscopy

CYB5 holoproteins are heterogeneous, with heme binding to the protein in two orientations [112, 141]. Peaks seen in the low field region of the NMR spectrum correspond to specific substituents in the porphyrin ring. Signals arising from the heme in both bMcb5 and rOMb5 have been previously assigned using multi dimensional NMR experiments [87, 112]. The corresponding signals in the mutants are assigned based on the similarity in spectra to the wild type proteins, peak integrals and changes in peak integrals as heme isomer ratio changes. As an example, the differences in spectra of Mc2m and Mc4m are shown (see figure 4.6).

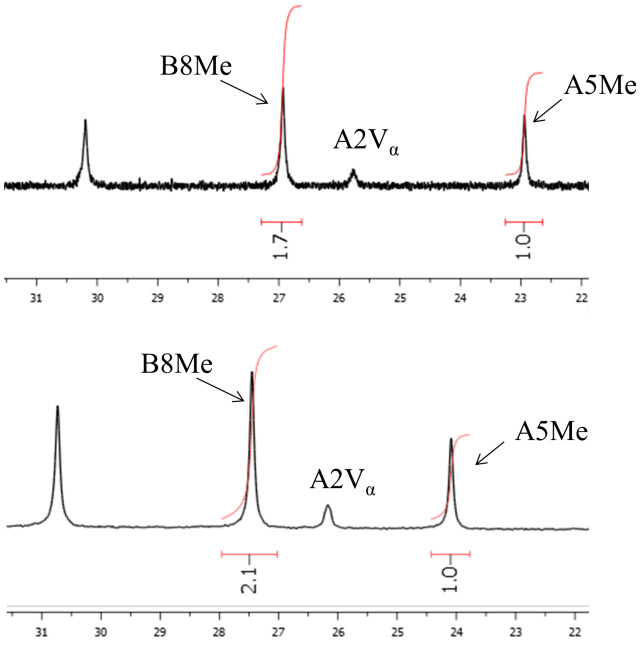

Figure 4.6: ^{1}H NMR spectra (22- 35 ppm) of Mc2m (top) and Mc4m (bottom) after equilibration. Integrals corresponding to specific peaks are indicated in red. For evaluation purposes, the integral of the A5 methyl peak is assigned as 1.0.

A qualitative approach was used to evaluate the relative heme binding strengths in the mutant holoproteins. This involved analysis of the spectra immediately after holoprotein purification followed by incubation of the holoprotein sample at 5 °C temperature increments till there was a change in heme isomer ratio. Additional spectra were obtained every 24- 48 hours until no further change in the heme isomer ratio was observed. A potential problem from this approach is the inability to obtain rate constants of heme isomer equilibration for all proteins in the study, given the wide differences in temperature required to observe equilibration. However relative heme binding strength can be estimated by the lowest temperature at which the first change in heme isomer ratio is observed. Using this method, the wild type rOMb5 was also analyzed as a control. Spectra obtained at equilibrium are shown in figure 4.7 and the temperature at which the heme isomer ratio changes is given in table 4.2.

Protein	Temperature (° C)	Initial isomer ratio (B:A)	Final Isomer ratio (B:A)	Time
bMcb5[‡]	< 25	1:1	1:8	48 hours at 25 °C
McS71L[‡]	< 25	1:1	8:1	30 hours at 25 °C
Mc2m	25	1.7:1	1.3:1	72 hours at 37 °C
Mc4m	30	1:1	2:1	< 24 hrs at 42 °C
Mc6m	42	1:1	2.3:1	5 days at 42 °C
hybb5	52	1:1	1.5:1	5 days at 52 °C
rOMb5[§]	65	1:1	1.2:1	8 hours at 68 °C

Table 4.2: Temperature at which heme isomer ratio first changes and final isomer ratio in each mutant. [‡]Previously in ref [135] [§]Previously in ref [125]

NMR data revealed that all mutations introduced in bMcb5, except the S71L point mutation, increased the heme binding strength. As noted above, the Ser to Leu mutation in bMcb5 switched the isomer preference in heme binding compared to bMcb5 with isomer B being the major isoform bound to the holoprotein. Restoration of heme binding properties similar to wt rOMb5 is seen as more mutations are progressively introduced to core 1 of bMcb5. The final mutant in the series, hybb5, displays a final isomer ratio that is very similar to that of rOMb5. This is expected since core 1 of hybb5 is the most similar to core 1 of rOMb5 (see figure 4.4) when compared to the rest of the mutants. However the heme binding strength of rOMb5 is not replicated in hybb5. Though the final equilibrium heme isomer ratio in hybb5 is similar to rOMb5, the temperature at which the first observable change in heme isomer ratio occurs is 13 °C lower than that of rOMb5. In addition, when the spectra of hybb5 and rOMb5 are compared (11-32 ppm region, see figure 4.6), positions of specific peaks are different in the two proteins. This indicates that the heme binding environment of rOMb5 is not completely reproduced in hybb5.

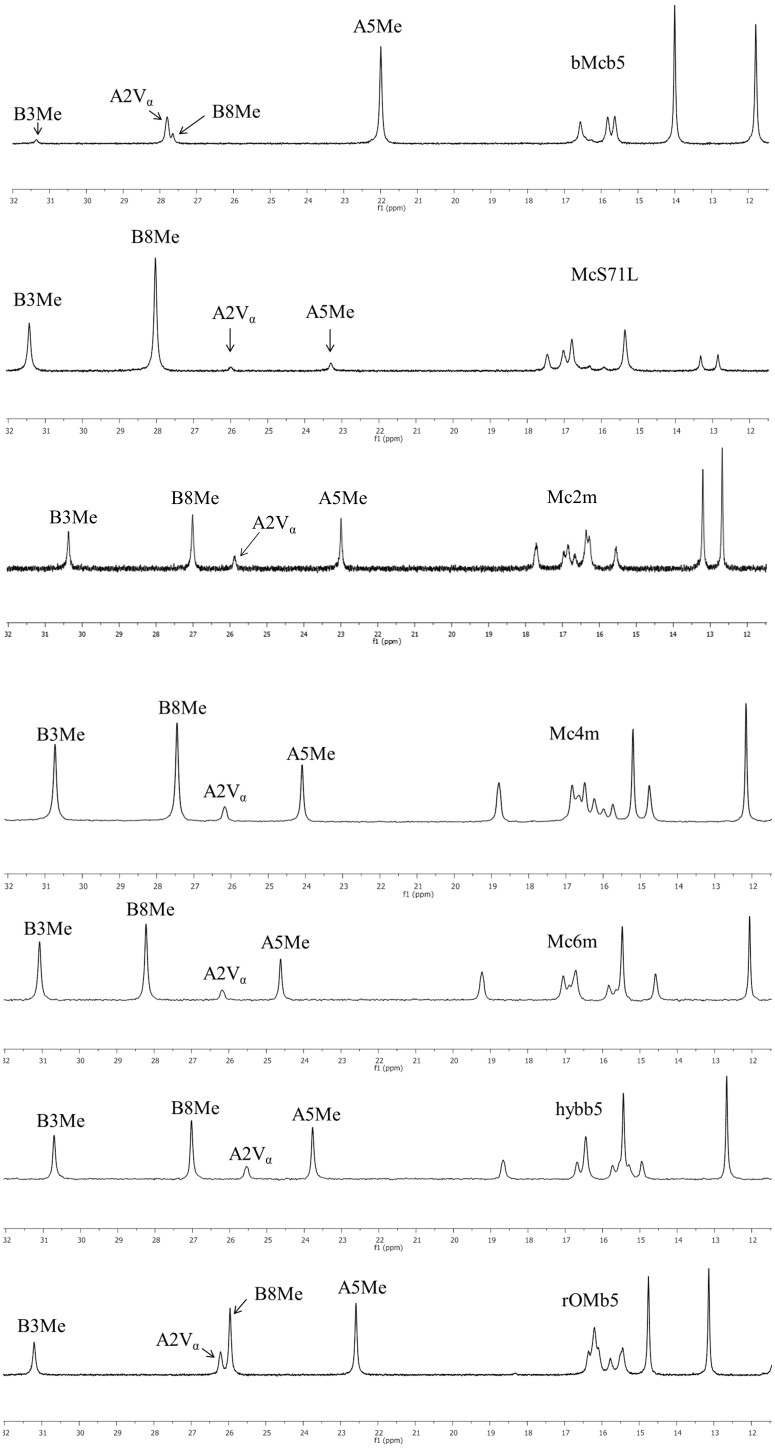

Figure 4.7: NMR spectra of the holoproteins at equilibrium. Integrals of specific peaks B8Me and A5Me are used to calculate heme isomer ratios as presented in Table 4.2.

Comparison of the hydrophobic patch in hybb5 and rOMb5 The X-ray crystal structure of hybb5 was solved to a reslution of 1.7 Å (PDB code 3OZZ) and compared with the recently solved structure of rOMb5 (PDB code 3MUS). As hown in figure 4.8c, the mutations introduced in hybb5 have not altered the

CYB5 fold significantly. In terms of backbone, most of the mutations introduced in hybb5 introduce small differences compared to the corresponding residues in rOMb5, some amino acid residues in hybb5 adopt different side chain conformations when compared to rOMb5 (see figures 4.8a and 4.8b). Most prominent among them are the residues Met23, Leu36, Leu47 and Thr21. The Leu36 and Leu47 side chains are solvent-exposed, and therefore may be expected to explore multiple conformational states. Differences in their conformations relative to wild-type rOMb5 may thus reflect differences in crystallization conditions and/or crystal morphology. Moreover, the different conformations observed for these surface residues in the hybb5 structure may necessitate the altered conformations adopted by the buried residues Thr21 and Met23. Nonetheless, it is reasonable to conclude that the rOMb5 hydrophobic patch has not been perfectly recapitulated in hybb5. This is further suggested by the NMR data in figure 4.7, which reveals differences in heme chemical shifts for the two proteins. These differences may contribute to the weaker heme binding of hybb5 in comparison to rOM b5.

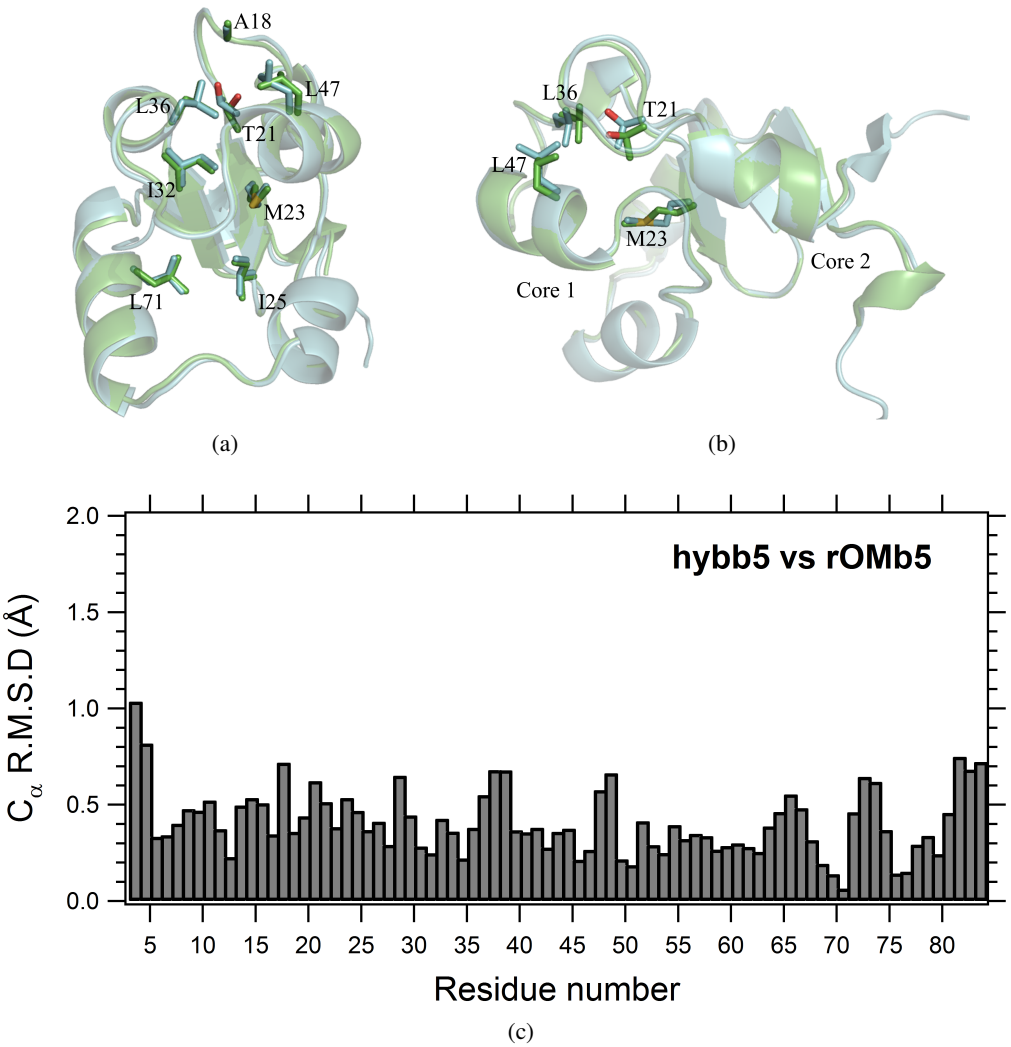

Figure 4.8: Structural alignment of hybb5 and rOMb5. Alternate views of the overlay of the structures of hybb5 (green) and rOMb5 (blue) are shown in (a) and (b). The polypeptide is shown as cartoon with specific amino acids depicted in stick form. For sake of clarity, heme is not shown. (c) C_α RMSD plot of hybb5 and rOMb5.

When the results from the holoprotein thermal denaturation and NMR spectroscopy experiments are considered together, it led us to hypothesize that the increased T_m value seen in McS71L in comparison to bMcb5 is a consequence of increased apo protein stability (see equation 4.1). The greater thermal stability of hybb5 relative to rOM b5, despite evidence of weaker heme binding, also seems likely to be explained by greater apoprotein stability. To investigate this possibility, apo proteins of the two mutants (McS71L and hybb5) were subjected to examination.

4.2.3 Native gel electrophoresis and Apoprotein thermal denaturation

In our lab dynamic light scattering and native gel electrophoresis have been used to investigate the biophysical differences between apo bMcb5 and apo rOMb5. DLS studies give a quantitative estimation of the

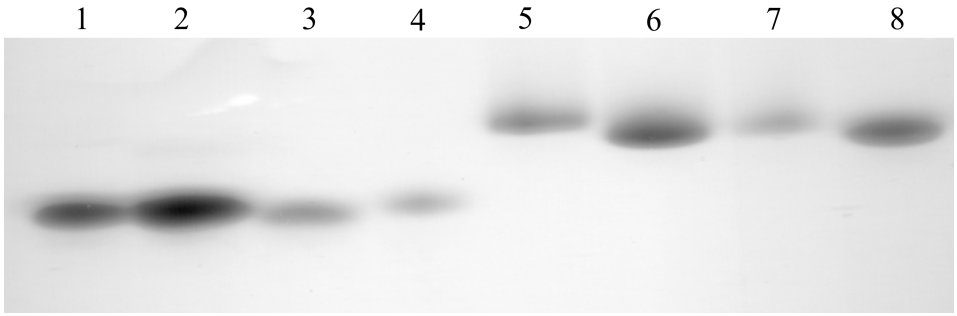

Figure 4.9: Native gel electrophoresis of holo and apo CYB5. Lanes 1, 2, 3 and 4 correspond to holo forms of bMcb5, McS71L, hybb5 and rOmb5 respectively. Lanes 5, 6, 7 and 8 correspond to apo forms of bMcb5, McS71L, hybb5 and rOmb5 respectively.

differences in the change in protein size that accompanies loss of heme in different proteins. Native gel electrophoresis provides a more qualitative estimate of these differences by observation of migration rates. The earliest study using this approach [29] revealed that apo bMcb5 had a 10 % increase in its hydrodynamic radius (R_H) compared to its holoprotein state. In contrast, apo rOMb5 only had a 3% increase in R_H compared to its holoprotein state. This revealed that apo rOMb5 was more compact than apo bMcb5 due to a more collapsed empty heme binding pocket. Native gel elecrophoresis data showed that migration of apo rOMb5 was faster than apo bMcb5, confirming the results obtained by DLS studies. Using this approach, the studies were expanded to include the L71S mutant of rOMb5 [30] and McS71L [135]. The rOMb5 L71S mutant in its apo state had an empty heme binding pocket even more expanded than that in apo-bMc b5, with conformation disorder extending into core 2. This result, when compared to apo rOMb5, is mainly due to the loss of a hydrophobic collapse when Leu was replaced with Ser. In contrast apo McS71L had a more compact empty heme binding pocket when compared to apo bMcb5. This same approach was used to evaluate the effect of the amino acid substitutions on the properties of apo hybb5. DLS studies could not be performed effectively given the tendency of the apo hybb5 to aggregate at high concentrations. Results of native gel electrophoresis are presented in figure 4.9

Native gel electrophoresis reveals that the apo forms of CYB5 migrate at a slower rate than the corresponding holoproteins. Two factors contribute to this retardation: (1) loss of the two negative charges from the heme propionates; and (2) expansion of the heme pocket and, thus, increase in polypeptide volume. It is also seen that the introduction of 12 mutations in bMcb5, to give hybb5, has not affected the the electrophoretic mobility of the holoprotein. Apo hybb5 migrates at a faster rate than apo bMcb5 indicating that the compactness of the empty heme binding pocket introduced in apo McS71L is maintained in apo hybb5. This also confirms the role of Leu at position 71 in maintenance of the compact heme binding pocket.

Apoprotein thermal denaturation experiments on apo McS71L using CD spectroscopy and differential scanning calorimetry (DSC) had been previuosly performed by Dr. Aaron Cowley in our lab, but have not been published. Thermal denaturation of apo hybb5 was studied using only CD spectroscopy and differential scanning calorimetry. DSC experiments on apo hybb5 failed due to reproducible aggregation of the unfolded apo protein at high temperatures. This was a consequence of the larger protein concentration requirement for

an effective DSC experiment when compared to the protein concentrations used in a typical CD experiment. Thus, only CD thermal denaturation experiments are reported in this dissertation.

CD spectroscopy on both apo McS71L and apo hybb5 revealed identical spectra in each case, both prior to and after thermal denaturation experiments. This indicated that the unfolding of apo hybb5 and apo S71L were reversible (See figure). Evidence that thermal unfolding occured in a cooperative two state process was provided by the presence of iso-dichroic behavior in CD spectra recorded as a function of temperature. As an example, temperature dependent far UV CD spectra of hybb5 are shown in figure 4.10.

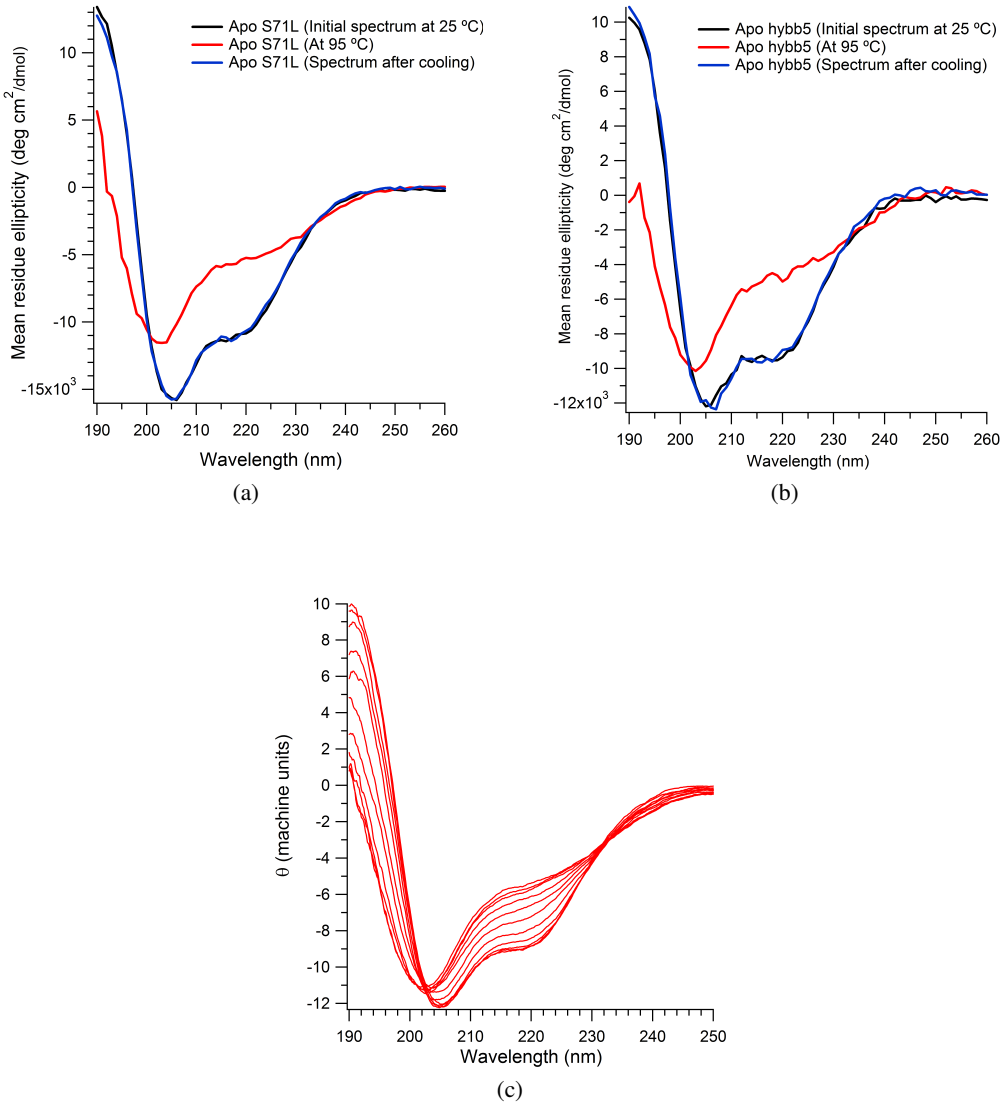

Figure 4.10: Demonstration of reversibility and Isodichroic behaviour during apoprotein thermal denaturation (a) Far UV CD spectrum of Apo S71L (b) Far UV CD spectrum of Apo hybb5 (c) Temperature dependent far UV CD spectra of apo hybb5. As temperature increases, θ at 222 nm steadily increases. Note the isodichroic points corresponding to wavelengths 203 nm and 232 nm

Protein	T_m (ºC)
apo bMcb5[§]	44.0 ± 0.4
apo McS71L[*]	62.2 ± 0.6
apo hybb5	56.2 ± 0.7
apo rOMb5[§]	50.4 ± 0.4

Table 4.3: Results from thermal denaturation experiments of apoproteins using CD spectroscopy. [§]Obtained from reference [29] [*]Obtained from the data fit in a single experiment.

CD thermal denaturation unfolding curves and corresponding fits are presented in figure 4.11 for apo McS71L and apo hybb5 along with previously published data [29] for apo bMcb5 and apo rOMb5. Tm values obtained from fits of the denaturation data are reported in table 4.3. The equation used to fit the data describes two state unfolding and accounts for sloping baselines [26].

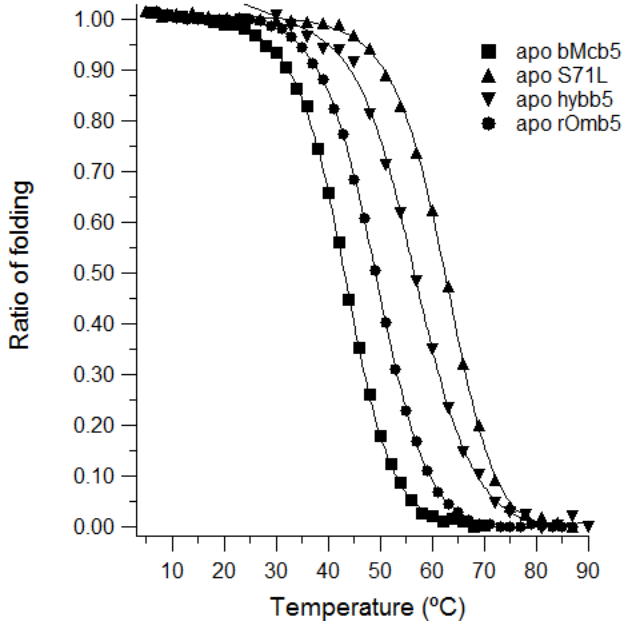

Figure 4.11: Thermal denaturation of apo proteins.

As seen from the data, the introduction of Leu at position 71 caused a large increase (18 ºC) in the T_m value when compared to apo bMcb5. This is quite remarkable given the location of Leu is in the disordered part of the apo protein. Additional mutations introduced in hybb5, though also occurring in the unstructured region, decreased the T_m value of the corresponding apoprotein when compared to apo McS71L. The T_m value of apo hybb5 is 6 ºC lower than that of apo McS71L but is still 5.8 ºC higher than that of apo rOMb5. This helps in understanding discrepancy in the holoprotein T_m trends (hybb5 > rOMb5 > McS71L > bMcb5) and the heme binding strengths (rOMb5 > hybb5 > bMcb5 > McS71L) and it can be concluded that increased apo protein stability has masked the weakening of heme binding in the mutants.

4.3 Conclusions

By the systematic incorporation of amino acids present in the heme binding pocket of rOMb5 into bMcb5, we successfully created a hybrid mutant (hybb5) that displayed holoprotein thermal stability similar to that of rOMb5. However the apparent increase in thermal stability was due at least in part, to an increase in apoprotein stability much greater than predicted on the basis of available data for apo-rOM b5 and apo-bMc b5. This initially masked the fact that hybb5 failed to fully recapitulate the heme binding properties of rOMb5. An important observation from this study was that mutations introduced even in the disordered region of the apo protein influence stability, especially by altering the compactness of the empty heme binding pocket. Within this disordered region, a key role is played by the nature of the amino acid at position 71. In a previous study [91], Lecomte and coworkers showed that mutations in core 1 that exerted a large impact on holoprotein stability exerted little effect on apoprotein stability, not surprising giving the location of the mutations in disordered core 1. The ability of residue 71 to exert a large impact on apoprotein stability can be attributed to its location near the point at which core 1 merges with core 2. When Leu occupies this position, its hydrophobic side chain can engage in non-specific interactions with apolar side chains of other residues on the core 1 side of the β sheet [135]. The polar side chain of Ser71 however is unable to engage in such interactions, and would prefer solvation by water.

Position 71 also provides clues as to the evolutionary divergence of CYB5 proteins. Sequence alignment of CYB5 proteins acquired from plants, fungi and insects indicated that position 71 is occupied by a hydrophobic amino acid (Leu or Met) [30]. With respect to this, CYB5 from *Musca domestica* (housefly) has a Met at position 71. The crystal structure of housefly CYB5 reveals that Met71 participates in interactions similar to conserved Leu71 in mammals [142]. Thus the progenitor of mammalian CYB5 also had a hydrophobic residue at position 71 whose change to Ser in the line leading to Mcb5s altered the biophysical properties of the holoprotein. Though the thermodynamic studies performed here do not reflect physiological conditions, it is possible that altered biophysical properties may have been the first step in functional divergence of the two CYB5 isoforms.

Chapter 5: Divergence of biochemical properties of CYB5; insight into the redox potential difference between isoforms

5.1 Introduction

Heme is a prosthetic group used by many proteins to carry out their diverse biochemical functions, which include electron transfer (cytochrome b_5, cytochrome c [73]), oxygen transport and storage (myoglobin, hemoglobin [73]), drug metabolism (cytochrome P450 [45]), cell signaling (guanylate cyclase [63]) and gene expression control (Bach1 [136]). Among hemes, the molecule heme-b (also called protoheme IX, see figure 5.1) is the most well studied since it is a co factor in many classes of molecules including the globins, peroxidases, CYB5 and cytochrome P450 (CYP450) [22].

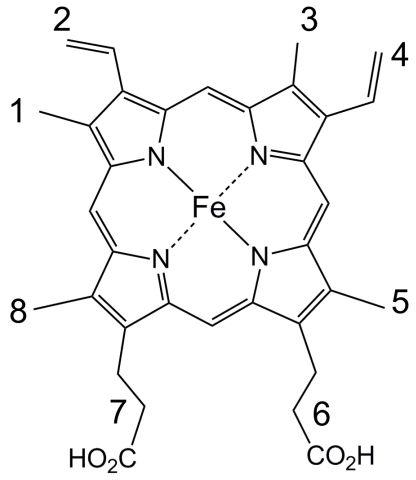

Figure 5.1: Structure of heme-b. Methyl groups are present in position 1,3,5 and 8; vinyl groups at positions 2 and 4; propionate groups are present in positions 6 and 7 of the porphyrin ring

5.1.1 Heme binding in CYB5

As seen in figure 5.1 iron in heme b is coordinated to four nitrogen atoms of the porphyrin ring (also called equatorial ligands) . This leaves two axial ligation sites, at least one of which in heme proteins is ligated by an amino acid side chain. CYB5, the subject of this thesis, is hexa-coordinated, with the side chains of two histidine residues serving as axial ligands (His39 and His63 based on the numbering scheme introduced in [83]). The coordination of the heme iron by His39 and His63 is the strongest interaction between the protein and heme. Binding of heme in the protein core is supplemented through Van der Waals interactions between the porphyrin ring and hydrophobic amino acid side chains. Characteristic properties of heme binding sites include the presence of highly aliphatic amino acid side chains (Ala, Leu, Met, Ile, Val) lining the heme binding pocket. Aromatic amino acids (Tyr, Trp, Phe) are also common features, within the heme binding pocket, whose side chains interact with the porphyrin ring [108].

In CYB5, one of the propionate groups of heme extends into solvent, while the other forms hydrogen bonds with both the side chain and backbone of invariant residue Ser64 (see figure 5.2b). This provides

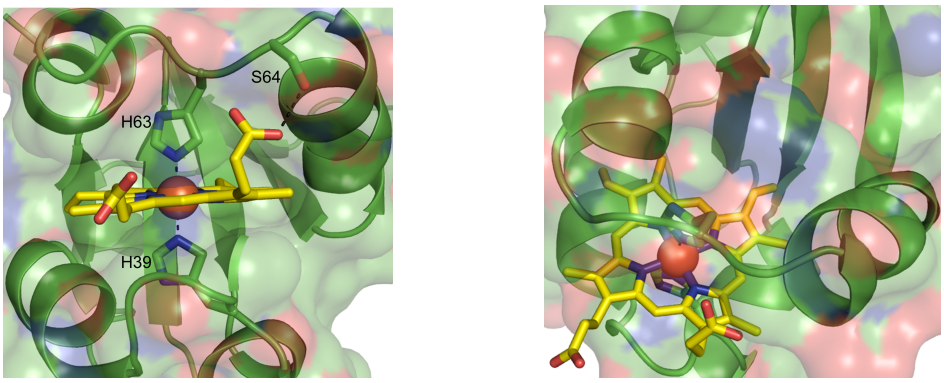

(a) (b)

Figure 5.2: Heme binding in CYB5. The structure of CYB5A (PDB id 1CYO) [35] is shown with the polypeptide in green cartoon and surface representation. The heme is colored yellow with the iron atom shown as a red sphere. (a) Bis- His coordination in CYB5A. The two His residues are shown as sticks, the coordination bonds (axial ligand) and the hydrogen bond between Ser 64 and the heme propionate are shown as black dashes. (b) This figure shows the burial of the hydrophobic components of heme further into the protein and the different dispositions of the two propionate groups.

stability to the protein, as demonstrated in studies in which heme is replaced by its dimethyl ester analog [110, 50].

5.1.2 Redox potentials of CYB5

Microsomal cytochrome b5 (CYB5A) and outer mitochondrial cytochrome b5 (CYB5B) differ from each other with respect to their biophysical properties (thermal stability, stability towards chaotropic agents) [6] and their redox potentials (also known as midpoint potentials, or E_m values) [7]. Early electrochemical studies revealed that the E_m value of bovine CYB5A (bCYB5A) is + 0.8 mV vs the standard hydrogen electrode (SHE) [141] and is considerably more positive than the E_m value of rat CYB5B (rCYB5B, -102 mV vs SHE) [114]. Various experiments have been performed on CYB5 and other proteins in an attempt to delineate the factors responsible for redox potential control in heme binding proteins. The details of the experiments and the conclusions are summarized below.

Electrochemical studies of wild type CYB5 Many studies have investigated the redox potential modulation of wild type CYB5 proteins and it has been seen that E_m values of CYB5 proteins are extremely sensitive to experimental conditions. Electrochemical studies of CYB5 proteins have utilized both voltammetric (kinetic) and potentiometric (equilibrium) methods. We will focus on the latter, since we used redox potentiometry in the work described herein. Initial redox potentiometry studies were performed in 'open' systems wherein anaerobic conditions were maintained by a positive pressure of N_2 or Ar. The first redox potentiometry study on CYB5 proteins was performed on bCYB5A isolated from beef heart that gave an E_m value of -9.0 mV vs SHE [111]. This study used only one mediator compound to facilitate communication with the measuring electrode. A subsequent study, using three mediator compounds, performed on the same protein revealed a more positive redox potential (-1.9 mV vs SHE) [141]. It was also seen that the usage

of three mediators decreased the electrochemical equilibration time thus reducing any 're-oxidation' caused by accidental oxygen leakage [141]. Other CYB5A proteins investigated include rCYB5A (E_m = 5 mV vs SHE) [82] and human CYB5A (hCYB5A, E_m = -9 mV vs SHE) [75]. Electrochemical studies on CYB5B proteins were first performed on the protein from rat [114]. rCYB5B had a more negative redox potential (E_m = -102.8 mV vs SHE) when compared to rCYB5A and bCYB5A. Subsequent studies on human CYB5B (hCYB5B) revealed that it also had a more negative redox potential (E_m = -40 mV vs SHE) but was significantly more positive than the E_m value of rCYB5B) [7].

Variation in E_m values of CYB5 have been reported on account of ionic strength [114] and temperature [111]. Recently it has been shown that E_m values of CYB5 change depending on the type of experimental method used [8]. Specifically, use of voltammetry typically gives more positive redox potentials than are obtained via potentiometry.

Cyclic voltammetry is a direct electrochemical measurement method that makes use of an electrode that also acts as the electron source to cause changes at the redox active center (Fe atom in the heme). In this method, reduction or oxidation are diffusion controlled processes [9] and involve only a thin layer of protein molecules surrounding the electrode. For some heme proteins, interaction with the electrode is prevented due to unfavorable electrostatic interactions, or because the heme is too deeply buried within the protein matrix [148]. To facilitate 'communication' with the electrode, researchers have used chemically modified electrodes, for example introducing positively charged groups that allow a negatively charged protein to interact electrostatically. An alternative approach is to utilize soluble polyions such as polylysine [146, 114] for mediating protein-electrode interactions. Typical problems with this approach are that these chemical modifications and polyions also interacted with the redox center and shift E_m values of CYB5 proteins [8, 114].

Redox potentiometry is an equilibrium based technique. The redox state of the protein is modulated by the systematic addition of a reducing agent (sodium dithionite) or an oxidising agent (potassium ferricyanide) which provide voltage ranges far exceeding typical biological E_m values [36]. Redox potentiometric experiments of CYB5 are extremely time consuming experiments as the redox active center (the heme iron embedded within the protein matrix) fails to interact effectively with the electrode. To enable communication with the electrode (not direct interaction as in cyclic voltametry), a mixture of redox active compounds (mediators) are added. The mediator molecules effectively act as a buffer to maintain the net potential of the reaction mixture and prevent any spontaneous process (for example oxidation by adventitious oxygen) from disturbing the equilibrium achieved [36]. The methodology used for analyzing CYB5 proteins in this dissertation is redox potentiometry since it avoids usage of agents that can affect the intrinsic potential of the proteins. This is particularly important when comparing E_m values of wild type and mutant CYB5 proteins.

5.1.3 Factors that modulate redox potential in heme proteins

Redox potential is calculated using the Nernst equation which can be written as follows

$$-nFE_m = \Delta G = \triangle G_{Fe^{3+}} - \triangle G_{Fe^{2+}} = -RTln\left[K_a^{Fe^{3+}}/K_a^{Fe^{2+}}\right] \tag{5.2}$$

where n is the number of electrons involved in the redox experiment, F is Faraday's constant, T is temperature, R is the gas constant and K_a is the affinity of the heme in the corresponding oxidation state [36, 108]. Equation 5.2 indicates that E_m values in CYB5 proteins are, in essence, free energy differences between the oxidized and the reduced species of the heme in the protein which can be extended to differences in the affinity of the protein to heme in its respective oxidation state.

The increasing availability of structures of heme proteins has enabled theoretical and experimental procedures to delineate the factors responsible for mid point potential (E_m) modulation [102].The major components that control redox potential in heme proteins include (i) the nature of porphyrin i.e. identity of substituent groups on the porphyrin ring [72] (ii) the type of ligation present on the heme [108] (iii) the hydrophobicity/ polarity of the environment in which the heme resides [85](iv) solvent accessibility of the heme [102] (v) structural / steric effects that cause heme distortion [99] and (vi) orientation of the heme within the protein complex [141]. In heme binding proteins, the type of ligation and the type of heme bound to the protein contributes most to the wide range of E_m values seen in nature (spanning 1000 mV) [108]. This chapter deals with CYB5 proteins that are bis-histidine coordinated to a type b heme. Hence, two factors responsible for modulating the redox potential specifically the nature of the pophyrin and the type of ligation are not explained in detail.

Modulating the dielectric surrounding the heme; hydrophobic, electrostatic effects and solvent accessibility of the heme. Controlling the micro-environment of the heme is a well studied mechanism of tuning redox potentials. The heme in the Fe^{3+} (ferric) state has a formal charge of +1 while in the Fe^{2+} (ferrous) state, it is formally neutral. The relative micro-environment of heme also determines the relative stabilization of the oxidation state of the iron in the heme. Thus, presence of the heme in a highly polar environment would stabilize the Fe^{3+} state relatively more than the Fe^{2+} state making the redox potential more negative. The dielectric of the heme reduces as it enters a hydrophobic matrix such as a protein, and based on the amino acid residues in the heme binding site, the relative polarity of the heme binding site influences the redox potentials [64]. Initial studies in bCYB5A [50] involved mutating Ser64, a residue involved in hydrogen bonding with the propionate group of heme (see figure 5.2). This residue was mutated to Ala. E_m values of the mutant revealed a more negative shift when compared to the E_m value of wild type bCYB5A (S64A mutant E_m= -4 mV vs SHE, wt bCYB5A = 3 mV vs SHE as reported) [50].

Further spectroelectrochemical experiments involving bCYBA [150] showed that mutation of Phe35 (a conserved residue in the heme binding pocket) to Tyr decreased the redox potential from 2 mV to -64 mV vs SHE. In the same study, the mutation of Phe35 to His resulted in a more positive E_m (-49 mV vs SHE) when compared to the F35Y mutant of bMcb5. This result correlated well with the hypothesis that hydrophobicity within the heme binding pocket was one of the factors responsible in tuning the redox potential of CYB5.

Solvent accessible surface area of the heme also relates to the microenvironment of heme in that increased solvent exposure generates a more polar environment for the heme thus stabilizing the Fe^{3+} state and decreasing redox potentials [108, 102]. A correlation between increasing solvent exposure of the heme and decreasing redox potential was observed by analysis of crystal structures of various heme binding proteins [137]. X-ray crystal structures of rat CYB5B mutants (V45I, V61I) also showed a decrease in heme

exposure when compared to the wild type rCYB5B structure that correlated well with the difference in redox potential (E_m V45I/V61I = -63 mV vs SHE, E_m wild type rCYB5B = -102 mV vs SHE) [113].

Electrostatic effects relate to the presence / absence of charged amino acids (Asp, Glu, Lys, Arg) in the heme binding pocket. Positively charged amino acids destabilize the Fe^{3+} state and will cause a positive shift in the E_m value. Conversely, negatively charged residues will stabilize Fe^{3+} relative to Fe^{2+} and cause a negative shift in redox potential. The E_m value is also dependent on the number of charged amino acids surrounding the heme. A classic study involving E_m shift due to charged residues was that published by Rodgers and Silgar [117]. In this study, they created a series of bCYB5A mutants in bCYB5A that involved replacing negatively charged residues on the protein surface with neutral amino acids at single and multiple sites. They also mutated 2 negatively charged residues in bCYB5A (Asp66 and Glu44) to lysines that completely reversed the charges. Shifts in E_m values of these mutants, when compared to wt bCYB5A, were in the direction expected for the type of mutation i.e. introduction of more negatively charged amino acids caused a negative shift in the E_m value while the substitutions involving positively charged amino acids showed a positive shift in E_m. Also disruption of a cluster of negatively charged amino acids by replacement with neutral analogues (Glu 44 $\rightarrow$ Gln, Glu 48 $\rightarrow$ Gln, Asp 60 $\rightarrow$ Asn) resulted in a more positive E_m value when compared to wt bCYB5A [117]. However the differences in E_m values of the single point mutants, when compared to wild type bCYB5A, were too small to interpret as significant (maximum difference as measured = 10 mV). Only the triple mutant of bCYB5A was observed to have a significant difference in E_m when compared to wt bCYB5A. The authors concluded that the redox potential of CYB5 was not significantly affected by the single point mutations that affected charge properties, but could be modulated by differences in overall surface electrostatic properties along with changes in the interior of the heme binding pocket.

Further studies were conducted on Val 61 in bCYB5A that was mutated to Glu and to Lys [149]. Val 61 is a highly conserved hydrophobic amino acid at the edge of the heme binding pocket and is positioned very close to the heme ligand His 63. The authors observed that the V61E mutation (increase in negative charge of the heme binding pocket that stabilizes the Fe^{3+} state) decreased the redox potential to -25 mV vs SHE and the V61K (an increase in positive charge of the heme binding pocket that destabilizes the Fe^{3+} state) mutation increased the redox potential to 17 mV vs SHE when compared to the wild type bMcb5 (-10 mV vs SHE in their study).

5.1.4 Heme within the heme binding pocket; orientation of the heme and His ligands

CYB5 proteins are heterogeneous because heme can bind in two orientations that differ by a 180° rotation about its α, γ meso axis (See figure 3.2). A study using bCYB5A [141] revealed a significant difference in E_m values when comparing wt bCYB5A with freshly heme reconstituted apo bCYB5A. Freshly reconstituted bCYB5A contains a 1:1 ratio of the two heme orientations, but at pH 7.0 and at 25 ºC equilibration to the thermodynamic ratio (A:B ~ 8:1) occurs within two days [141] (See chapter 3). On the basis of A:B orientation equilibrium values (obtained by NMR spectroscopy) and and time-dependent redox potentiometric data measurements, they calculated that the $E_m$value for the major orientation (orientation A, E_m = -1.9 mV vs SHE) was more positive than that of the minor orientation (orientation B, E_m = -26.2 mV vs SHE).

Though the difference in the E_m value was not considered to be physiologically significant, it is interesting given that the heme environment is identical in both orientations.

Another aspect with respect to heme orientation in CYB5 proteins is the relative angle between the heme and the histidine ligands. The definition of the vectors defining the heme and the histidine used to calculate this angle is important here given the heterogeneity of the heme binding to CYB5 proteins (detailed in the results section). Using rCYB5A as a model, it was seen that a point mutation in the heme binding pocket (A67V) altered the angle of heme binding in bCYB5A, as predicted by the researchers, without affecting the heme orientation [120] compared to wt rCYB5A. Furthermore, electrochemical analysis revealed that the A67V mutant of rCYB5A had an E_m value more negative (Em = -2.8 mV vs SHE) than that of wt bCYB5A (Em = 16.2 mV vs SHE). One might expect a positive shift in the E_m value given that the A67V mutation in the heme binding pocket decreases the polarity of the heme binding environment (thus making Fe^{2+} state more stable) and also leads to a reduced heme solvent exposure, but this is not the case. The authors attributed the negative shift seen in the rCYB5A A67V mutant to the change in heme- histidine angle that increased the stability of the Fe^{2+} state more than the Fe^{3+} state.

5.1.5 Heme distortion and steric effects

Free heme-b in solution has a planar conformation. When high quality crystal structures of heme proteins were analyzed, it was seen that the protein matrix introduces structural distortions in the heme porphyrin. These distortions are similar and conserved within functional classes of proteins [80] including in CYB5. Heme distortions may play important functional roles in many proteins. One well-known example is control of oxygen-binding affinity by doming of heme in hemoglobin [1, 15, 96]. Evidence that heme distortion can modulate E_m values was recently provided for in the heme nitric oxide/oxygen binding (H-NOX) protein from the thermophile *Thermoanaerobacter tengcogensis* [99]. In this study, using conservative mutations that altered the extent of heme non-planar distortion, they observed a 171 mV decrease in E_m value as the porphyrin became more planar [99]. When CYB5A and CYB5B structures are compared, only minor differences in heme distortion are seen. Moreover, heme is resolved in both orientations in rCYB5B and in many of its mutants (including ones generated for this dissertation), making it extremely difficult to detect changes in heme distortion. However, the possibility of heme distortion in modulating CYB5 redox potentials cannot be discounted.

5.2 Project goals

Various mutants were generated (see chapter 3) in order to delineate factors responsible for the large stability difference between bCYB5A and rCYB5B. In this chapter, we describe results of studies aimed at investigating the effects of the mutations on the redox potentials. We also report studies of human CYB5A and CYB5B (hCYB5A and hCYB5B respectively) and rat CYB5A (rCYB5A). The crystal structures of hybb5 and McS71L were solved in order to get a better understanding of the structure function relationships in these mutants. These structures are compared to the X-ray structures of bCYB5A (PDB code 1CYO), rCYB5B (pdb code 3MUS) and hCYB5B (PDB code 3NER). To get a better understanding of the dynamics

of the protein and its relation to modulation of redox potential, we performed 10 ns MD simulations on all of the above mentioned proteins. The results have provided an interesting insight into the biochemical evolution of the two proteins.

5.3 Results and Discussion

5.3.1 Experiments with holoproteins: Redox potentiometry and thermal denaturation studies

As mentioned in the introduction, redox potentiometry experiments are extremely time consuming. However, potentiometry is preferable to voltammetry because it doesn't require direct interaction between the protein and the electrode, which can cause shifts in the intrinsic redox potential especially if modified electrodes or mediators such as polylysine are used. Our approach to shorten total experiment times included performing the experiment in an anaerobic chamber and usage of a large number of mediators (each at a very low concentration) that covered the entire voltage range needed in the experiment. Nonetheless, a typical redox titration required 12-15 hours because equilibration at each potential took at least 10-13 minutes.

Changes in oxidation state of the heme during the redox potentiometry experiments were monitored via UV/Vis spectrophotomtery, using the heme α band at 557 nm. Isosbestic behavior was observed (See figure 5.3a) indicating absence of any intermediate species. Before performing redox potentiometry experiments with the mutants, wild type CYB5 proteins from different mammals were analyzed in order to compare results with published values. The wild type proteins used were bCYB5A, hCYB5A and hCYB5B, rCYB5A and rCYB5B. Representative data and fits of hCYB5A and hCYB5B redox titrations are presented in figure 5.3b and E_m values obtained for all wild type proteins are presented in table 5.1.

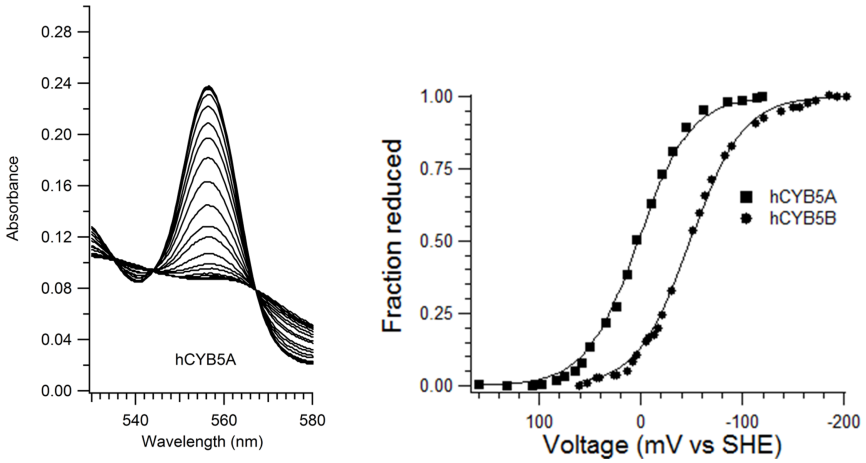

(a) (b)

Figure 5.3: Typical redox experiment data and Nernstian fit. (a) Demonstration of isosbestic behavior in visible spectra during a redox experiment with hCYB5A. The region corresponding to the α band used to calculate relative populations of reduced and oxidized protein is shown. Absorbance at 557 nm steadily increases as more aliquots of reducing agent are added. (b) Data from redox potentiometry experiments for hCYB5A and hCYB5B. The data points are fit to a one electron Nernst equation

Protein	E_m (mV vs SHE)[¥]	E_m(mV vs SHE)[§]
bCYB5A	6 ± 2	-1.9 [141]
rCYB5A	1.3 ± 0.7	5 [82]
hCYB5A	4 ± 1	-9 [75]
hCYB5B	-54 ± 1	-40 [7]
rCYB5B	-55 ± 1	-102.8 [114]

Table 5.1: E_m values of wild type proteins. [¥]Values represent the average and standard deviation from three independent experiments. [§]Previously published values and references

Our first redox potentiometric measurement was with hCYB5B. The E_m value obtained by us for hCYB5B was more negative than the published value (see table 5.1). It has to be taken into account that the experiment design with respect to the published $E_m$of hCYB5B [7] was similar to our experiment design except that an anaerobic environment was achieved without using a glove box.

Our next measurement was with rCYB5B which gave us a more positive E_m value than the published result (see table 5.1). The published E_m measurement was performed using an optically transparent thin layer electrode (OTTLE) [114]. Personal communication with Prof. Rivera revealed potential problems with the OTTLE setup. The experiments performed using OTTLE used a very high concentration of protein (mM range) in a very small volume (200-500 μL). This experimental design also lacks the ability to maintain a constant temperature in the system and temperature may increase as the experiment progresses. Previously published results indicate that as temperature increases, the E_m value becomes more negative. Our experiments were performed in a glove box and with strict temperature control. Our reaction cell volume was greater than 5 mL and the experiment was performed with constant stirring and a low protein concentration (~ 10 μM). The apparatus allowed for strict temperature control, temperature measurements performed every hour indicated little deviation ($\pm$ 1 ºC) from the target temperature (25 ºC). Reliability of our data is further strengthened by the low standard deviation and reproducibility we obtained during our experiments.

We next performed a redox titration with the well studied bCYB5A protein. The E_m value for bCYB5A obtained by us was consistent with previously published results [111, 141]. This further supported reliability of our experimental method and increased our confidence in the E_m values obtained for hCYB5B and rCYB5B.

When comparing CYB5 proteins from other mammals, it is interesting to note that all wild type CYB5A proteins tested here display an E_m value significantly more positive than the corresponding CYB5B proteins. The shift in E_m values between the two isoforms (in both rat and human) is ~ 60 mV. Given the conservation of sequences across organisms, we can reasonably hypothesize that a redox potential difference of 60 mV exists for the two CYB5 isoforms from all mammals.

An important conclusion from these redox potentiometric titrations is that redox potentials of rCYB5B and hCYB5B determined in this work are virtually identical (approximately -55 mV). As indicated in the introduction, the E_m values of CYB5 proteins are extremely sensitive to experimental conditions. We are

confident that the redox potentials determined in this study for rCYB5B and hCYB5B are valid for the stated conditions. There is little difference when comparing the protein sequences of rCYB5B and hCYB5B. In addition MD studies described in Chapter 3 revealed that there is little statistical difference in the average solvent accessible surface area of the heme in the two proteins. Finally, previously published cyclic voltammetry data for bCYB5A and rCYB5B recorded in the presence of varying concentrations of divalent metal ions revealed a constant ~ 70 mV difference in E_m values [114]. The difference in E_m values between bCYB5A and rCYB5B, as obtained in our work (~ 60 mV), is nearly the same as reported in [114].

After the methodology had been established, we shifted our attention to the mutant proteins. Included in this study were the mutants McS71L, Mc6m and hybb5 (see chapter 2 and chapter 4) which were compared to bCYB5A and rCYB5B. Results from redox potentiometry experiments for all the proteins are presented in table 5.2. Fits of the data obtained for bCYB5A, rCYB5B and the mutants McS71L, Mc6m and hybb5 are presented in figure 5.4.

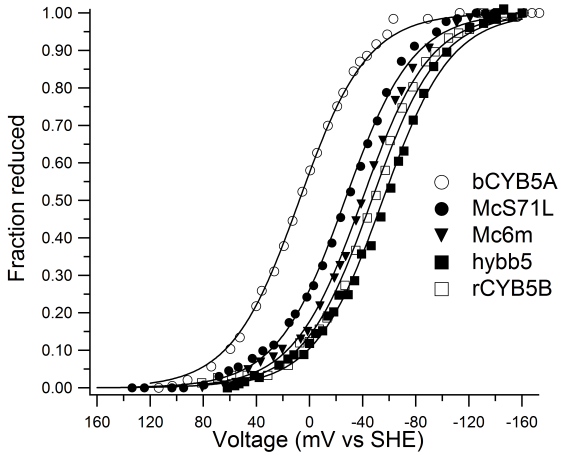

Figure 5.4: Redox titrations of wild type proteins compared to mutants.

Protein	E_m (mV vs SHE)
bCYB5A	6 ± 2
McS71L	-29.7 ± 0.7
Mc6m	-42.6 ± 0.8
hybb5	-61 ± 1
rCYB5B	-55 ± 1

Table 5.2: E_m values of the mutants compared to wild type proteins

Model compound studies in our lab [65, 28] using bis-Histidine ligated heme peptides (a model of heme iron coordination present in CYB5 proteins) have provided some insight into control of redox potential. In those studies, stability as indicated by strength of His to iron ligation was increased by (a) introduction of interactions between heme and the side chains of aromatic amino acids; and (b) decrease of peptide mobility

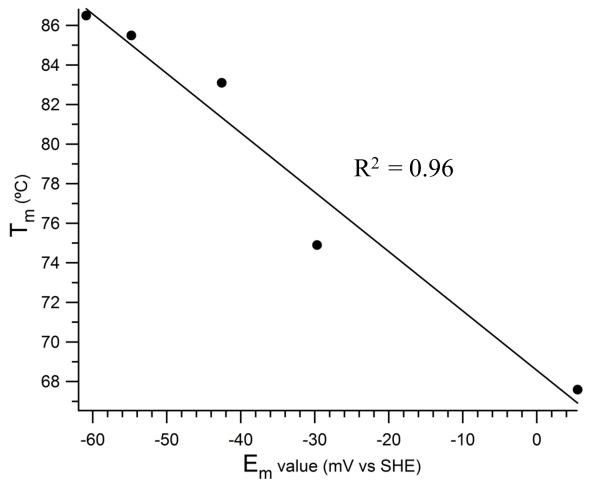

Figure 5.5: Correlation plot of thermal denaturation midpoints (T_m) and redox potentials (E_m values)

by the introduction of helices in the peptide through addition of 2,2,2-trifluoroethanol (TFE). It was seen that as the stability increased the redox potential became more negative. It was demonstrated that this occurred as a result of stabilizing His-Fe^{3+} ligation to a much greater extent than His-Fe^{2+} ligation. This occurred despite the fact that the aromatic side chain-heme interactions diminished heme solvent accessibility. Thus, changes in structure that alter His-heme affinity can outweigh other factors that are known to affect redox potential such as solvent exposure of the heme [28].

Stabilities of the holoproteins in this study (as indicated by their ferric T_m values) follow the trend bCYB5A< McS71L < Mc6m < rCYB5B $\leq$ hybb5 (T_m values of rCYB5B and hybb5 differ by only 1 ºC). The trend in E_m values for the same set of proteins is bCYB5A > McS71L > Mc6m > rCYB5B > hybb5. It should be noted that the energy difference between hybb5 and rCYB5B based on E_m values is only 0.15 kcal/mol. Nonetheless, these data reveal that increasing stability correlates well with decreasing redox potentials, as shown in Figure 5.5.

On the basis of the model studies described above, this led us to hypothesize that Fe^{3+} was being stabilized relative to Fe^{2+}, and that this was the primary determinant of the measured redox potential differences. Indeed, we had previously published a conjecture that differential stabilization of Fe^{3+} and Fe^{2+} was the basis of the difference in the rOM and bMc b5 redox potentials [28]. To evaluate relative stabilities of the various proteins in the Fe^{2+} state, we decided to perform thermal denaturation experiments of the ferrous form of the proteins. T_m values obtained in thermal denaturation experiments with CYB5 holoproteins have been used previously to compare stability in the oxidized and reduced states [144, 142].

Thermal denaturation midpoints of ferrous bCYB5A and rCYB5B have been reported previously [142]. Data corresponding to ferrous McS71L, Mc6m and hybb5 are reported here (see figure 5.6). Results from ferrous holoprotein thermal denaturation experiments are summarized in table 5.3. As a control, thermal denaturation of ferrous bCYB5A holoprotein was repeated.

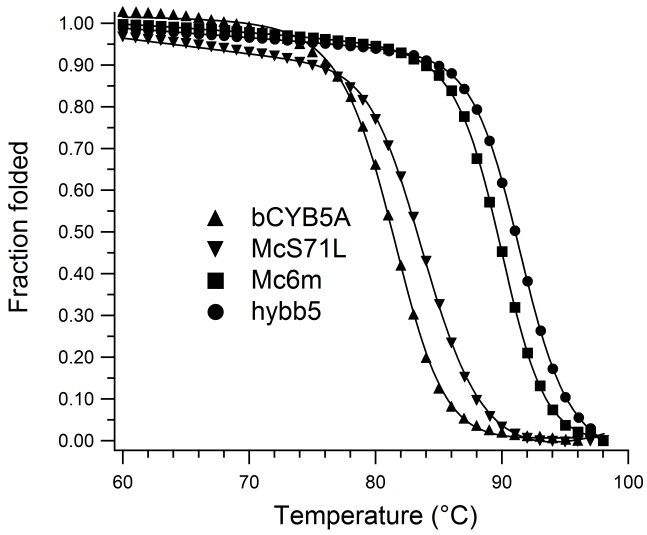

Figure 5.6: Representative plots of thermal denaturation of ferrous holoproteins and their corresponding fits

Protein	$T_m[Fe^{3+}]$ (ºC)§	$T_m[Fe^{2+}]$ (ºC)	$\triangle T_m[Fe^{3+}]$(ºC)	$\triangle T_m[Fe^{2+}]$(ºC)
bCYB5A¶	67.6 ± 0.3	79.4 ± 0.3	–	–
McS71L	74.9 ± 0.2	83.8 ± 0.7	7.3	4.4
Mc6m	83.1 ± 0.4	89.3 ± 0.1	8.2	6.5
hybb5	86.5 ± 0.3	90.9 ± 0.5	3.4	1.6
rCYB5B¶	85.5 ± 0.5	93.1 ± 0.9	–	–

Table 5.3: Results of thermal denaturation experiments. Average values and standard deviations from three individual runs are shown. §See chapter 3 ¶From reference [142]

Table 5.3 shows that mutations sequentially introduced into bCYB5A increased the T_m value of the ferric protein more than that of the ferrous protein, consistent with the above prediction. One problem with the above analysis is that heme orientation equilibration studies detailed in chapter 4 have revealed a trend in strength of ferric heme binding (Mcs71L < bCYB5A < Mc6m < hybb5 < rCYB5B) that is different from the trend in overall stability indicated by Tm values: bCYB5A < McS71L < Mc6m < rCYB5B < hybb5 (see chapter 4).

As demonstrated in Chapter 4, the higher T_m value of McS71L in comparison to bCYB5A, despite evidence of weaker ferric heme binding, is due to a large effect of the mutation on apoprotein thermal stability. Changes in apoprotein stability are likely to exert similar effects on thermal denaturation of the holoprotein in the Fe^{3+} and Fe^{2+} oxidation states. Table 5.3 shows that the S71L mutation increases Tm value in both the Fe^{+3} and Fe^{+2} states, but the increase is greater for the Fe^{+3} state. In light of the observation that ferric heme is bound less weakly in McS71L than in bCYB5A, we can reasonably conclude that the S71L

mutation has destabilized both the ferric and ferrous oxidation states, but has destabilized the ferrous state to a greater extent.

Each set of additional mutations also increases stability of the ferric state more than the stability of the ferrous state. Heme orientation equilibration data determined by NMR spectroscopy (see Chapter 4) have revealed that each set of mutations also substantially strengthens ferric heme binding. We can therefore conclude that each of these sets of mutations strengthens heme binding in both the ferric and ferrous oxidation states, but with a larger increase for the ferric state.

Recall from Chapter 3 that NMR spectroscopic studies of McS71L have revealed a reversal in the heme binding orientation within the protein relative to bCYB5A (McS71L [A:B] = 1:8.2, bCYB5A [A:B] = 8.2:1) [43]. In other words, the introduction of Leu at position 71 stabilized heme orientation B relative to heme orientation A. Our redox studies have now shown that this change in major heme orientation from A to B is accompanied by a 35 mV negative shift in redox potential. This is interesting in light of the studies by Walker et al [141] showing that the redox potential of bCYB5A with heme bound in orientation B is 27 mV more negative than that of bCYB5A with heme bound in preferred orientation A. That paper also presented a thermodynamic cycle indicating that the negative shift in redox potential was due to destabilization of Fe^{2+} relative to Fe^{3+}. In other work, Walker and others have argued that heme orientation B in bCYB5A is not only flipped by 180 degrees relative to orientation A, but is also rotated in plane [124]. This prompted us to obtain an X-ray crystal structure of the S71L mutant.

5.3.2 Crystal structure analysis of the McS71L mutant

McS71L crystallized with four molecules in the asymmetric unit (labeled A-D in the PDB file) and the structure was resolved to 2.4 Å. The crystal structure of McS71L (molecule C) is herein compared with the bCYB5A structure published by Durley and Mathews (PDB code 1CYO) [35]. It was interesting to note that crystallization of McS71L was notoriously difficult given the ease with which other CYB5 proteins and their mutants crystallized. We attributed this observation to the increased mobility of heme within the heme binding pocket as suggested in the original paper describing this mutant [135].

The overall structure of McS71L revealed that the secondary structure elements described in the CYB5 fold were maintained. A C_α backbone RMSD plot comparing McS71L and bCYB5A and the corresponding aligned structures is shown in figure 5.7. The RMSD plot indicates little difference between McS71L and bCYB5A (overall C_α RMSD (residues 3-84) = 0.5 Å).

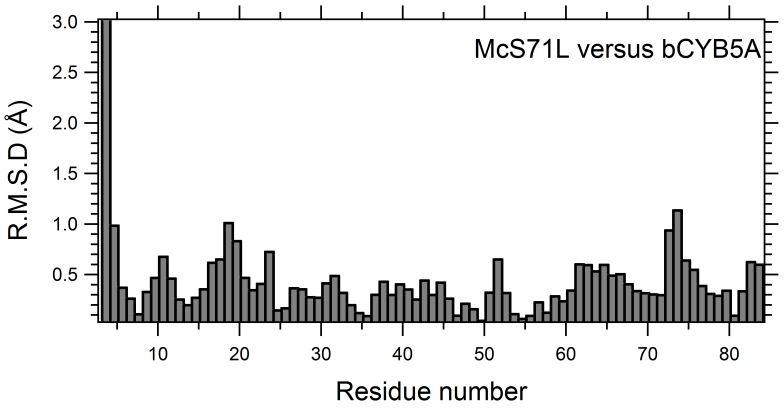

(a)

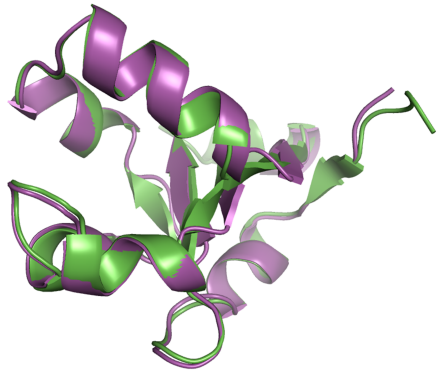

(b)

Figure 5.7: Structural alignment of McS71L and bCYB5A. (a) C_α RMSD plot showing the differences between McS71L and bCYB5A (b) Representation of the structural alignment with the proteins shown in cartoon form. McS71L is colored purple and bCYB5A is colored green

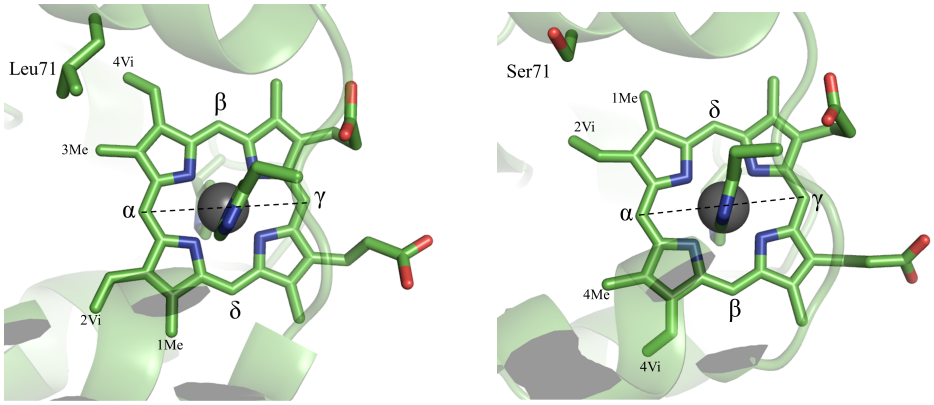

(a) McS71L [orientation B]

(b) bCYB5A (1CYO) [Orientation A]

Figure 5.8: Heme orientation difference in McS71L and bCYB5A. Comparison of the two structures reveals the rotation of heme about the α- γ axis (indicated as black dashes). The view of the structures is top down from His 63 (shown as sticks). The polypeptide is colored green and shown as cartoons. Fe atom is shown as a gray sphere. Heme and amino acid side chains are shown as sticks. Methyl and vinyl substituents on the porphyrin ring are abbreviated Me and Vi respectively.

Consistent with NMR analysis, McS71L crystallized with the heme bound in the B orientation (See 5.8).The effect of the Leu side chain on the heme orientation preference in McS71L became clearer when we compared the heme binding pockets of the McS71L and bCYB5A structures (See figure 5.8 and 5.9).

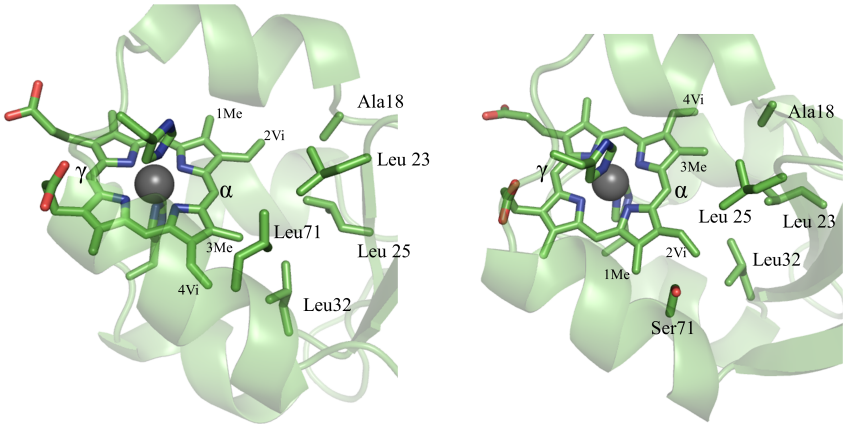

(a) Mcs71L (b) bCYB5A

Figure 5.9: Heme binding pocket comparison. The residues lining the heme binding pocket are compared in McS71L and bCYB5A. The polypeptide is colored green and shown as cartoons. Fe atom is shown as a gray sphere. Heme and amino acid side chains are shown as sticks. Methyl and vinyl substituents on the porphyrin ring are abbreviated Me and Vi respectively.

In bCYB5A, orientation A is more stable and the 4-vinyl and the 3- methyl groups of the porphyrin ring are involved in Van der Waals interactions with the side chains of Leu23 and Leu 25. The 2-vinyl group also has Van der Waals interactions with the side chain of Leu32 and the β-CH_2 group of Ser71. If heme is maintained in orientation A and a bulkier side chain is introduced at position 71 (as in McS71L), it introduces an unfavorable steric environment for the 2-vinyl group. This is due to a crowding effect that both Leu32 and Leu71 will exert, below and above respectively, on the heme. In McS71L, a 180º rotated heme (orientation B) is observed. This enables a smaller methyl group (3-methyl in case of McS71L) to interact with the Leu71 and Leu32 side chains and prevent steric clash. Support for this conclusion was provided by the fact that the mutant Mc2m (L32I/S71L) restored relative stabilization of orientation A as determined by NMR spectroscopy(See chapter 3). The predicted basis for this observation is that the branched side chain of Ile32 reduces the steric contact with the 2-vinyl group in orientation A thus restoring stabilization of orientation A [135].

5.3.3 Crystal structure analysis of hybb5

The asymmetric unit of hybb5 contained only one molecule and the structure of this mutant was solved to a final resolution of 1.7 Å. The crystal structure of hybb5 contained heme bound in two orientations (both A and B isomer) (See figure 5.10). This was consistent with NMR spectra of freshly purified hybb5 that showed equal population of the two orientations (A:B = 1:1).

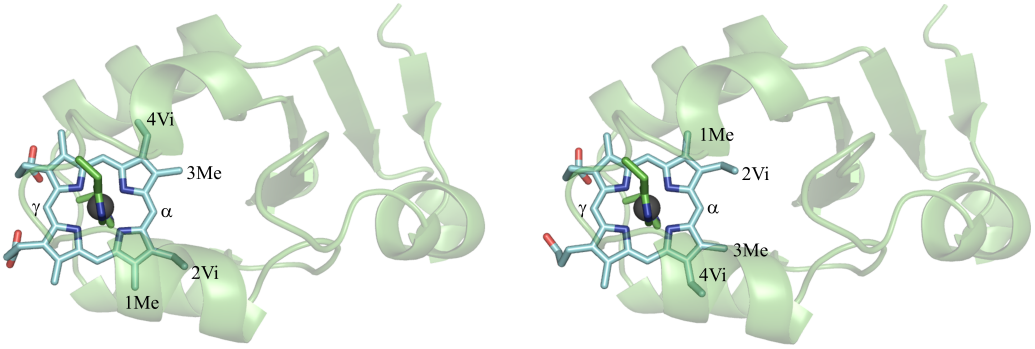

(a) Orientation A (b) Orientation B

Figure 5.10: View of the two heme orientations in hybb5. Consistent with NMR spectroscopy, hybb5 crystallized with heme present in both orientations. The heme is depicted as sticks and the Fe atom is shown as a gray sphere. The reader observes the protein such that His 63 is above the iron atom. The polypeptide is colored green and shown in cartoon form. His 63 and His 39 are shown as sticks.

Structural alignments of hybb5 with bCYB5A and rCYB5B are shown in figure 5.11a and 5.11b respectively. The backbone C_α R.M.S.D (residues 3- 84) comparing hybb5 with bCYB5A and rCYB5B are shown in figure 5.12a and 5.12b respectively. The structural alignment reveals that the twelve mutations introduced in hybb5 have not altered the overall CYB5 fold.

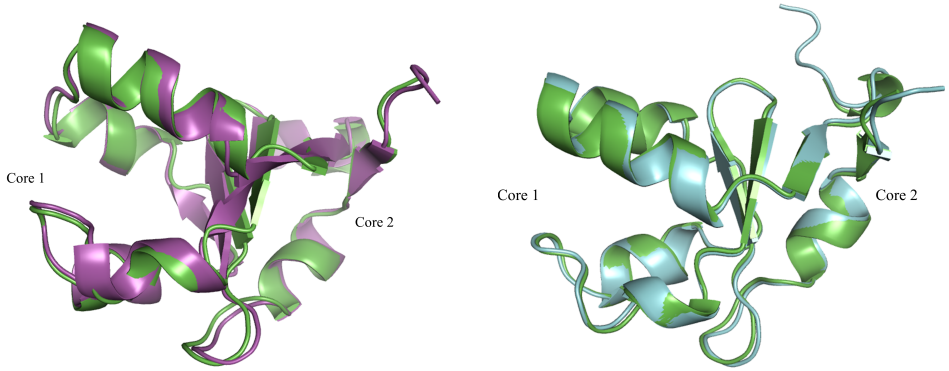

(a) (b)

Figure 5.11: Structural alignment of proteins. (a) hybb5 is aligned with bCYB5A, both proteins are depicted as cartoons, with hybb5 colored green and bCYB5A colored violet (b) hybb5 is aligned with rCYB5B, both proteins are depicted as cartoons, with hybb5 colored green and rCYB5B colored cyan. For sake of clarity, the heme is not shown.

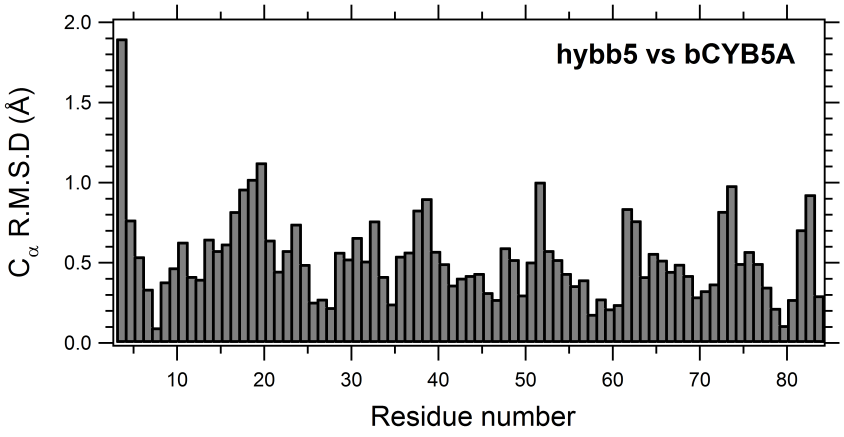

(a)

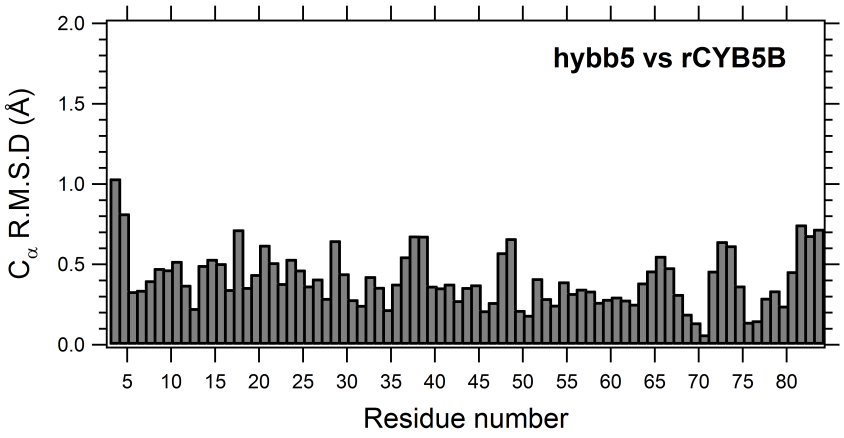

(b)

Figure 5.12: Comparison of hybb5 with (a) bCYB5A (PDB code 1CYO) and (b) rCYB5B (PDB code 3MUS)

The overall R.M.S.D, in case of hybb5 and bCYB5A, is 0.6 Å. The overall R.M.S.D when comparing hybb5 and rCYB5B is 0.5 Å. Distinct changes are seen in side chain orientations of residues located at the surface. Given the similarity in polypeptide structure in hybb5, bCYB5A and rCYB5B, we shifted our attention to the heme and its structural properties within the heme binding pocket.

5.3.4 A closer look at the heme

Histidine- heme angles A key amino acid within the heme binding pocket of CYB5 is at position 71. bCYB5A contains Ser while rCYB5B, hCYB5B, hybb5 and McS71L all contain Leu at position 71. To investigate the influence of Leu 71 on the heme of McS71L, we performed a structural alignment on the proteins (bCYB5A and McS71L) such that the side chain R.M.S.D of His63 (one of the iron ligating histidines) is minimized. This procedure did not significantly alter the overall backbone R.M.S.D of the polypeptide chains in any pair of proteins being compared. On visual inspection, a clear in-plane rotation and displacement of the heme was observed when comparing McS71L with bCYB5A.

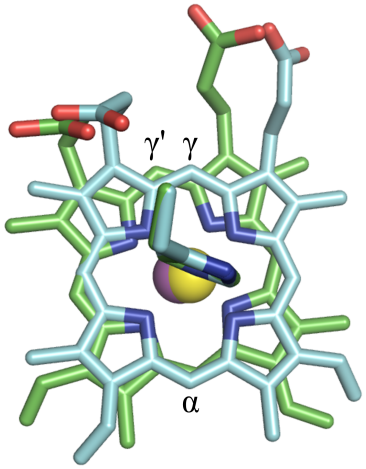

Figure 5.13: Heme in-plane rotation. The heme molecules and histidine residues are shown as sticks. Structural alignment of the two proteins was such that R.M.S.D of the His 63 side chain was less than 0.1 Å. The heme molecule corresponding to McS71L is colored green, the Fe atom in McS71L is shown as a purple sphere. Similarly the heme molecule corresponding to bCYB5A is colored blue and the Fe atom is shown as a yellow sphere. For reference, if the α position of the heme is assumed constant, the relative rotation can be seen by the shift in γ position (γ (rCYB5A)$\rightarrow$ γ'(McS71L)).

In order to quantitate the in plane rotation, we needed an unambiguous method of measuring the relative angle between the cooordinated histidine and heme i.e. a measurement method that would give the relative angle no matter what the orientation of the heme (A or B) was. A literature search revealed an algorithm [47] used to measure histidine heme angles and we adopted the method to study the differences in heme binding for the wild type and mutant proteins. A description of the method is presented in the following text.

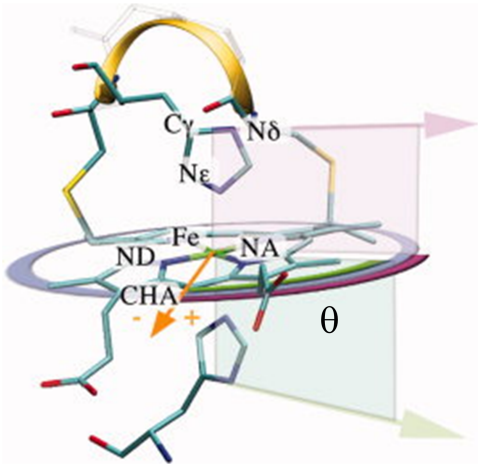

Figure 5.14: Heme angle calculation. The purple and blue arrows define the histidine vector from above and below the plane of the heme. The orange arrow depicts the heme basis vector. Rectangles extending to the plane of the heme depict the projection of the histidine vectors onto the plane of the heme. This picture is reproduced from [47] and is copyrighted. ©Wiley-Liss Inc, License number: 2805570692479

As shown in figure 5.14, the angle θ describes the angle between the ligating histidine and heme. For our analysis we chose His63, which is coordinated to the iron atom via its N_ε atom. Consider a heme basis vector Fe- CHA and a histidine vector C_γ- N_δ. The heme plane is defined as the least squares plane calculated using the atoms of the porphyrin ring. θ is the angle between the projected histidine vector onto the heme plane, and the heme basis vector [47].

Protein	θ
bCYB5A	108 º
McS71L	121 º

Table 5.4: Heme-histidine angles of bCYB5A and McS71L

The relative angles between the histidine and heme of bCYB5A and McS71L are are presented in table 5.4. The data show that the S71L mutation has caused an ~ 13º in-plane rotation of the heme. As reported in the introduction, Sarma *et al* successfully created a mutant in rCYB5A (McA67V) that changed the relative His63-heme angle by 17º without changing the relative in plane heme orientation [120]. Electrochemical studies of McA67V also showed that its E_m was 19 mV more negative than that of wt bCYB5A. Here, when comparing McS71L and wt bCYB5A, we have a 13º in-plane heme displacement combined with a change in the heme orientation. We have also shown that the E_m value of McS71L is 35 mV more negative than that of wt bCYB5A. This led us to hypothesize that the change in E_m of McS7L when compared to bCYB5A was not only due simply to a change in heme orientation from A to B but rather due to an in-plane rotation of the heme within the heme binding pocket.

His63-heme angles were also analyzed using the same method for rCYB5B, hybb5 and hCYB5B. Both hybb5 (PDB code 3OZZ), hCYB5B (PDB code 3NER) produced crystal structures with the heme modeled in both orientation A and orientation B. Unfortunately, in the crystal structure of rCYB5B (PDB code 3MUS) heme was modeled only in orientation B. Given this problem, a new crystal structure of rCYB5B (rCYB5Bnew) was recently solved by Dr. Scott Lovell at the Protein Structure laboratory, University of Kansas (PSL- KU). However, due to lack of time, histidine-heme angles were not calculated.

The values of θ measured for hybb5, rCYB5B and hCYB5B are presented in table 5.5. Heme was modeled in both the A and B orientations in hybb5 and hCYB5B, and thus His63-heme angles could be calculated for both orientations. The proteins rCYB5B, hCYB5B and hybb5 displayed a change in His-heme angle of about 11- 13 º when compared to bCYB5A. In fact when compared to McS71L, the His-heme angles are nearly identical in each case. More interestingly, both orientations of heme (A and B), as seen in hCYB5B and hybb5 have nearly identical His-heme angles (see figure 5.15). Virtually identical in-plane rotations, for heme orientations A and B, were also seen in the new crystal structure of rCYB5B (rCYB5Bnew, see figure 5.15c).

Protein	θ
hybb5 (A orientation)	119 °
hybb5 (B orientation)	120 °
rCYB5B (B orientation)	122 °
hCYB5B (A orientation)	120 °
hCYB5B (B orientation)	121 °

Table 5.5: Histidine heme angles of hybb5, rCYB5B and hCYB5B.

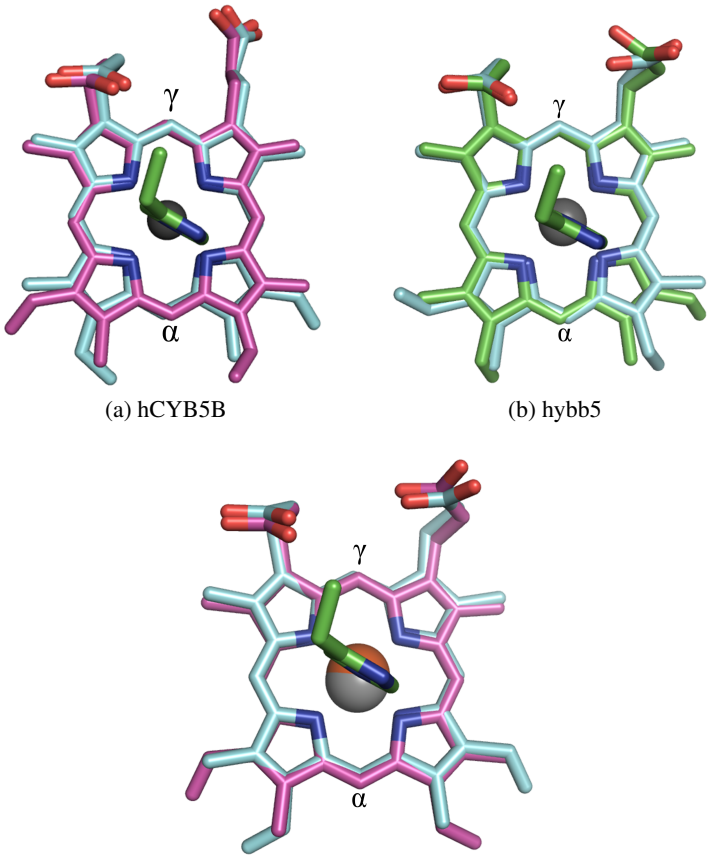

(a) hCYB5B (b) hybb5

(c) rCYB5Bnew

Figure 5.15: Rotation of heme in hCYB5B, hybb5 and rCYB5Bnew. The two orientations of heme are well placed one on top of the other indicating little displacement relative to one another. (a) Heme orientations in hCYb5B, with orientation A colored green and orientation B colored magenta (b) Heme displacement in hybb5, with orientation A colored cyan and orientation B colored green. (c) Heme displacement in rCYB5Bnew, with orientation A colored magenta and orientation B colored cyan. For all figures His 63 and the hemes are depicted as sticks. The iron atom is shown as a gray sphere.

The common feature among McS71L, hCYB5B, rCYB5B and hybb5 is the presence of Leu at position 71. In all four of these proteins, heme displays an 11- 13 ° in-plane rotation when compared to heme in

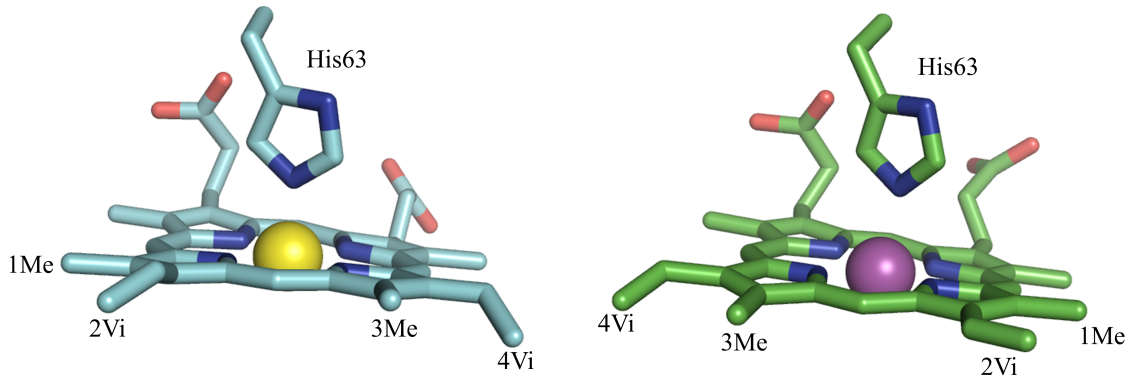

(a) bCYB5A (b) McS71L

Figure 5.16: Comparison of heme structures in bCYB5A and McS71L. The heme and His 63 are shown as sticks. Methyl and Vinyl groups on the porphyrin ring are abbreviated Me and Vi respectively (a) Heme and the histidine present in bCYB5A are colored blue with the iron atom shown as a yellow sphere. (b) Heme and the hisidine residue present in McS71L are colored green, the iron atom is shown as a purple sphere.

bCYB5A, regardless of whether it is in orientation A or orientation B (see 5.15). As discussed in Chapter 4, these four proteins exhibit little preference for binding of heme in these two orientations (equilibrium A:B ratios all ~1:1). On the basis of these observations, we hypothesized that approximately half of the ~60 mV more negative redox potential of rOM b5 in comparison to bMc b5 can be attributed to in-plane heme rotation. Moreover, an 11- 13 ° in-plane rotation of heme appears to be a consistent feature that differentiates mammalian CYB5B proteins from their CYB5A counterparts.

5.3.5 Effect of the vinyl group: experiments with mesoheme incorporated CYB5

Close comparison of the heme in the bCYB5A and McS71L crystal structures revealed an important difference between the two heme structures. As shown in figure 5.16a, both vinyl groups (2- vinyl and 4-vinyl) present in the bCYB5A are tilted out of the plane of the porphyrin ring whereas only one vinyl group in McS71L (4-vinyl, see figure 5.16b) is tilted out of porphyrin ring plane. Vinyl groups are electron withdrawing groups on account of their double bond character. When electrons are withdrawn from the porphyrin ring system, this causes a relative stabilization of the Fe^{2+} state. To achieve maximum effect of electron withdrawing from the porphyrin system, the π bonds of the vinyl groups should be in the same plane as the porphyrin π system as observed for the 2-vinyl group in the McS71L structure. Increased co-planarity with the heme corresponds to a more negative E_m value [109, 72]. In support of this, site directed mutagenesis studies on CYP450 BM3 provide evidence in that vinyl group orientation can be modulated by steric groups surrounding it which in turn affects the E_m value [23]

This observation was important since it provided an additional mechanism that could explain the more positive E_m value of bCYB5A when compared to McS71L. In order to examine the role of the vinyl group in the modulation of redox potential, we performed a 'heme mutation' by preparing holoproteins incorporated with mesoporphyrin-IX (mesoheme). Mesoheme differs from heme in that the vinyl groups at positions 2 and 4 are replaced by ethyl groups (see figure 5.17). This eliminates the electron withdrawing effect of the

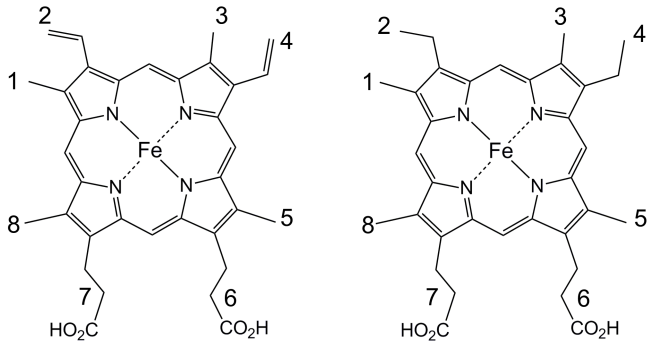

(a) Heme b (b) Mesoheme

Figure 5.17: Comparison of heme and mesoheme. Note the difference in substitutions on the porphyrin ring at positions 2 and 4.

vinyl substituents and hence the E_m value will have a much weaker dependence on the orientation of the substituent group.

To prepare mesoheme incorporated protein, apoCYB5 was prepared from purified holoCYB5 as described in chapter 2. Mesoheme dissolved in DMSO was slowly titrated into apo CYB5 at room temperature and then subjected to one round of purification using a Q sepharose column. This generated a pure sample of CYB5 incorporated with mesoheme. The proteins subjected to mesoheme incorporation were bCYB5A (bCYB5A$_{mh}$), McS71L (McS71L$_{mh}$) and rCYB5B (rCYB5B$_{mh}$). We examined the effect of these heme "mutations" on thermal denaturation of bCYB5A and rCYB5A.Thermal denaturation experiments on McS71L$_{mh}$ were not performed.

Thermal denaturation experiments Results from the thermal denaturation experiments are shown in table 5.6. The data and corresponding fits are shown in figure 5.18 The experimental procedure is the same as described in chapter 3 except that unfolding of the holoprotein incorporated with mesoheme was monitored using the Soret band at 404 nm. Mesoheme incorporated holoprotein thermal denaturation reactions were only partially reversible, similar to the thermal denaturation experiments performed with holoproteins bound to heme.

Protein	T_m(ºC)	T_m(ºC) [protoheme]
bCYB5A$_{mh}$	64.9 $\pm$0.1	67.6 $\pm$ 0.3
rCYB5B$_{mh}$	85.8 $\pm$ 0.2	85.5 $\pm$ 0.5

Table 5.6: Thermal denaturation midpoints (T_m) of mesoheme CYB5

Protein	Heme isomer ratio (A:B)	Mesoheme isomer ratio (A:B)
bCYb5A	8:1	7.1:1
McS71L	1:8	~ 100% B
rCYB5B	1:1.2	1:1.6

Table 5.7: Isomer ratios of proteins bound to different porphyrins

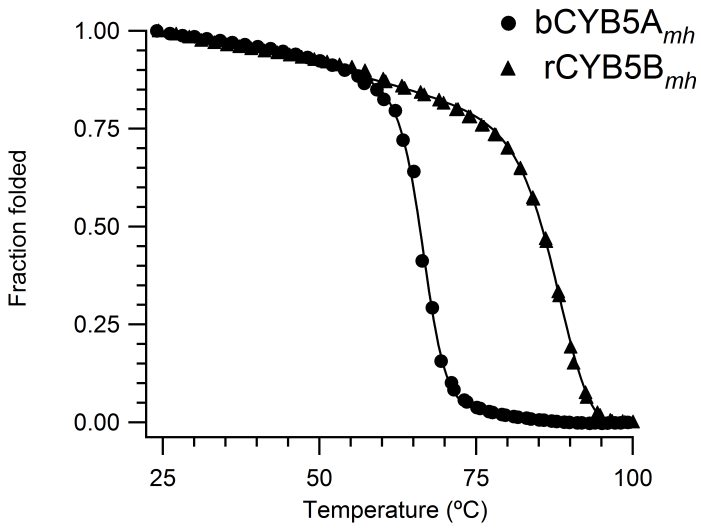

Figure 5.18: Thermal denaturation data and associated fits of mesoheme incorporated CYB5

As seen from the data, replacing the heme in bCYB5A and rCYB5B with mesoheme exerted only minor effects on the T_m values. This is consistent with a small steric difference between ethyl groups (mesoheme) and vinyl groups (protoheme).

Recall that CYB5 proteins are heterogeneous due to the observation that heme binds in two orientations. As reported in chapter 3, the heme isomer ratio (A:B) at equilibrium for bCYB5A, McS71L and rCYB5B are 8:1, 1:8 and 1:1.2 respectively. To check the ratio of orientation when mesoheme is incorporated into CYB5, we performed 1D NMR spectroscopy on the proteins. NMR spectra and equilibrium ratios are reported in figure 5.19.

1D NMR spectra reveal that the heme isomer ratios present in mesoheme incorporated CYB5s were only slightly different from those of holo CYB5s as seen from table 5.7. We next proceeded to perform redox potentiometry on these proteins.

Protein	E_m (mV vs SHE)[§]
bCYB5A$_{mh}$	- 54.0 $\pm$ 0.7
McS71L$_{mh}$	- 87 $\pm$ 1
rCYB5B$_{mh}$	- 127.2 $\pm$ 0.6

Table 5.8: E_m values of mesoheme-CYB5 proteins. [§]Represents the average of two independent experiments. Error values reported are the average errors obtained from each fit.

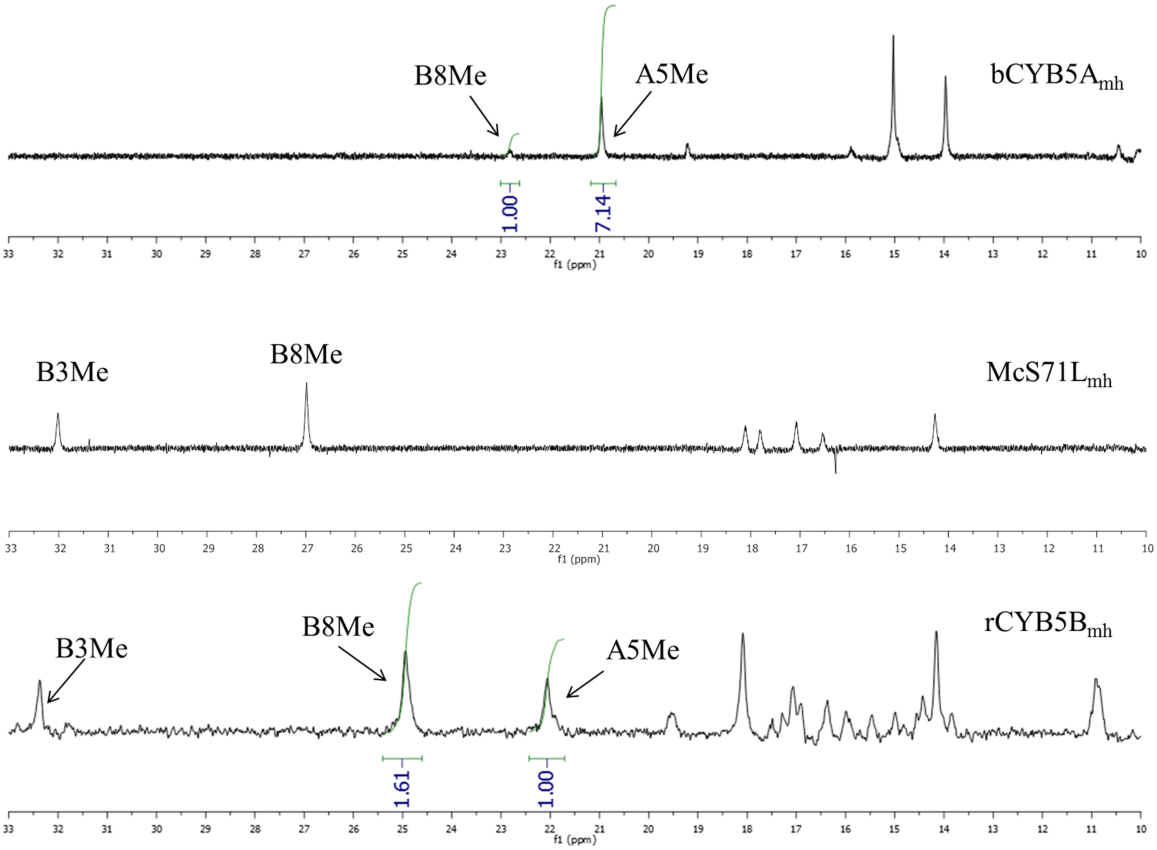

Figure 5.19: 1D NMR spectra of holoproteins incorporated with mesoheme. Selected peak assignment was based on previously reported spectra as seen in chapter 3. Integrals corresponding to specific peaks are shown in green. It was difficult to detect the A5Me peak in the NMR spectrum of McS71L$_{mh}$

Redox potentiometry experiments on mesoheme incorporated CYB5 The procedure used in evaluating oxidation states in mesoheme-CYB5s differs slightly from that described for the protoheme-CYB5s. In mesoheme-CYB5, the mesoheme α peak (used to monitor oxidation states) occurs at 546 nm (see figure 5.20b) compared to 557 nm in heme-CYB5 proteins (see section 2.2.1). Results from the redox titration and fits are given in figure 5.20. E_m values are reported in table 5.8.

Mesoheme- proteins display negatively shifted $E_m$values when compared to the proteheme forms. This is due to stabilization of the Fe^{3+} state relative to the Fe^{2+} state resulting from replacement of the vinyl

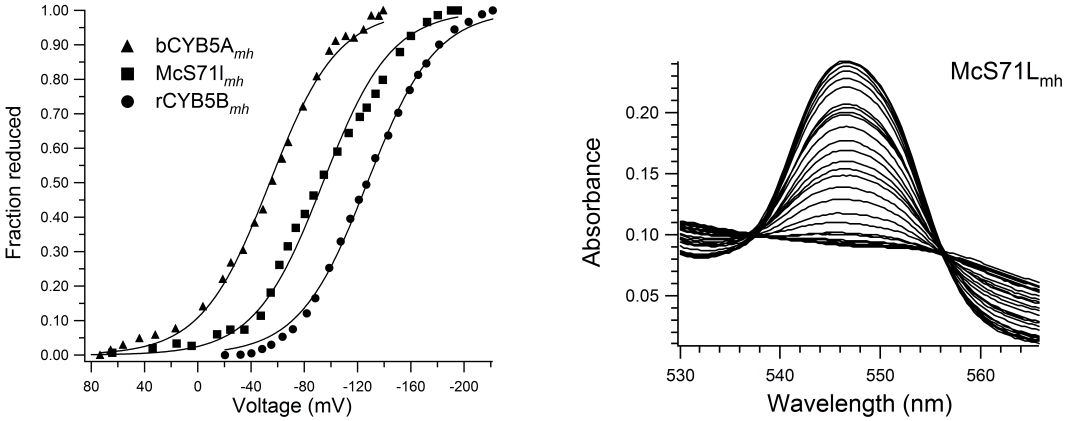

(a) (b)

Figure 5.20: Redox potentiometric experiments of mesoheme CYBs. (a) Data points and fits corresponding to redox titrations (b) Isosbestic behavior in visible spectra used to monitor oxidation states. Note the peak at 546 nm corresponding to the α band present in mesoheme- CYB5s.

groups with more electron donating ethyl groups [123]. Also, the trend in $E_m$values for mesoheme-CYB5 proteins is bCYB5A$_{mh}$ > McS71L$_{mh}$ > rCYB5B$_{mh}$. This is identical to the trend seen for holo CYB5 proteins bound to heme. In fact, the difference between the $E_m$values of McS71L and bCYB5A is nearly identical irrespective of the type of porphyrin it is bound to (35.2 mV in case of protoheme vs 32.7 in case of mesoheme). The same is true for rCYB5B vs. bCYB5A (60.3 mV in case of protoheme vs 73.2 mV in case of mesoheme). This allows a conclusion that the more negative redox potential of S71L in comparison to bCYB5A is not due to differences in heme vinyl orientation. It can likewise be concluded that the more negative redox potential of rCYB5B in comparison to bCYB5A is not due to differences in vinyl group orientations. On the basis of these observations, we can reasonably conclude that in-plane rotation of heme in both orientation A and orientation B will be associated with a negative shift in redox potential and that the magnitude of the shift will be similar for both orientations.

5.3.6 Molecular dynamics (MD) simulations of wild type proteins and hybb5

MD simulations of 10 nanosecond length were performed for bCYB5A, McS71L, rCYB5B and hybb5. For rCYB5B and hybb5, the polypeptide with heme bound in orientation B was used generate the MD trajectories. Visual inspection of the McS71L MD trajectory revealed an increased mobility of the heme within the heme binding pocket leading to errant His- Fe bond lengths and bond angles. Hence results pertaining to MD simulations of McS71L are not reported. Apparently, a more careful initial model-building step is required in future systems.

Previous MD simulation studies [6, 131, 71] comparing bCYB5A and rCYB5B revealed that bCYB5A displayed more dynamic behavior than rCYB5B. The increased dynamics were localized to a cleft opening event, in a region separating core 1 and core 2 of bCYB5A, which was not seen in the rCYB5B simulations. Subsequently this event was shown to be a result of crystal contact effects (in the bCYB5A starting structure). A change in procedure that accounted for this effects allowed MD simulations (8.5 ns) of rCYB5B

and bCYB5A that showed little difference in dynamic behavior [24]. For the purposes of this dissertation, we generated new MD trajectories of bCYB5A (PDB code 1CYO) and rCYB5B (PDB code 3MUS) in order to compare with the MD trajectory of hybb5 (PDB code 3OZZ) aimed at generating new insight into the modulation of redox potential of CYB5 proteins.

Basic Structural analysis of MD simulations Analysis of MD simulations of the proteins indicated that the average polypeptide backbone structures were very similar to those of the starting experimental structures. The root mean square deviation (RMSD) and fluctuation (RMSF) of both the polypeptide backbone and the heme prosthetic group are given in Table 5.9.

	Backbone RMSD	Backbone RMSF	Heme RMSD	Heme RMSF
bCYB5A	0.7	0.5	0.8	1.0
rCYB5B	0.9	0.9	0.7	0.9
hybb5	0.6	0.7	0.8	1.0

Table 5.9: Backbone RMSD and RMSF of the three simulations (Å). Backbone atoms are defined by Cα, C and N atoms of amino acid residues 3-82

None of these proteins showed a significant deviation from their crystal structure coordinates as seen by the low RMSD and RMSF values in table 5.9. Individual amino acid residue RMSDs and RMSFs in all three proteins are shown in Figure 5.21

No significant difference could be seen in the dynamic behavior of the three proteins. The simulation results for rCYB5B and bCYB5A are consistent with previous results [24]. As part of the analysis we calculated the solvent accessible surface area (SASA) of the amino acid side chains averaged over the length of the MD simulations (see figure 5.22).

The differences in average SASA values calculated for the three proteins are not statistically significant. Unfortunately, the MD simulations provided no suggestions regarding potential roles of the polypeptide in governing the redox potentials of the proteins. This could be due to the fact that the simulations were on a relatively short time scale. Indeed, hydrogen-deuterium exchange studies of bCYB5A and rCYB5B, monitored by NMR spectroscopy, have revealed greater conformational mobility in bCYB5A [127]. In addition, all simulations were performed with the iron in the Fe^{3+} state. NMR studies of the rat microsomal CYB5 in both the oxidized and reduced form [11, 13] have revealed a decrease in backbone dynamics as the protein goes from the oxidized to the reduced state. MD simulations comparing rat microsomal CYB5 in both the oxidized and reduced form indicated that the minor structural changes observed upon reduction were due to changes in surface charge distribution that was influenced by the oxidation state of the heme [51]. It is necessary to increase the length of MD simulations along with changes in the oxidation state of the iron, in order to correlate structural motions in CYB5 to observed biophysical and biochemical properties.

We also used MD to analyze the heme binding environment . Recall that solvent exposure of heme plays an important role in modulating the E_m value of CYB5. Average heme SASA values for the three proteins are presented in 5.10.

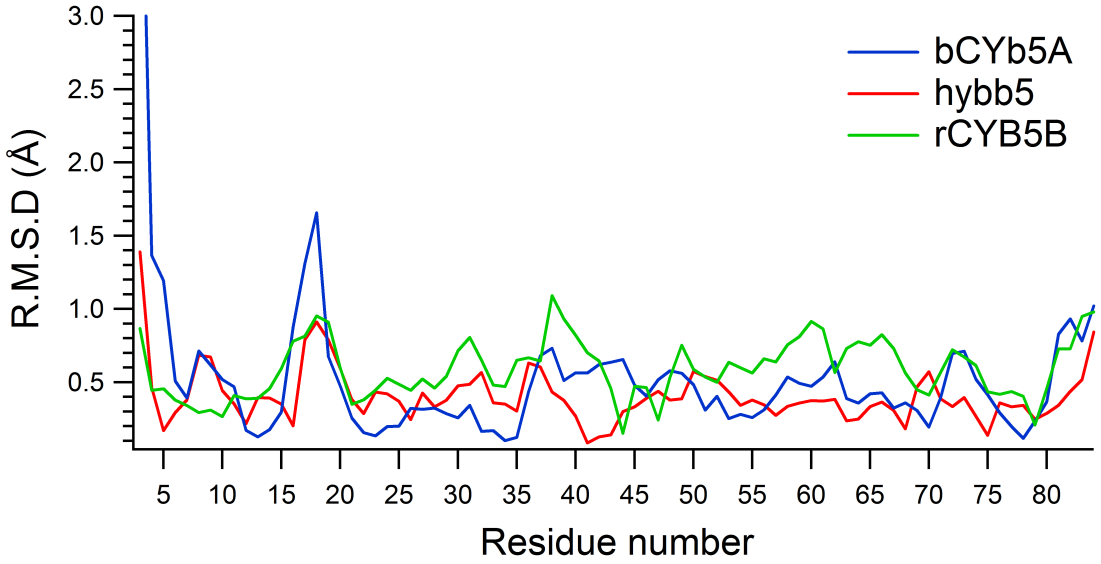

(a)

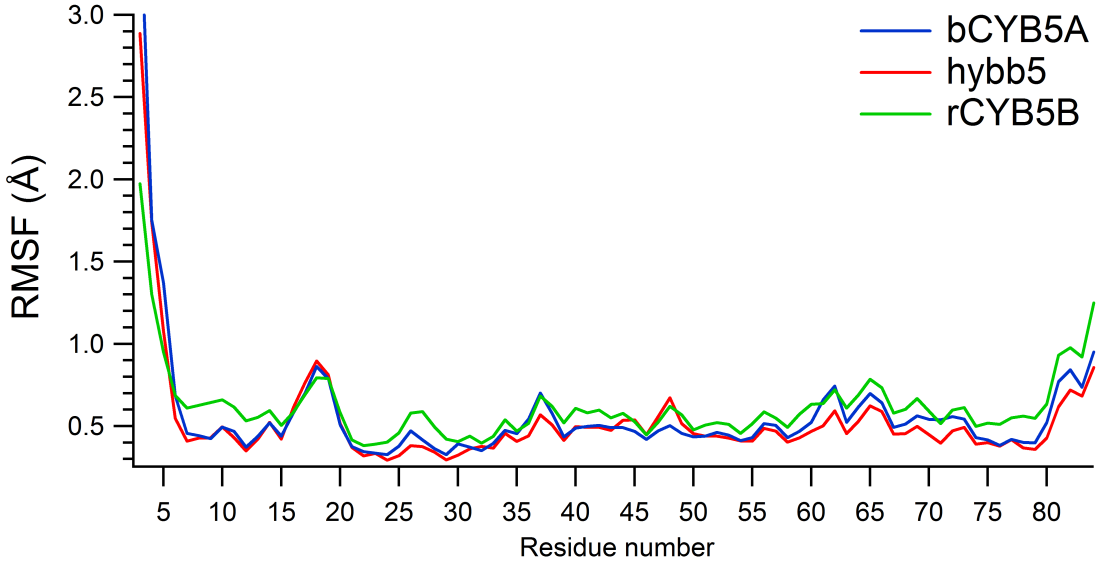

(b)

Figure 5.21: (a) Backbone RMSD plots of the average trajectory structure and the starting X- ray coordinates in the 10ns simulations. (b) Backbone RMSF plots in the three simulations.

Protein	Heme SASA (Å^2)
bCYB5A	249 ±18 (206.8)
hybb5	235 ± 18 (193.8)
rCYB5B	242 ± 18 (221.7)

Table 5.10: Average heme SASA in the three simulations. Values in parentheses indicate heme SASA calculated from the X-ray crystal structure

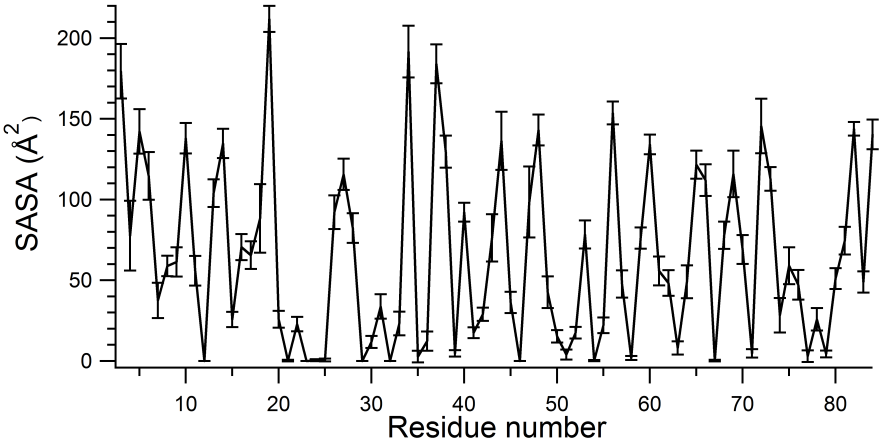

(a) bCYB5A

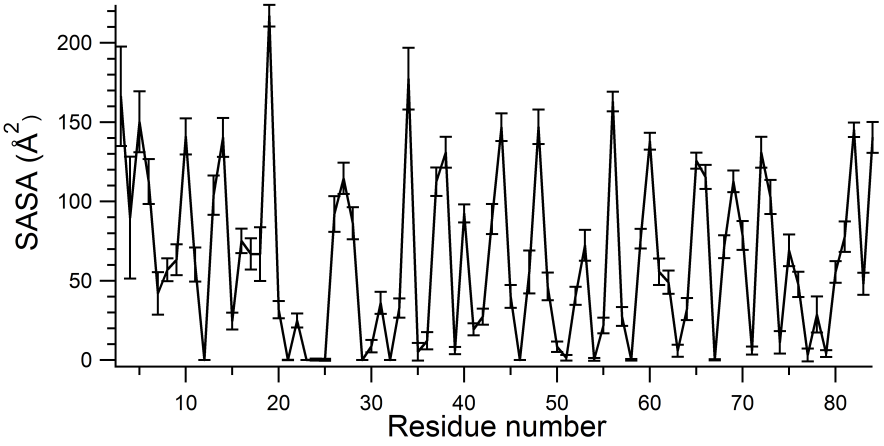

(b) hybb5

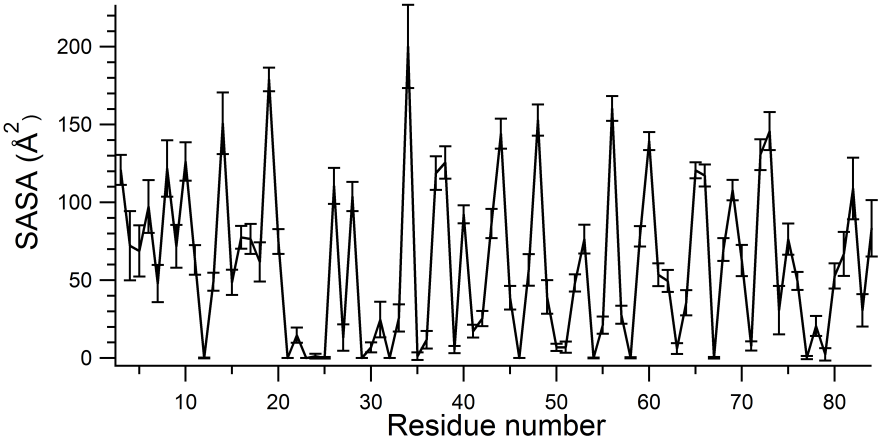

(c) rCYB5B

Figure 5.22: Average SASA of the three MD simulations. Error bars indicate the standard deviation. (a) bCYB5A, (b) hybb5 and (c) rCYB5B

Neither the crystal structure heme SASA nor the MD heme SASA data correlate with the difference in E_m values observed for the proteins. If crystal structure data are considered alone, hybb5 (on account of having a lower SASA) should have a higher E_m value than either bCYB5A or rCYB5B. Moreover, MD data suggest that the average heme SASA for these proteins are in essence identical. The heme SASA data lead us to believe that the redox potential difference seen in the holoproteins is not due to difference in the heme solvent exposure.

One marked difference between the hemes, is the conserved difference in the His63-heme angle when bCYB5A is compared to rCYB5B, hCYB5B and hybb5. As part of analyzing the heme, we used the algorithm (described above) to calculate average His63-heme angles (θ) during the course of the MD simulation. The results are presented in table 5.11.

Protein	Average θ(°)
bCYB5A	101± 10 (108.2)
hybb5 (B orientation)	114 ± 9 (120.1)
rCYB5B (B orientation)	111 ± 9 (121.9)
hCYB5B (A orientation)	104 ± 9 (120.1)
hCYB5B (B orientation)	114 ± 11 (121.3)

Table 5.11: Average heme-histidine angles calculated during the MD simulations. Values in parentheses are θ values from the crystal structure

When only the average values of θ are taken into consideration, it is seen that the His63-heme angle difference between bCYB5A and the other proteins (as observed in the crystal structure) is maintained throughout the MD simulation in the case of orientation B, but not in the case of orientation A (for rCYB5B only orientation B could be considered as heme could only be modeled in that orientation in the structure we used; 3MUS). This suggests the possibility that in-plane heme rotation in these proteins (relative to orientation A in bMc b5) is more important for orientation B than for orientation A, perhaps for steric reasons. Nonetheless, when the standard deviations are taken into account, the difference in all cases becomes insignificant. As a consequence we cannot use these data in support of our conclusion that in-plane heme rotation changes are the source of the negatively shifted redox potential that accompanied conversion of bCYB5A to McS71L. Personal discussions with Prof. Kuczera revealed a possible source of error. The CHARMM force field (used in this work) parameters of heme are very approximate and provide a simple model of heme. To accurately model His- Fe coordination, we need detailed models and additional bonding parameters such as orbital overlap and associated quantum mechanical properties. The current force field in CHARMM [19] is insufficient in estimating subtle molecular changes including heme angle calculations. Additional MD simulations performed with a more sophisticated force field are needed in regard to this.

5.3.7 Conclusions

The biochemical differences and redox behavior of CYB5A and CYB5B have been analyzed using mutant CYB5 proteins and wild type proteins. Our results indicate that a consistent ~ 60 mV difference in E_m values is maintained between the CYB5A and CYB5B isoforms in mammals. Structural analysis of the proteins provides insight into redox potential modulation by CYB5 proteins. A key finding from MD studies is that the source of differences in redox potential of CYB5s is not differences in heme solvent exposure. In fact bCYB5A and rCYB5B display virtually identical heme SASA but have distinctly different E_m values. Also mesoheme studies have shown that the differences in heme vinyl group orientations in bCYB5A and rCYB5B contribute little if anything to the differences in E_m values.

The major finding from this study is that differences in E_m values are dependent on the in-plane heme orientation within the heme binding pocket. The change in E_m when comparing McS71L and bCYB5A is a good example of this concept. McS71L (which binds heme in orientation B) has a 35 mV more negative E_m value compared to bCYB5A (which binds heme in orientation A). In addition we see a constant 11- 13 º in-plane rotation of the heme within the heme binding pocket when comparing McS71L, hybb5, rCYB5B and hCYB5B with bCYB5A, regardless of whether heme is bound in orientation A or orientation B. This in-plane heme rotation, which alters the angle between heme and both of its His ligands, appears to contribute about half of the difference in redox potentials exhibited by bCYB5A and rCYB5B. The explanation for this effect may relate to the fact that the in-plane rotation moves the histidine plane closer to an N-Fe-N line of the heme, which increases steric interactions [28]. Studies with both model compounds and natural proteins have revealed greater sensitivity of His-Fe^{2+} bonds than of His-Fe^{3+} bonds to steric interactions [28]. Another possibility is that the in-plane rotation destabilizes Fe^{2+} relative to Fe^{3+} because it differentially alters the nature of orbital interactions [121] between heme and the ligand. Our results further suggest that the remaining ~30 mV difference in rOM and bMc b5 redox potentials is due to the tendency of mutations that stabilize His-Fe coordination to stabilize the ferric form of the protein more than the ferrous form, as established in the Benson group using model compounds [28].

Sequence alignments of proteins across the cytochrome b5 superfamily have allowed us to conclude that the common ancestor of CYB5A and CYB5B contained Leu at position 71. Hence, after the CYB5A and CYB5B genes duplicated, residue 71 in the CYB5A line became mutated to Ser. We have shown herein that this change resulted in an in-plane heme rotation of ~13 degrees, which appears to be a key source of its more positive redox potential. This may have contributed to the ability of the CYB5A line to evolve distinct roles within the cell, and ultimately to a different subcellular locations for the two isoforms.

Chapter 6: Conclusions

This dissertation focusses on the variation in sequences of Mcb5 and OMb5 that is reflected in the difference in biophysical and biochemical properties in the two isoforms. It has also revealed the capability of the CYB5 fold to withstand mutations during the evolutionary progress of these two isoforms. Across mammalian organisms, both OMb5 and Mcb5 display remarkable sequence identity and similarity. However subtle changes exist within an isoform that impart changes in the dynamic behavior of the proteins. This is best exemplified by the work described in chapter 3. Recall that the human OMb5, at amino acid position 21, differs from the rat OMb5 by incorporating a bulkier amino acid (Leu in hOMb5, Thr in rOMb5). The significance of this amino acid difference is not reflected in the biophysical and biochemical properties of the two proteins given the observation that both hOMb5 and rOMb5 have identical thermal denaturation midpoints and redox potentials. It can be argued that macroscopic properties associated with a given protein are a consequence of both structural integrity and dynamic behavior of the proteins. Structural integrity, in this case to maintain the CYB5 fold, hOMb5 compensates for a deeply buried bulkier amino acid by incorporating two well-ordered water molecules between β4 and β5. These water molecules mediate the hydrogen bonding that occurs between beta strands β4 and β5. An important result from the molecular dynamics simulation described in chapter 3 is that one of these water molecules (WAT 11 in the chapter) mediating the hydrogen bond between the beta strands is found to be highly dynamic. Equally important is the role of the second water molecule (WAT 194) in maintenance of the intact CYB5 fold. WAT194, at a physiological temperature, plays an important role in the maintenance of the hOMb5 structure by continuing to mediate the hydrogen bond between the beta strands. When WAT194 and WAT 11 are removed and the protein is subjected to MD simulations, the resultant structure shows presence of strain. This is due to the unnatural conformation adopted by the side chain of Leu21. Thus, the presence of WAT 194 within the crystal structure of hOMb5 shows a possible mechanism by which the CYB5 fold is able to maintain its integrity in spite of a non-conservative mutation. Additionally, the MD simulations and the movement of the water molecule between the beta strands provides a major insight into a possible folding mechanism of CYB5 proteins, in that the water molecules between the two beta strands may represent a folding intermediate in the formation of the CYB5 beta sheet network. The third hydrogen bond in the between β4 and β5 is between the amino acid residues Ala54 and Val24). Ala54 is an invariant residue that is present in all mammalian forms of Mcb5 and Omb5. Complete separation of the beta strands in the CYB5 fold and thus protein unfolding is accomplished only after the hydrogen bond (between Ala54 and Val24) is broken. The work here in chapter 3 not only highlights the stability of the CYB5 fold in accommodating mutations but also provides insight into the interactions that are important in maintaining the stable CYB5 fold.

In chapter 4, amino acids of bCYB5A was systematically incorporated into rCYB5B to create a hybrid mutant (hybb5) that displayed holoprotein thermal stability similar to that of rOMb5. However the apparent increase in thermal stability was due, at least in part, to an increase in apoprotein stability much greater than predicted on the basis of available data for apo-rOM b5 and apo-bMc b5. The weaker heme binding ability of hybb5, when compared to rOMb5, was masked due to the stability of the apo-protein. This is in support of our initial model that the overall stability of the CYB5 holoprotein is a combination of the stability of the apo-protein and the strength of heme binding. When a direct comparison of rOMb5 and hybb5 is made, it

can be concluded from the results in chapter 4 that introduction of bMcb5 residues in the non heme binding core (core 1) has weakened the heme binding strength of hybb5 despite the fact that residues lining the heme binding core (core 2) in both hybb5 and rOMb5 are in essence identical. An important observation from this study was that mutations introduced even in the disordered region of the apo protein influence stability, especially by altering the compactness of the empty heme binding pocket. Within this disordered region, a key role is played by the nature of the amino acid at position 71. Recall that at position 71, all Mcb5 proteins contain a Ser while all Omb5 proteins contain Leu. The difference in the nature of amino acid at position 71 has a major effect on the stability primarily because position 71 occurs at the boundary where core 1 ends and core 2 begins. Core 1 is predominantly unstructured and a non-polar amino acid, such as Leu, can engage in non-specific hydrophobic interactions with the hydrophobic side chains of residues present in the unfolded core 1. This additionally increases the compactness of the empty heme binding pocket. However if Ser is present at position 71, the polar side chain of Ser fails to engage in similar hydrophobic interactions. This is responsible for the increased hydrodynamic radius of apoMcb5 when compared to apo OMb5. The empty heme binding core of hybb5 also shows the same level of compactness as that of rOMb5 given that both the proteins have Leu at position 71. Position 71 also provides clues as to the evolutionary divergence of CYB5 proteins. It is possible that the progenitor of mammalian CYB5 also had a hydrophobic residue at position 71 whose change to Ser in the line leading to Mcb5s has manifested in the form of altered biophysical properties. It is true that thermodynamic studies in this thesis do not reflect physiological conditions but this chapter initiates careful analysis of the biochemical properties which vary due to the amino acid at position 71 as described in chapter 5 and in the following text.

In chapter 5, the careful measurements of the redox potential of Mcb5, OMb5 and other mutants generated in the course of chapter 4 have been carried out. These experiments along with structural and computational studies have helped us delineate factors responsible for the difference in redox potentials between the two protein isoforms. Systematic analysis of factors classically known to modulate redox potential differences including solvent accessible surface are and polarity surrounding the heme have been found not to be contributing to the redox potential differences between the two isoforms. In addition the vinyl substituents of the heme group do not contribute to the redox potential differences. The major finding from this study is that differences in between Mcb5 and Omb5 arise due to two main factors (i) the nature of heme orientation within the heme binding pocket and (ii) a constant 11- 13 ° in-plane rotation of the heme within the heme binding pocket. This however could not be further investigated using MD simulation because of incorrect parameters used when modeling hee protein interactions. In addition, the time scale of MD simulations are not long enough to simulate experimental time scales. Thus, longer simulations of the CYB5 proteins combined with an improved parameter set that better models heme protein interactions should be used in order to further understand the redox potential differences between OMb5 and Mcb5 proteins.

Within this chapter it is seen that proteins with Ser (all mammalian Mcb5) have a significantly more positive redox potential than the corresponding proteins that contain Leu at position 71. Thus a key step leading to functional divergence in these two proteins is the difference in the amino acid at position 71. Recall that in mammals, erythrocytes contain an alternatively spliced variant of Mcb5. This CYB5 lacks the membrane anchor that is present in the classical Mcb5. It also shows a more positive redox potential similar

to Mcb5 when compared to the Omb5 proteins. One of the physiological roles that erythrocyte CYB5 performs is the maintenance of hemoglobin in the reduced state. Circulating hemoglobin, to be functional, must maintain the heme iron in the Fe (II) state. Sometimes the iron is oxidized and the resulting hemoglobin (methemoglobin) is incapable of binding oxygen. CYB5A acts as an electron transfer protein that transfers electrons to methemoglobin from nicotinamide adenine dinucleotide (NADH) bound in NADH-CYB5 reductase (CYB5R3). A medical case also exists where a person with congenital methemoglobinaemia (a disease characterised by increased concentration of methemoglobin) was linked to a deficiency of CYB5A. The higher redox potential of erythrocyte CYB5 partly assists this process given that it requires lesser effort to maintain the erythrocyte b5 in the reduced state. With respect to this hypothesis, it is interesting to note that a CYB5 (Ascyb5) found in a parasitic nematode, Ascaris suum, interacts in similar fashion to oxygenated myoglobin (metmyoglobin) present in its circulatory system. A. suum, a parasite of the small intestine in pigs, has a more positive redox potential (78 mV vs SHE) that helps in maintenance of reduced myoglobin in the parasite's blood [151]. The presence of Ser at position 71 provides further credence to the hypothesis that a key factor involved in more positive redox potentials is the presence of Ser at position 71. In addition, house fly CYB5 (only one isoform is known) has a redox potential of -25 mV vs SHE and it contains Met at position 71. It is possible that evolutionary divergence of the CYB5 isoforms in mammals started with the variation in amino acids at position 71. The retention of Ser at position 71 enabled Mcb5 (and the erythrocyte isoform) to maintain a more positive redox potential that helps it perform its function in a highly oxidative environment as present within erythrocytes. A change at position 71 to a non-polar amino acid (Leu in the case of Omb5s) decreases the redox potential of the CYB5 protein. Recall that a more negative redox potential indicates that more energy is needed in order for the protein to be in a reduced state. The more negative redox potential may be beneficial for OMb5 to perform its biological function within the mitochondria (the organelle where Omb5 is localized). The mitochondria has a more reducing environment than the normal cell environment. It can be hypothesized that on the basis of its redox potential and its binding partners, the CYB5 isoforms were localized to different organelles which in turn have different redox conditions. On the basis of the work performed in this dissertation, it can be hypothesized that the specific subcellular localization of CYB5 was preceded by the evolutionary split of the progenitor protein, wherein the amino acid type at position 71 provided two different proteins that separately evolved with specific biochemical functions.

References

[1] John A. Shelnutt, Xing-Zhi Song, Jian-Guo Ma, Song-Ling Jia, Walter Jentzen, and Craig J. Medforth. Nonplanar porphyrins and their significance in proteins. *Chemical Society Reviews*, 27(1):31, 1998.

[2] P. D. Adams, P. V. Afonine, G. Bunkoczi, V. B. Chen, I. W. Davis, N. Echols, J. J. Headd, L. W. Hung, G. J. Kapral, R. W. Grosse-Kunstleve, A. J. McCoy, N. W. Moriarty, R. Oeffner, R. J. Read, D. C. Richardson, J. S. Richardson, T. C. Terwilliger, and P. H. Zwart. Phenix: a comprehensive python-based system for macromolecular structure solution. *Acta Crystallogr D Biol Crystallogr*, 66(Pt 2):213–21, 2010.

[3] D.J. Allen, M. P.; Tildesley. *Computer- Simulations of Liquids*. Oxford Science Publications, London, 1987.

[4] A. Altuve, S. Silchenko, K. H. Lee, K. Kuczera, S. Terzyan, X. Zhang, D. R. Benson, and M. Rivera. Probing the differences between rat liver outer mitochondrial membrane cytochrome b5 and microsomal cytochromes b5. *Biochemistry*, 40(32):9469–83, 2001.

[5] A. Altuve, L. J. Wang, D. R. Benson, and M. Rivera. Mammalian mitochondrial and microsomal cytochromes b(5) exhibit divergent structural and biophysical characteristics. *Biochemical and Biophysical Research Communications*, 314(2):602–609, 2004.

[6] Adriana Altuve, S Silchenko, K H Lee, K Kuczera, S Terzyan, X Zhang, D R Benson, and M Rivera. Probing the differences between rat liver outer mitochondrial membrane cytochrome b5 and microsomal cytochromes b5. *Biochemistry*, 40(32):9469–83, August 2001.

[7] Adriana Altuve, Lijun Wang, David R Benson, and Mario Rivera. Mammalian mitochondrial and microsomal cytochromes b5 exhibit divergent structural and biophysical characteristics. *Biochemical and Biophysical Research Communications*, 314(2):602–609, February 2004.

[8] Tomomi Aono, Yoichi Sakamoto, Masahiro Miura, Fusako Takeuchi, Hiroshi Hori, and Motonari Tsubaki. Direct electrochemical analyses of human cytochromes b5 with a mutated heme pocket showed a good correlation between their midpoint and half wave potentials. *Journal of biomedical science*, 17(1):90, January 2010.

[9] Fraser a. Armstrong, H. Allen O. Hill, and Nicholas J. Walton. Direct electrochemistry of redox proteins. *Accounts of Chemical Research*, 21(11):407–413, November 1988.

[10] F Arnesano, L Banci, I Bertini, and I C Felli. The solution structure of oxidized rat microsomal cytochrome b5. *Biochemistry*, 37(1):173–84, January 1998.

[11] F Arnesano, L Banci, I Bertini, I C Felli, and D Koulougliotis. Solution structure of the B form of oxidized rat microsomal cytochrome b5 and backbone dynamics via 15N rotating-frame NMR-relaxation

measurements. Biological implications. *European journal of biochemistry / FEBS*, 260(2):347–54, March 1999.

[12] Franca Ascoli, Maria Rosaria Rossi Fanelli, and Eraldo Antonini. Preparation and Properties of Apohemoglobin and Reconstituted Hemoglobins. *Methods in Enzymology*, 76:72– 87, 1981.

[13] L Banci, I Bertini, F Ferroni, and a Rosato. Solution structure of reduced microsomal rat cytochrome b5. *European journal of biochemistry / FEBS*, 249(1):270–9, October 1997.

[14] L Banci, I Bertini, a Rosato, and S Scacchieri. Solution structure of oxidized microsomal rabbit cytochrome b5. Factors determining the heterogeneous binding of the heme. *European journal of biochemistry / FEBS*, 267(3):755–66, February 2000.

[15] Damián E Bikiel, Flavio Forti, Leonardo Boechi, Marco Nardini, F Javier Luque, Marcelo a Martí, and Darío a Estrin. Role of heme distortion on oxygen affinity in heme proteins: the protoglobin case. *The journal of physical chemistry. B*, 114(25):8536–43, July 2010.

[16] M J Billen and E J Squires. The role of porcine cytochrome b5A and cytochrome b5B in the regulation of cytochrome P45017A1 activities. *The Journal of steroid biochemistry and molecular biology*, 113(1-2):98–104, January 2009.

[17] E. Blanc, P. Roversi, C. Vonrhein, C. Flensburg, S. M. Lea, and G. Bricogne. Refinement of severely incomplete structures with maximum likelihood in buster-tnt. *Acta Crystallographica Section D-Biological Crystallography*, 60:2210–2221, 2004.

[18] Fabian Bös and Jürgen Pleiss. Multiple molecular dynamics simulations of TEM beta-lactamase: dynamics and water binding of the omega-loop. *Biophysical journal*, 97(9):2550–8, November 2009.

[19] B. R. Brooks, 3rd Brooks, C. L., Jr. Mackerell, A. D., L. Nilsson, R. J. Petrella, B. Roux, Y. Won, G. Archontis, C. Bartels, S. Boresch, A. Caflisch, L. Caves, Q. Cui, A. R. Dinner, M. Feig, S. Fischer, J. Gao, M. Hodoscek, W. Im, K. Kuczera, T. Lazaridis, J. Ma, V. Ovchinnikov, E. Paci, R. W. Pastor, C. B. Post, J. Z. Pu, M. Schaefer, B. Tidor, R. M. Venable, H. L. Woodcock, X. Wu, W. Yang, D. M. York, and M. Karplus. Charmm: the biomolecular simulation program. *J Comput Chem*, 30(10):1545–614, 2009.

[20] A. T. Brunger, P. D. Adams, G. M. Clore, W. L. DeLano, P. Gros, R. W. Grosse-Kunstleve, J. S. Jiang, J. Kuszewski, M. Nilges, N. S. Pannu, R. J. Read, L. M. Rice, T. Simonson, and G. L. Warren. Crystallography and nmr system: A new software suite for macromolecular structure determination. *Acta Crystallographica Section D-Biological Crystallography*, 54:905–921, 1998.

[21] A. T. Brunger and M. Karplus. Polar hydrogen positions in proteins: empirical energy placement and neutron diffraction comparison. *Proteins-Structure Function and Genetics*, 4(2):148–56, 1988.

[22] S. Chapman, S. Daff, and A. Munro. Heme: The most versatile redox centre in biology? *Metal Sites in Proteins and Models*, 88:39–70, 1997.

[23] Zhucheng Chen, Tobias W B Ost, and Johannes P M Schelvis. Phe393 mutants of cytochrome P450 BM3 with modified heme redox potentials have altered heme vinyl and propionate conformations. *Biochemistry*, 43(7):1798–808, February 2004.

[24] Q Cheng, DR Benson, and Mario Rivera. Influence of point mutations on the flexibility of cytochrome b5: molecular dynamics simulations of holoproteins. *Biopolymers*, 83(2006):297–312, 2006.

[25] Ramu Chenna, Hideaki Sugawara, Tadashi Koike, Rodrigo Lopez, Toby J Gibson, Desmond G Higgins, and Julie D Thompson. Multiple sequence alignment with the Clustal series of programs. *Nucleic Acids Research*, 31(13):3497–3500, July 2003.

[26] a J Constans, M R Mayer, S F Sukits, and J T Lecomte. A test of the relationship between sequence and structure in proteins: excision of the heme binding site in apocytochrome b5. *Protein science*, 7(9):1983–93, September 1998.

[27] Aaron B Cowley, Adriana Altuve, Olga Kuchment, Simon Terzyan, Xuejun Zhang, Mario Rivera, and David R Benson. Toward engineering the stability and hemin-binding properties of microsomal cytochromes b5 into rat outer mitochondrial membrane cytochrome b5: examining the influence of residues 25 and 71. *Biochemistry*, 41(39):11566–81, October 2002.

[28] Aaron B Cowley, Michelle L Kennedy, Svetlana Silchenko, Gudrun S Lukat-Rodgers, Kenton R Rodgers, and David R Benson. Insight into heme protein redox potential control and functional aspects of six-coordinate ligand-sensing heme proteins from studies of synthetic heme peptides. *Inorganic chemistry*, 45(25):9985–10001, December 2006.

[29] Aaron B Cowley, Mario Rivera, and David R Benson. Stabilizing roles of residual structure in the empty heme binding pockets and unfolded states of microsomal and mitochondrial apocytochrome b 5. *Protein science*, 1(13):2316–2329, 2004.

[30] Aaron B Cowley, Na Sun, Mario Rivera, and David R Benson. Divergence in nonspecific hydrophobic packing interactions in the apo state, and its possible role in functional specialization of mitochondrial and microsomal cytochrome b5. *Biochemistry*, 44(44):14606–15, November 2005.

[31] Ronald B Davis and Juliette T J Lecomte. Structural propensities in the heme binding region of apocytochrome b5. I. Free peptides. *Biopolymers*, 90(4):544–55, January 2008.

[32] M De Silvestris, a D'Arrigo, and N Borgese. The targeting information of the mitochondrial outer membrane isoform of cytochrome b5 is contained within the carboxyl-terminal region. *FEBS letters*, 370(1-2):69–74, August 1995.

[33] Bin Deng, Sudharsan Parthasarathy, WenFang Wang, Brian R Gibney, Kevin P Battaile, Scott Lovell, David R Benson, and Hao Zhu. Study of the individual cytochrome b5 and cytochrome b5 reductase domains of Ncb5or reveals a unique heme pocket and a possible role of the CS domain. *Journal of Biological Chemistry*, 285(39):30181–91, September 2010.

[34] Hultquist E. Donald and Philip G. Passon. Catalysis of Methaemoglobin reduction by erythrocyte cytochrome b5 and cytochrome b5 reductase. *Nature New Biology*, 229:252–254, 1971.

[35] R. C. Durley and F. S. Mathews. Refinement and structural analysis of bovine cytochrome b5 at 1.5 a resolution. *Acta Crystallogr D Biol Crystallogr*, 52(Pt 1):65–76, 1996.

[36] P Leslie Dutton. Redox Potentiometry: Determination of Midpoint Potentials of Oxidation-Reduction Components of Biological Electron-Transfer Systems. *Methods in Enzymology*, 54:411–435, 1978.

[37] P. Emsley, B. Lohkamp, W. G. Scott, and K. Cowtan. Features and development of coot. *Acta Crystallographica Section D-Biological Crystallography*, 66:486–501, 2010.

[38] U. Essmann, L. Perera, M. L. Berkowitz, T. Darden, H. Lee, and L. G. Pedersen. A smooth particle mesh ewald method. *Journal of Chemical Physics*, 103(19):8577–8593, 1995.

[39] P. Evans. Scaling and assessment of data quality. *Acta Crystallogr D Biol Crystallogr, 2006*, D62:72–82, 2006.

[40] C J Falzone, Y Wang, B C Vu, N L Scott, S Bhattacharya, and J T Lecomte. Structural and dynamic perturbations induced by heme binding in cytochrome b5. *Biochemistry*, 40(15):4879–91, April 2001.

[41] C. J. Falzone, Y. Wang, B. C. Vu, N. L. Scott, S. Bhattacharya, and J. T. Lecomte. Structural and dynamic perturbations induced by heme binding in cytochrome b5. *Biochemistry*, 40(15):4879–91, 2001.

[42] Christopher J Falzone, Michael R Mayer, Eileen L Whiteman, Cathy D Moore, and Juliette T J Lecomte. Design Challenges for Hemoproteins : The Solution Structure of Apocytochrome b 5. *Biochemistry*, 35(21):6519–6526, 1996.

[43] S. E. Feller, Y. H. Zhang, R. W. Pastor, and B. R. Brooks. Constant-pressure molecular-dynamics simulation - the langevin piston method. *Journal of Chemical Physics*, 103(11):4613–4621, 1995.

[44] J S Finer-Moore, a a Kossiakoff, J H Hurley, T Earnest, and R M Stroud. Solvent structure in crystals of trypsin determined by X-ray and neutron diffraction. *Proteins*, 12(3):203–22, March 1992.

[45] R. D. Finn, L. A. McLaughlin, S. Ronseaux, I. Rosewell, J. B. Houston, C. J. Henderson, and C. R. Wolf. Defining the in vivo role for cytochrome b5 in cytochrome p450 function through the conditional hepatic deletion of microsomal cytochrome b5. *Journal of Biological Chemistry*, 283(46):31385–93, 2008.

[46] Robert D Finn, Lesley a McLaughlin, Catherine Hughes, Chengli Song, Colin J Henderson, and C Roland Wolf. Cytochrome b (5) null mouse: a new model for studying inherited skin disorders and the role of unsaturated fatty acids in normal homeostasis. *Transgenic research*, 20(3):491–502, June 2011.

[47] Christian Fufezan, Jun Zhang, and M R Gunner. Ligand preference and orientation in b- and c-type heme-binding proteins. *Proteins*, 73(3):690–704, November 2008.

[48] H. Fukushima, G. F. Grinstead, and J. L. Gaylor. Total enzymic synthesis of cholesterol from lanosterol. cytochrome b5-dependence of 4-methyl sterol oxidase. *Journal of Biological Chemistry*, 256(10):4822–6, 1981.

[49] K. Fukushima and R. Sato. Purification and characterization of cytochrome b5-like hemoprotein associated with outer mitochondrial membrane of rat liver. *J Biochem*, 74(1):161–73, 1973.

[50] W D Funk, T P Lo, M R Mauk, G D Brayer, R T MacGillivray, and a G Mauk. Mutagenic, electrochemical, and crystallographic investigation of the cytochrome b5 oxidation-reduction equilibrium: involvement of asparagine-57, serine-64, and heme propionate-7. *Biochemistry*, 29(23):5500–8, June 1990.

[51] Andrea Giachetti, Giovanni La La Penna, Angelo Perico, and Lucia Banci. Modeling the backbone dynamics of reduced and oxidized solvated rat microsomal cytochrome b5. *Biophysical journal*, 87(1):498–512, July 2004.

[52] Hervé Guillou, Sabine D'Andrea, Vincent Rioux, Romain Barnouin, Stéphanie Dalaine, Frédérique Pedrono, Sophie Jan, and Philippe Legrand. Distinct roles of endoplasmic reticulum cytochrome b5 and fused cytochrome b5-like domain for rat Delta6-desaturase activity. *Journal of lipid research*, 45(1):32–40, January 2004.

[53] V. M. Guzov, H. L. Houston, M. B. Murataliev, F. A. Walker, and R. Feyereisen. Molecular cloning, overexpression in escherichia coli, structural and functional characterization of house fly cytochrome b5. *Journal of Biological Chemistry*, 271(43):26637–45, 1996.

[54] E. Hegesh, J. Hegesh, and A. Kaftory. Congenital methemoglobinemia with a deficiency of cytochrome b5. *N Engl J Med*, 314(12):757–61, 1986.

[55] W. Humphrey, A. Dalke, and K. Schulten. Vmd: Visual molecular dynamics. *Journal of Molecular Graphics*, 14(1):33–38, 1996.

[56] T.E. Huntley and P. Strittmatter. The effect of heme binding on the tryptophan residue and the protein conformation of cytochrome b5. *Journal of Biological Chemistry*, 247(14):4641, 1972.

[57] M. Ihara, S. Takahashi, K. Ishimori, and I. Morishima. Functions of fluctuation in the heme-binding loops of cytochrome b5 revealed in the process of heme incorporation. *Biochemistry*, 39(20):5961–70, 2000.

[58] A. ITO. Cytochrome b5-like Hemoprotein of Outer Mitochondrial Membrane; OM Cytochrome bI. Purification of OM Cytochrome b from Rat Liver Mitochondria and Comparison of Its Molecular Properties with Those of Cytochrome b5. *Journal of Biochemistry*, 87(1):63, 1980.

[59] A. Ito, S. Hayashi, and T. Yoshida. Participation of a cytochrome b5-like hemoprotein of outer mitochondrial membrane (om cytochrome b) in nadh-semidehydroascorbic acid reductase activity of rat liver. *Biochem Biophys Res Commun*, 101(2):591–8, 1981.

[60] G Jagow. b-Type Cytochromes. *Annual Review of Biochemistry*, 49:281–314, 1980.

[61] S. Jo, T. Kim, V. G. Iyer, and W. Im. Charmm-gui: a web-based graphical user interface for charmm. *J Comput Chem*, 29(11):1859–65, 2008. .

[62] W. Kabsch. Automatic-indexing of rotation diffraction patterns. *Journal of Applied Crystallography*, 21:67–71, 1988.

[63] David S Karow, Duohai Pan, Joseph H Davis, Sönke Behrends, Richard a Mathies, and Michael a Marletta. Characterization of functional heme domains from soluble guanylate cyclase. *Biochemistry*, 44(49):16266–74, December 2005.

[64] RJ Kassner. Effects of nonpolar environments on the redox potentials of heme complexes. *Proceedings of the National Academy of Sciences of*, 69(8):2263–2267, 1972.

[65] M L Kennedy, S Silchenko, N Houndonougbo, B R Gibney, P L Dutton, K R Rodgers, and D R Benson. Model hemoprotein reduction potentials: the effects of histidine-to-iron coordination equilibrium. *Journal of the American Chemical Society*, 123(19):4635–6, May 2001.

[66] R Kuroda, T Ikenoue, M Honsho, S Tsujimoto, J Y Mitoma, and a Ito. Charged amino acids at the carboxyl-terminal portions determine the intracellular locations of two isoforms of cytochrome b5. *The Journal of biological chemistry*, 273(47):31097–102, November 1998.

[67] GN La Mar, PD Burns, JT Jackson, KM Smith, KC Langry, and P. Strittmatter. Proton magnetic resonance determination of the relative heme orientations in disordered native and reconstituted ferricytochrome b5. Assignment of heme resonances by deuterium labeling. *Journal of Biological Chemistry*, 256(12):6075–6079, 1981.

[68] Florence Lederer. The cytochrome b5 fold: An adaptable module. *Biochimie*, 76(7):674–692, 1994.

[69] Florence Lederer, Rachid Guiard, Sylvie Cortial, and Akio Ito. Two Homologous Cytochromes b5 in a Single Cell. *European journal of biochemistry / FEBS*, 132(1):95–102, 1983.

[70] B. Lee and F. M. Richards. Interpretation of protein structures - estimation of static accessibility. *Journal of Molecular Biology*, 55(3):379–400, 1971.

[71] K. H. Lee and K. Kuczera. Molecular dynamics simulation studies of cytochrome b5 from outer mitochondrial and microsomal membrane. *Biopolymers*, 69(2):260–9, 2003.

[72] Kang Bong Lee, Eunsoon Jun, Gerd N. La Mar, Irene N. Rezzano, Ravindra K. Pandey, Kevin M. Smith, F. Ann Walker, and Daniel H. Buttlaire. Influence of heme vinyl- and carboxylate-protein contacts on structure and redox properties of bovine cytochrome b5. *Journal of the American Chemical Society*, 113(9):3576–3583, April 1991.

[73] Albert L. Lehninger, David L. Nelson, and Michael M. Cox. *Lehninger principles of biochemistry*. W.H. Freeman, New York, 5th edition, 2008.

[74] Dahui Liu, David a. Williamson, Michelle L. Kennedy, Todd D. Williams, Martha M. Morton, and David R. Benson. Aromatic Side Chain- Porphyrin Interactions in Designed Hemoproteins. *Journal of the American Chemical Society*, 121(50):11798–11812, December 1999.

[75] E Lloyd, J C Ferrer, W D Funk, M R Mauk, and a G Mauk. Recombinant human erythrocyte cytochrome b5. *Biochemistry*, 33(38):11432–7, September 1994.

[76] R Loris, P P Stas, and L Wyns. Conserved waters in legume lectin crystal structures. The importance of bound water for the sequence-structure relationship within the legume lectin family. *The Journal of biological chemistry*, 269(43):26722–33, October 1994.

[77] S. C. Lovell, I. W. Davis, 3rd Arendall, W. B., P. I. de Bakker, J. M. Word, M. G. Prisant, J. S. Richardson, and D. C. Richardson. Structure validation by calpha geometry: phi,psi and cbeta deviation. *Proteins-Structure Function and Bioinformatics*, 50(3):437–50, 2003. Lovell, Simon C Davis, Ian W Arendall, W Bryan 3rd de Bakker, Paul I W Word, J Michael Prisant, Michael G Richardson, Jane S Richardson, David C GM-15000/GM/NIGMS NIH HHS/United States GM-61302/GM/NIGMS NIH HHS/United States Research Support, Non-U.S. Gov't Research Support, U.S. Gov't, P.H.S. Validation Studies United States Proteins Proteins. 2003 Feb 15;50(3):437-50.

[78] S C Lovell, J M Word, J S Richardson, and D C Richardson. The penultimate rotamer library. *Proteins*, 40(3):389–408, August 2000.

[79] Yipin Lu, Renxiao Wang, Chao-Yie Yang, and Shaomeng Wang. Analysis of ligand-bound water molecules in high-resolution crystal structures of protein-ligand complexes. *Journal of chemical information and modeling*, 47(2):668–75, 2007.

[80] J G Ma, J Zhang, R Franco, S L Jia, I Moura, J J Moura, P M Kroneck, and J a Shelnutt. The structural origin of nonplanar heme distortions in tetraheme ferricytochromes c3. *Biochemistry*, 37(36):12431–42, September 1998.

[81] A. D. Mackerell, M. Feig, and C. L. Brooks. Extending the treatment of backbone energetics in protein force fields: Limitations of gas-phase quantum mechanics in reproducing protein conformational distributions in molecular dynamics simulations. *Journal of Computational Chemistry*, 25(11):1400–1415, 2004.

[82] S a Martinis, C Sotiriou, C K Chang, and S G Sligar. Characterization of cytochrome b5 reconstituted with a ferric chlorin and a ferric oxochlorin. *Biochemistry*, 28(2):879–84, January 1989.

[83] F. S. Mathews, M. Levine, and P. Argos. Structure of calf liver cytochrome b5 at 2.8 a resolution. *Nature-New Biology*, 233(35):15, 1971. K1780 Times Cited:76 Cited References Count:13.

[84] F S Mathews, M Levine, and P Argos. Three-dimensional Fourier synthesis of calf liver cytochrome b 5 at 2-8 A resolution. *Journal of molecular biology*, 64(2):449–64, March 1972.

[85] a. Grant Mauk and G. R. Moore. Control of metalloprotein redox potentials: what does site-directed mutagenesis of hemoproteins tell us? *Journal of Biological Inorganic Chemistry*, 2(1):119–125, February 1997.

[86] M R Mauk and a G Mauk. Interaction between cytochrome b5 and human methemoglobin. *Biochemistry*, 21(19):4730–4, September 1982.

[87] S.J. McLachlan, G.N. La Mar, and K.B. Lee. One-and two-dimensional nuclear Overhauser effect studies of the eletronic/molecular structure of the heme cavity of ferricytochrome b5. *Biochimica et Biophysica Acta (BBA)-Protein Structure and Molecular Enzymology*, 957(3):430–445, 1988.

[88] Lesley A Mclaughlin, Sebastien Ronseaux, Robert D Finn, Colin J Henderson, and C Roland Wolf. Deletion of Microsomal Cytochrome b 5 Profoundly Affects Hepatic and Extrahepatic Drug Metabolism. *Molecular Pharmacology*, 78(2):269–278, 2010.

[89] J. Mitoma and Akio Ito. The carboxy-terminal 10 amino acid residues of cytochrome b5 are necessary for its targeting to the endoplasmic reticulum. *The EMBO journal*, 11(11):4197, 1992.

[90] C D Moore and J T Lecomte. Structural properties of apocytochrome b5: presence of a stable native core. *Biochemistry*, 29(8):1984–9, February 1990.

[91] Kunal Mukhopadhyay and Juliette T J Lecomte. A relationship between heme binding and protein stability in cytochrome b5. *Biochemistry*, 43(38):12227–36, September 2004.

[92] Derek Murphy, Jeremy Parker, Minglong Zhou, Faisal M Fadlelmola, Christian Steidl, Aly Karsan, Randy D Gascoyne, Hong Chen, and Diponkar Banerjee. Constitutively overexpressed 21 kDa protein in Hodgkin lymphoma and aggressive non-Hodgkin lymphomas identified as cytochrome B5b (CYB5B). *Molecular cancer*, 9:14, January 2010.

[93] G. N. Murshudov, A. A. Vagin, and E. J. Dodson. Refinement of macromolecular structures by the maximum-likelihood method. *Acta Crystallographica Section D-Biological Crystallography*, 53:240–255, 1997.

[94] Manabu T Nakamura and Takayuki Y Nara. Structure, function, and dietary regulation of delta6, delta5, and delta9 desaturases. *Annual review of nutrition*, 24:345–76, January 2004.

[95] J. Navaza. Amore - an automated package for molecular replacement. *Acta Crystallographica Section A*, 50:157–163, 1994.

[96] Saburo Neya, Masaaki Suzuki, Tyuji Hoshino, Hirotaka Ode, Kiyohiro Imai, Teruyuki Komatsu, Akira Ikezaki, Mikio Nakamura, Yuji Furutani, and Hideki Kandori. Molecular insight into intrinsic heme distortion in ligand binding in hemoprotein. *Biochemistry*, 49(27):5642–50, July 2010.

[97] F G Nóbrega, P S Araujo, M Pasetto, and I Raw. Some properties of cytochrome b5 from liver microsomes of man, monkey, pig and chicken. *The Biochemical journal*, 115(4):849–56, December 1969.

[98] M. Nunez, E. Guittet, D. Pompon, C. van Heijenoort, and G. Truan. Nmr structure note: oxidized microsomal human cytochrome b5. *J Biomol NMR*, 47(4):289–95, 2010.

[99] Charles Olea, John Kuriyan, and Michael a Marletta. Modulating heme redox potential through protein-induced porphyrin distortion. *Journal of the American Chemical Society*, 132(37):12794–5, September 2010.

[100] Paul R. Ortiz de Montellano. *Cytochrome P450 : structure, mechanism, and biochemistry*. Kluwer Academic/Plenum Publishers, New York, 3rd edition, 2005.

[101] Z. Otwinowski and W. Minor. Processing of x-ray diffraction data collected in oscillation mode. *Macromolecular Crystallography, Pt A*, 276:307–326, 1997.

[102] Massimo Paoli, Jon Marles-Wright, and Ann Smith. Structure-function relationships in heme-proteins. *DNA and cell biology*, 21(4):271–80, April 2002.

[103] Sheldon Park and Jeffery G Saven. Statistical and molecular dynamics studies of buried waters in globular proteins. *Proteins*, 60(3):450–63, August 2005.

[104] Sudharsan Parthasarathy, Adriana Altuve, Simon Terzyan, Xuejun Zhang, Krzysztof Kuczera, Mario Rivera, and David R Benson. Comparison of Human and Rat Type B (Mitochondrial) Cytochrome b 5. *Biochemistry*, 2011.

[105] W Pfeil. Thermodynamics of apocytochrome b5 unfolding. *Protein science*, 2(9):1497–501, September 1993.

[106] Todd D Porter. The roles of cytochrome b5 in cytochrome P450 reactions. *Journal of biochemical and molecular toxicology*, 16(6):311–6, January 2002.

[107] V. V. Reddy, D. Kupfer, and E. Caspi. Mechanism of c-5 double bond introduction in the biosynthesis of cholesterol by rat liver microsomes. *Journal of Biological Chemistry*, 252(9):2797–801, 1977.

[108] Charles J Reedy and Brian R Gibney. Heme protein assemblies. *Chemical reviews*, 104(2):617–49, March 2004.

[109] Lorne S Reid, Anthony R Lim, and A Grant Mauk. Role of Heme Vinyl Groups in Cytochrome b5 Electron Transfer. *Biochemistry*, 108(26):8197–8201, 1986.

[110] Lorne S. Reid, Marcia R. Mauk, and a. Grant Mauk. Role of heme propionate groups in cytochrome b5 electron transfer. *Journal of the American Chemical Society*, 106(7):2182–2185, April 1984.

[111] L.S. Reid, V.T. Taniguchi, H.B. Gray, and A.G. Mauk. Oxidation-reduction equilibrium of cytochrome b5. *Journal of the American Chemical Society*, 104(26):7516–7519, 1982.

[112] M Rivera, C Barillas-Mury, K A Christensen, J W Little, M a Wells, and F a Walker. Gene synthesis, bacterial expression, and 1H NMR spectroscopic studies of the rat outer mitochondrial membrane cytochrome b5. *Biochemistry*, 31(48):12233–40, December 1992.

[113] M Rivera, R Seetharaman, D Girdhar, M Wirtz, X Zhang, X Wang, and S White. The reduction potential of cytochrome b5 is modulated by its exposed heme edge. *Biochemistry*, 37(6):1485–94, February 1998.

[114] M Rivera, M a Wells, and F a Walker. Cation-promoted cyclic voltammetry of recombinant rat outer mitochondrial membrane cytochrome b5 at a gold electrode modified with beta-mercaptopropionic acid. *Biochemistry*, 33(8):2161–70, March 1994.

[115] Mario Rivera, F Qiu, R a Bunce, and R E Stark. Complete isomer-specific 1H and 13 C NMr assignments of the heme resonances of rat liver outer mitochondrial membrane cytochrome b5. *Journal of Biological Inorganic Chemistry*, 4:87–98, 1999.

[116] Karla K Rodgers, Thomas C Pochapsky, and Stephen G Sligar. Probing the Mechanisms of Macromolecular Recognition: The Cyochrome b5 Cytochrome c Complex. *Science*, 240(4859):1657–1659, 1988.

[117] Karla K Rodgers and Stephen G Sligar. Surface Electrostatics, Reduction potentials and the Internal dielectric constant of proteins. *Journal of the American Chemical Society*, 113(24):9419–9421, 1991.

[118] M J Rodríguez-Marañón, F Qiu, R E Stark, S P White, X Zhang, S I Foundling, V Rodríguez, C L Schilling, R a Bunce, and M Rivera. 13C NMR spectroscopic and X-ray crystallographic study of the role played by mitochondrial cytochrome b5 heme propionates in the electrostatic binding to cytochrome c. *Biochemistry*, 35(50):16378–90, December 1996.

[119] J. P. Ryckaert, G. Ciccotti, and H. J. C. Berendsen. Numerical-integration of cartesian equations of motion of a system with constraints - molecular-dynamics of n-alkanes. *Journal of Computational Physics*, 23(3):327–341, 1977.

[120] S Sarma, B Dangi, C Yan, R J DiGate, D L Banville, and R D Guiles. Characterization of a site-directed mutant of cytochrome b5 designed to alter axial imidazole ligand plane orientation. *Biochemistry*, 36(19):5645–57, May 1997.

[121] S Sarma, R J DiGate, D B Goodin, C J Miller, and R D Guiles. Effect of axial ligand plane reorientation on electronic and electrochemical properties observed in the A67V mutant of rat cytochrome b5. *Biochemistry*, 36(19):5658–68, May 1997.

[122] John B Schenkman and Ingela Jansson. The many roles of cytochrome b5. *Pharmacology and Therapeutics*, 97(2):139–152, February 2003.

[123] J M Shifman, C C Moser, W a Kalsbeck, D F Bocian, and P L Dutton. Functionalized de novo designed proteins: mechanism of proton coupling to oxidation/reduction in heme protein maquettes. *Biochemistry*, 37(47):16815–27, November 1998.

[124] N. V. Shokhirev and F. a. Walker. The effect of axial ligand plane orientation on the contact and pseudocontact shifts of low-spin ferriheme proteins. *Journal of Biological Inorganic Chemistry*, 3(6):581–594, December 1998.

[125] S Silchenko, M L Sippel, O Kuchment, D R Benson, a G Mauk, a Altuve, and M Rivera. Hemin is kinetically trapped in cytochrome b(5) from rat outer mitochondrial membrane. *Biochemical and biophysical research communications*, 273(2):467–72, July 2000.

[126] M. Simeonov, A. Altuve, M. A. Massiah, A. Wang, M. A. Eastman, D. R. Benson, and M. Rivera. Mitochondrial and microsomal ferric b5 cytochromes exhibit divergent conformational plasticity in the context of a common fold. *Biochemistry*, 44(26):9308–19, 2005.

[127] Mario Simeonov, Adriana Altuve, Michael a Massiah, An Wang, Margaret a Eastman, David R Benson, and Mario Rivera. Mitochondrial and microsomal ferric b5 cytochromes exhibit divergent conformational plasticity in the context of a common fold. *Biochemistry*, 44(26):9308–19, July 2005.

[128] Lorna J Smith, Abdullah Kahraman, and Janet M Thornton. Heme proteins–diversity in structural characteristics, function, and folding. *Proteins*, 78(10):2349–68, August 2010.

[129] Penny Soucy and Van Luu-The. Assessment of the ability of type 2 cytochrome b5 to modulate 17,20-lyase activity of human P450c17. *The Journal of steroid biochemistry and molecular biology*, 80(1):71–5, January 2002.

[130] Lawrence Spatz and Phillipp Strittmatter. A Form of Cytochrome b5 That Contains an Additional Hydrophobic Sequence of 40 Amino Acid Residues. *Proceedings of the National Academy of Sciences of the United States of America*, 68(5):1042–1046, 1971.

[131] E M Storch and V Daggett. Molecular dynamics simulation of cytochrome b5: implications for protein-protein recognition. *Biochemistry*, 34(30):9682–93, August 1995.

[132] C.F. Strittmatter and E.G. Ball. A hemochromogen component of liver microsomes. *Proceedings of the National Academy of Sciences of the United States of America*, 38(1):19–25, 1952.

[133] P. Strittmatter, P. Fleming, M. Connors, and D. Corcoran. Purification of cytochrome b5. *Methods Enzymol*, 52:97–101, 1978.

[134] P. Strittmatter and S.F. Velick. The isolation and properties of microsomal cytochrome. *Journal of Biological Chemistry*, 221(1):253–264, 1956.

[135] Na Sun, An Wang, Aaron B Cowley, Adriana Altuve, Mario Rivera, and David R Benson. Enhancing the stability of microsomal cytochrome b5: a rational approach informed by comparative studies with the outer mitochondrial membrane isoform. *Protein engineering, design & selection : PEDS*, 18(12):571–9, December 2005.

[136] Hiroshi Suzuki, Satoshi Tashiro, Shusuke Hira, Jiying Sun, Chikara Yamazaki, Yukari Zenke, Masao Ikeda-Saito, Minoru Yoshida, and Kazuhiko Igarashi. Heme regulates gene expression by triggering Crm1-dependent nuclear export of Bach1. *The EMBO journal*, 23(13):2544–53, July 2004.

[137] F. Akif Tezcan, Jay R. Winkler, and Harry B. Gray. Effects of Ligation and Folding on Reduction Potentials of Heme Proteins. *Journal of the American Chemical Society*, 120(51):13383–13388, December 1998.

[138] D. E. Tronrud, L. F. Teneyck, and B. W. Matthews. An efficient general-purpose least-squares refinement program for macromolecular structures. *Acta Crystallographica Section A*, 43:489–501, 1987.

[139] A. Vagin and A. Teplyakov. Molecular replacement with molrep. *Acta Crystallographica Section D-Biological Crystallography*, 66:22–25, 2010.

[140] G Vergéres and L Waskell. Cytochrome b5, its functions, structure and membrane topology. *Biochimie*, 77(7-8):604–20, January 1995.

[141] F Ann Walker, David Emrick, Jenny E Rivera, Bernard J Hanquet, and Daniel H Buttlaire. Effect of Heme Orientation on the Reduction Potential of Cytochrome b5. *Journal of the American Chemical Society*, 110(15):6234–6240, 1988.

[142] Lijun Wang, Aaron B Cowley, and David R Benson. Enhancing the thermal stability of mitochondrial cytochrome b 5 by introducing a structural motif characteristic of the less stable microsomal isoform. *Protein Engineering Design and Selection*, 20(10):511–520, 2007.

[143] Lijun Wang, Na Sun, Simon Terzyan, Xuejun Zhang, and David R Benson. A histidine/tryptophan pi-stacking interaction stabilizes the heme-independent folding core of microsomal apocytochrome b5 relative to that of mitochondrial apocytochrome b5. *Biochemistry*, 45(46):13750–9, November 2006.

[144] Z Q Wang, Y H Wang, W H Wang, L L Xue, X Z Wu, Y Xie, and Z X Huang. The effect of mutation at valine-45 on the stability and redox potentials of trypsin-cleaved cytochrome b5. *Biophysical chemistry*, 83(1):3–17, January 2000.

[145] M a Williams, J M Goodfellow, and J M Thornton. Buried waters and internal cavities in monomeric proteins. *Protein science*, 3(8):1224–35, August 1994.

[146] Marc Wirtz, Vaheh Oganesyan, Xuejun Zhang, Joe Studer, and Mario Rivera. Modulation of redox potential in electron transfer proteins: Effects of complex formation on the active site microenvironment of cytochrome b5. *Faraday Discussions*, 116:221–234, 2000.

[147] J. Wu, J. H. Gan, Z. X. Xia, Y. H. Wang, W. H. Wang, L. L. Xue, Y. Xie, and Z. X. Huang. Crystal structure of recombinant trypsin-solubilized fragment of cytochrome b(5) and the structural comparison with val61his mutant. *Proteins-Structure Function and Bioinformatics*, 40(2):249–57, 2000.

[148] Yunhua Wu and Shengshui Hu. Biosensors based on direct electron transfer in redox proteins. *Microchimica Acta*, 159(1-2):1–17, April 2007.

[149] L L Xue, Y H Wang, Y Xie, P Yao, W H Wang, W Qian, Z X Huang, J Wu, and Z X Xia. Effect of mutation at valine 61 on the three-dimensional structure, stability, and redox potential of cytochrome b5. *Biochemistry*, 38(37):11961–72, September 1999.

[150] P. Yao, Y. Xie, Y. H. Wang, Y. L. Sun, Z. X. Huang, G. T. Xiao, and S. D. Wang. Importance of a conserved phenylalanine-35 of cytochrome b5 to the protein's stability and redox potential [published erratum appears in Protein Eng 1997 Aug;10(8):983]. *Protein Engineering Design and Selection*, 10(5):575–581, May 1997.

[151] Takehiro Yokota, Yoshitaka Nakajima, Fumiyuki Yamakura, Shigetoshi Sugio, Muneaki Hashimoto, and Shinzaburo Takamiya. Unique structure of Ascaris suum b5-type cytochrome: an additional alpha-helix and positively charged residues on the surface domain interact with redox partners. *The Biochemical journal*, 394(Pt 2):437–47, March 2006.

[152] Haoming Zhang, Sang-Choul Im, and Lucy Waskell. Cytochrome b5 increases the rate of product formation by cytochrome P450 2B4 and competes with cytochrome P450 reductase for a binding site on cytochrome P450 2B4. *The Journal of biological chemistry*, 282(41):29766–76, October 2007.